PREPARATION AND CHARACTERIZATION OF POLYMER BASED COMPOSITE NANOSPHERES FOR BONE INFECTION PREVENTION

A Thesis Submitted to
The Graduate School of Engineering and Sciences of
İzmir Institute of Technology
in Partial Fulfillment of the Requirements for the Degree of

MASTER OF SCIENCE

in Chemical Engineering

by
Ceren KIMNA

June, 2018
İZMİR

We approve the thesis of **Ceren KIMNA**

Examining Committee Members:

_____
Prof. Dr. Funda TIHMINLIOĞLU
Department of Chemical Engineering, İzmir Institute of Technology

_____
Prof. Dr. Oğuz BAYRAKTAR
Department of Chemical Engineering, Ege University

_____
Asst. Prof. Dr. Ayben TOP
Department of Chemical Engineering, İzmir Institute of Technology

27 June 2018

_____
Prof. Dr. Funda TIHMINLIOĞLU
Supervisor,
Department of Chemical Engineering,
İzmir Institute of Technology

_____
Prof. Dr. Erol ŞEKER
Head of the Department of Chemical Engineering

_____
Prof. Dr. Aysun SOFUOĞLU
Dean of the Graduate School of Engineering and Sciences

ACKNOWLEDGMENTS

Firstly, I would like to express my warmest gratitude to Prof. Dr. Funda Tıhmınlıoğlu for her supervision, guidance and support during my thesis studies.

I would like to thank Dr. Gülnihal Yelken, Dr. Özlem Çağlar Duvarcı and Evrim Paşık for their advice and helping for the analyses. I thank Mustafa Umut Mutlu for his help and suggestions in the electrospraying process. I also acknowledge to Mehmet Onur Cirit for his valuable recommendations and friendship.

I am thankful to my lab and office mates Dr. Sedef Tamburacı and Sibel Değer for their help and support. They were always more than a colleague throughout this thesis.

I am grateful to my lovely parents, Mediha and Ertan Kımna for their endless support and understanding during my whole education life. I knew they will always be with me whenever I need them. I ought to thank Cenk Girman for making this journey fun with his motivation and support.

This study was financially supported by The Scientific and Technological Research Council of Turkey (TUBITAK) under the name of Development of Controlled Antibiotic Releasing Chitosan/Silica Based Composite Scaffolds and Investigation of Their Potential for Hard Tissue Engineering Applications (#116M096).

ABSTRACT

PREPARATION AND CHARACTERIZATION OF POLYMER BASED COMPOSITE NANOSPHERES FOR BONE INFECTION PREVENTION

Currently, bone tissue engineering applications comprise the development of smart materials that can induce tissue regeneration meanwhile supporting the defect site of the body. Despite of the advancements, inflammation is still a serious problem that threatens human health at the post-implantation period. To overcome potential inflammations, antibiotic therapy is commonly employed in clinical trials. However, antibiotic therapy causes some side effects such as ototoxicity and nephrotoxicity, especially when applied in high doses. Therefore, local drug delivery systems play a vital role in bone disorders due to the elimination of disadvantages introduced by conventional methods.

In the presented study, it was aimed to develop chitosan-based composite nanospheres as a controlled drug delivery system against bone infections. Accordingly, chitosan and montmorillonite nanoclay was homogenized with microfluidizer and electrosprayed to obtain spherical nanoparticles. The optimum electrospraying conditions were investigated using response surface methodology. Vancomycin and Gentamicin antibiotics were incorporated in the polymeric matrix to provide controlled release at the defect region to overcome inflammations after implantation. The prepared nanospheres were characterized in terms of morphology, hydrodynamic size distribution, surface charge, drug encapsulation efficiency and release profiles. The dominant drug release mechanism was determined by empirical mathematic models.

Drug loaded nanospheres have been successfully produced with a size range of 180-350 nm. High encapsulation efficiency was achieved (80-95%) with a controlled drug release up to 30 days. Fickian diffusion was found as the main mechanism in drug delivery from spherical CS/MMT nanocomposites. The *in vitro* release medium of nanospheres showed strong antimicrobial activity against gram-positive *S. aureus* and gram-negative *E. coli* bacteria. Furthermore, it was found that the nanospheres did not show any cytotoxic effect to 3T3 and SaOS-2 cell lines. These results demonstrated that the prepared nanospheres can be a promising option for bone infection prevention.

ÖZET

KEMİK ENFEKSİYONLARININ ÖNLENMESINE YÖNELİK POLİMER BAZLI KOMPOZİT NANOKÜRELERİN HAZIRLANMASI VE KARAKTERİZASYONU

Günümüzde, kemik doku mühendisliği uygulamaları iyileşme sürecinde destek olabilen aynı zamanda da doku rejenerasyonunu tetikleyen akıllı malzemelerin geliştirilmesini içermektedir. Ancak bu gelişmelerin yanısıra, transplantasyon sonrası dönemde yaşanan inflamasyon sorunu, insan sağlığını tehdit eden ciddi bir problemdir. Genellikle klinik çalışmalarda olası inflamasyon probleminin üstesinden gelebilmek için hastalara antibiyotik tedavisi uygulanmaktadır. Fakat antibiyotik tedavisi özellikle yüksek dozda uygulandığında ototoksisite ve nefrotoksisite gibi bazı yan etkilere yol açmaktadır. Bu nedenle, lokal ilaç salım sistemleri geleneksel yöntemlerin dezavantajlarını kaldırarak kemik defektlerinde hayati bir rol oynamaktadır.

Bu çalışmada, kemik enfeksiyonlarına karşı kontrollü ilaç salım sistemi olarak kitosan bazlı kompozit nanokürelerin geliştirilmesi amaçlanmıştır. Bu nedenle, kitosan ve montmorrilonit nanokil katkısı mikroakışkanlaştırıcı ile homojenize edilip elektrospreylenmiştir. Vankomisin ve Gentamisin antibiyotikleri defekt bölgede inflamasyonu engelleme amacıyla kontrollü salınım sağlanması için polimerik matrikse dahil edilmiştir. Hazırlanan nanoküreler, morfoloji, hidrodinamik boyut dağılımı, yüzey yükü, enkapsülasyon verimi ve ilaç salınım profilleri açısından karakterize edilmiştir. Baskın ilaç salım mekanizması empirik matematik modelleri ile belirlenmiştir.

İlaç yüklü nanoküreler, 180-350 nm boyut aralığında başarıyla üretilmiştir. Hazırlanan nonükerelere yüksek miktarda ilaç yüklemesi (80-95%) sağlanarak 30 gün boyunca kontrollü ilaç salımı gerçekleştirilmiştir. Nanokompozit CS/MMT kürelerin ilaç salım davranışı difüzyon ile kontrol edilmiştir. Kürelerin salım sıvıları gram pozitif *S. aureus* ve gram negatif *E. coli* bakterilerine karşı antimikrobiyal aktivite göstermiştir. Ayrıca, nanoküreler 3T3 ve SaOS-2 hücre hatlarında herhangi bir sitotoksik etki göstermemiştir. Elde edilen sonuçlar, hazırlanan nanokürelerin kemik enfeksiyonuna karşı umut verici bir seçenek olabileceğini göstermektedir.

TABLE OF CONTENTS

LIST OF FIGURES

Figure **Page**

LIST OF TABLES

Table **Page**

CHAPTER 1

INTRODUCTION

There has been a significant increase in the bone disorders due to the population aging and the sedentary lifestyle of the people today. Musculoskeletal problems, severe bone tissue degeneration and advanced inflammatory problems cannot be treated with a medication. Consequently, there is an increasing demand for bone replacement materials to ensure adequate support during the healing process and promote new bone growth. However, inflammation is still a drawback of these operations which should immediately be overcome to prevent the biofilm formation. In the conventional procedure, the antibiotic treatment is applied via oral administration or high concentration vaccination. However, the possibility of the drug cannot be delivered to the defect site with therapeutic amounts in oral systems limits the application of this method by inducing the antibiotic resistance of the human body (Gao et al., 2011). In addition, the depot antibiotic application can cause autotoxicity and nephrotoxicity.

Nowadays, local controlled release can be served as an alternative to conventional methods to prevent inflammation in the defect site of the bone. The site-specific drug delivery systems supply an effective delivery and prevent the side effects due to the high dosage of the drug. These systems should be well-characterized to understand the underlying mechanism of the release kinetics.

The material selection to achieve sustained release is a challenging issue. Therefore, a wide range of materials has been utilized to adjust the release rate regarding the specific criteria specified in the system. The carrier material should be non-toxic to the human body, should protect the active agent and assist an efficient release profile. Thus, natural polymer-based nanoparticles can circumvent these issues. They come into prominence in drug delivery systems due to their biocompatibility, biodegradability and the ease in processability. They degrade to non-toxic monomers inside the body. Collagen, albumin, gelatin, alginate, chitosan, cyclodextrins are the mainly used natural polymers in drug delivery (Pillai and Panchagnula, 2001).

Chitosan is a natural aminoglycosidic polymer that has been commonly used in drug delivery systems according to its outstanding properties. The active amino groups

of positively charged chitosan provide reactive sites for various groups that make it an ideal candidate for carrying any types of drugs. Chitosan-based carrier systems have been evaluated and showed promising results in local antibiotic delivery in forms of the hydrogel, bead or film (Patel and Amiji, 1996; Anal and Stevens, 2005; Noel et al., 2008). However, chitosan biopolymer shows rapid degradation profile and high swelling degree. Therefore, chitosan-based materials should be modified to improve the stability which is substantial to design a rate-controlled drug delivery. In order to overcome these drawbacks, anionic excipients can be preferred to harden the polymer matrix and prolong the drug release period. Recently, composite formation with nanofillers has attained great interest according to the superior properties as compared to biopolymer itself. Polymer-clay nanocomposites are the hybrid materials composed of the synergistic effect of the organic polymer matrix and nanoscale organophilic clay fillers. Recent studies promoted that chitosan/clay nanocomposite systems show promising results with improved stability in drug delivery applications for cationic or anionic drugs (Depan et al., 2009; Yuan et al., 2010). Montmorillonite (MMT) is a smectite group of minerals that is the most commonly used nanofiller in composite systems. The layered structure of the MMT is suitable for reinforcement purposes and provides a tortuous pathway for drug delivery. The MMT surface is modified by replacing Na^+ ions with cations to make the platelets compatible with polymers.

The aim of this study is to develop a chitosan/nanoclay composite system for the delivery of gentamicin and vancomycin antibiotics which are recommended for bone infection treatment. Firstly, electrospray process variables were optimized in order to obtain spherical, uniformly distributed nanoparticles. Furthermore, homogenization parameters were optimized in terms of molecular weight, deacetylation degree and rheological properties of the chitosan. The chitosan/clay nanocomposite spheres were characterized regarding their morphology, size distribution, surface charges, chemical interactions and the drug entrapment efficiencies. *In vitro* drug release profiles of nanospheres with a different polymer to drug ratios were determined with the appropriate kinetic model. Antimicrobial activities of nanospheres were determined against *E. coli* and *S. aureus* microorganisms. The *in vitro* cell cytotoxicity assay of chitosan nanospheres were performed on the NIH/3T3 fibroblast and SaOS-2 bone osteosarcoma cell lines.

The organization of the dissertation is as follows: A brief information related to the nanocomposite drug delivery systems for bone infections and the aim of the research

were mentioned in Chapter 1. Chapter 2 presents a background on literature regarding bone tissue inflammation, controlled drug delivery systems and chitosan/clay nanocomposites as drug carrier systems. Chapter 3 provides information about production methods and characterization of the drug loaded nanospheres. The results and the discussion of the experiments are assessed in Chapter 4. Finally, Chapter 5 concludes the thesis with the goals and the suggestions for the future works with the composite nanocarrier system.

CHAPTER 2

LITERATURE REVIEW

2.1. Bone Tissue Engineering

2.1.1. Structure of Bone Tissue

The bone is a complex tissue involving the mineralized osseous tissue, marrow, endosteum and periosteum, vessels, nerves and cartilage (Porter et al., 2009). The principal functions of the bone can be noted as to provide mechanical support to the body, to protect interior organs and to store the minerals such as calcium and potassium. Bone has a biphasic structure containing both inorganic and organic elements. It is composed of 60% (w/v) mineral, 30% (w/v) matrix and 10% (w/v) water (Razak et al., 2012).

The irregular structure of the bone makes it heterogeneous and anisotropic. The structural components of the bone are tabulated in Table 2.1. According to the structure and the porosity, the macrostructure of the bone can be divided into two main parts named as compact and trabecular.

The highly mineralized outer layer is called as a compact bone (cortical layer). It includes osteons that provide a connection with the nervous system. The inner layer, trabecular bone, is the spongy part that fills the interior of the cortical layer. It has a porous architecture with a large surface area. The porosity of the trabecular bone is reported as 50-90% (Costa-Pinto et al., 2011). The main parts of the bone are illustrated in Figure 2.1.

The human bone extracellular matrix is composed of collagen matrix, mineral (mainly carbonated hydroxyapatite crystals), water, non-collagenous proteins (osteocalcin, osteonectin, alkaline phosphatase etc.) and proteoglycans (GAGs) (Lowenstam and Weiner, 1989). The most abundant protein in bone tissue is Type I collagen. Other types of collagens (collagen II, VI and V) are also present in the mature bone (Reznikov et al., 2014)

Table 2. 1. Components of the bone according to the hierarchical structure (Source: Rho et al., 1998)

Scale	Components
Macrostructure	Compact and trabecular bone
Microstructure (10-500 mm)	Haversian systems, osteons, single trabeculae
Sub-microstructure (1-10 mm)	Lamellae
Nanostructure (few hundred nanometers to 1 mm)	Fibrillar collagen and embedded mineral
Subnanostructure (below few hundred nanometers)	Mineral, collagen, non-collagenous organic proteins

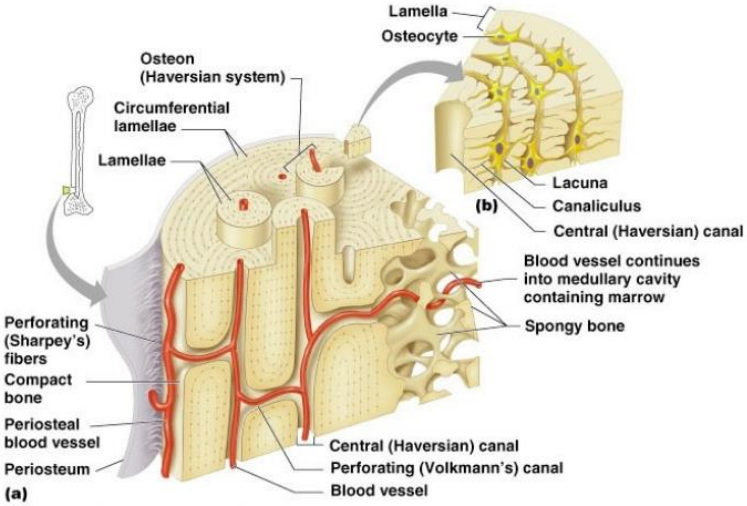

Figure 2. 1. The cross-sectional structure of the bone (Source: Marieb and Koehn, 2007)

Bone tissue comprises the osteoblasts, lining cells, osteoclasts on the bone surface and osteocytes permeated in the bone extracellular matrix. Osteoblasts, lining cells and osteocytes are derived from the osteoprogenitor cells while osteoclasts are differentiated from peripheral blood monocytes (Marks and Popoff, 1988). Osteoblasts are responsible for the production and the organization of the collagen fibrils; production of the bone proteins; mineralization of the bone matrix (osteoid) and the vascularization. The bone-lining cells cover the bone surface with their elongated structures. They serve as a semi-permeable barrier between the bone and body fluid and regulate crystal growth in the bone (Miller and Jee, 1987). Osteoclasts are the multinucleated cells that resorb the mineralized bone and the cartilage. They are responsible for the bone modeling and

remodeling during the development and repairing of the skeleton by their resorptive functions. Osteocytes are responsible for maintaining extracellular matrix and calcium homeostasis. They placed concentrically around the central vessels forming Haversian systems with the increase in organization and the density of the bone.

2.1.2. Bone Tissue Engineering Applications

The bone itself has a high potential for regeneration, especially before adulthood stage. However, surgical operations are necessary for the large bone defects when the bone cannot repair itself. Osteoporosis (reduction of bone mass), arthritis, osteomalacia (bone mineralization defects) and scoliosis are the crucial musculoskeletal problems for the bone tissue regeneration which generally ends up with surgical operations. In addition, according to the aging of the population and the decrease in the physical activity, bone disorders are getting importance and reducing the quality of the human life.

The bone tissue degeneration and inflammation cases are intervened with the operational methods when the drug therapy alone cannot be sufficient. Generally, conventional methods are applied to the bone disorders by filling the defects known as grafting. Autograft, allograft, and xenograft are the three main approaches to bone grafting. Autologous grafting, called the gold standard of the reconstructive surgery, grafts the tissue from another part of the body to fill the defected region. These operations do not end up with the immunologic complications in general but contain several drawbacks such as the need for additional surgery, donor pain or insufficient source to fill the gaps (Wagh, 2004). Allografting is the grafting between different members of the same species. Cadaver bones are generally used in this technique. Allografts bring the risk of disease transmission and immunogenicity. Xenograft is the method of tissue grafting between the members of different species. However, they have the major drawbacks such as the risk of donor-site pain, need of an additional operation and the limited donor site.

The limitations in conventional grafting and need for the substitutionary material to fill the bone defects becomes crucial in case of critical-sized defects. Hence, the bone substitutes are preferred to promote the osteoblast differentiation (osteoinductive), foster the surrounding bone ingrowth (osteoconductive) and allow the integration into the tissue of the surrounding bone (osseointegration) (Stevens, 2008).

Bone tissue engineering allows functional bone regeneration with the combination of cells, signal molecules, and the engineered biomaterials. In this manner, site-specific bone substitutes can be transplanted successfully by minimizing the possible complications.

The natural function of the bone can be imitated by composite materials that contain organic and inorganic groups. The physicochemical and the biological properties of these substitutes can be adjusted with different processing techniques. 3D scaffolds can serve as a support material promoting the tissue regeneration at the defect side. However, they should be compatible with the defect and the surrounding tissues in physical, chemical and biological point of views. The scaffolds for the bone tissue engineering should supply key requirements such as:

- **Biocompatibility:** The bone scaffold and its degradation side products should support the biological activity without causing any toxic effects. It should be agreeable to the surrounding tissue and the body fluid so that it should not provoke an immune response, rejection or inflammation to host tissue.
- **Biodegradability:** The scaffold degradation rate should coincide with the rate of new tissue formation as much as possible. While the cells fabricate their own natural matrix, the scaffold must be able to provide the structural integrity within the body and break down leaving the newly formed tissue which will take the place over (Arca and Şenel, 2008).
- **Suitable architecture:** The scaffold surface should allow cell migration into defect from surrounding tissue with its interconnected pores. The bone scaffold should have a broad range of porosity to mimic the natural structure by allowing cell attachment; diffusion of nutrients and oxygen for cell survival and vascularization without risking the mechanical strength. Studies contended that scaffolds should have the required minimum pore size of 100 μm which is critical for the diffusion of nutrients and oxygen for cell survival (Hulbert et al., 1970). Besides, pore size range of 200-350 μm was found to be optimum for cell proliferation in bone tissue engineering (Murphy et al., 2010).
- **Mechanical properties:** The scaffold should serve temporary mechanical support and integration during the regeneration. The mechanical requirements must meet the physical demand of the healthy bone.

2.1.3. Inflammation at Post-transplantation

The bacterial adhesion, ending up with the bio-film formation at the implant site is still a major problem of the transplantation operations. In literature, infection followed by patient morbidity has been reported for 5% of total hip and joint replacement operations (Albuhairan et al., 2008). The period of 6 hours after the post-implantation is critical for the prevention of long-term infection. Bacteria can reach bone via the hematogenous route, spread from an external source or propagation from soft tissue infection which may lead to necrosis of trabecular bone (Hogan et al., 2013). In these cases, antibiotic treatment is needed after implantation to overcome any possible bone infection problems. The infection problem limits the compatibility of biomaterials and reduces the tissue integration.

The infection can be defined as a homeostatic imbalance between host tissue and the microorganisms. The microorganism concentration exceeding 10^5 organisms/tissue or presence of beta-hemolytic streptococci causes infection problems (Sussman and Bates-Jensen, 2012). The oral antibiotic treatment should be applied to decrease the bacterial infection to a minimum level at which healing process can start. Even though the infected/necrotic tissue is removed from the body, antibiotic therapy is required for the prevention of the wound. Studies asserted that at least 4-6 weeks of antibiotic therapy is required since the reconstruction of blood vessels takes 4 weeks (Mader and Adams, 1989; Salvati et al., 2003). Local antibiotics can shorten the therapy because of the long-term elution of antimicrobial agents.

2.1.4. Antibiotics Used in Bone Inflammations

Gentamicin, vancomycin, amikacin, and tobramycin are the generally preferred clinically relevant antibiotics against bone inflammation. The therapeutic and toxic ranges based on conventional administrations of these antibiotics through life-threatening infections were tabulated in Table 2.2. The common side effects that are limiting the usage in clinical operations can be listed as nephrotoxicity, neurotoxicity, auditory and vestibular ototoxicity (Song et al., 1998; Hidayat et al., 2006). Also, other side effects such as patient noncompliance and discomfort can occur with oral administrations since

it has higher plasma concentration than the minimum inhibitory concentration (MIC) of bacteria (Hammett-Stabler and Johns, 1998). Hence, local controlled delivery systems after a post-implantation period can increase the quality of the remission period.

Table 2. 2. Therapeutic and toxic concentrations of antibiotics through life-threatening infections (Source: Hammett-Stabler and Johns, 1998)

Drug	**Therapeutic concentration (mg/L)**	**Toxic concentration (mg/L)**
Gentamicin Sulphate	<2	>2
Vancomycin Hydrochloride	<2	>2
Amikacin	4-8	>10
Tobramycin	5-10	40

- **Gentamicin**

Gentamicin sulfate is an aminoglycosidic antibiotic that is generally used against Gram-negative bacteria by inhibiting the protein synthesis. It only shows antibacterial activity against aerobic bacteria (Sionkowska et al., 2016). Gentamicin was firstly isolated from *Micromonospora purpurea*. The antimicrobial activity of gentamicin against *Escherichia coli, Proteusbacillus vulgaris, Pseudomonas aeruginosa, Pneumobacillus, Salmonella bacteria, Shigella dysenteriae, Staphylococcus aureus* was reported in the literature (Rapoport et al., 1999; Balakumar et al., 2010; Lan et al., 2014). It is commonly used for the treatment of endocarditis, pelvic inflammations, meningitis, pneumonia, urinary tract infections, and sepsis. Besides, it is widely used for the bone tissue diseases such as osteomyelitis and infection treatments due to its favorable penetration to bone tissue (Blanco-Príeto et al., 2002; Darley and MacGowan, 2004). The Scanning Electron Microscopy (SEM) image of Gentamicin sulfate is depicted in Figure 2.2.

- **Vancomycin**

Vancomycin hydrochloride, the hydrochloride salt of vancomycin, is the branched tricyclic glycosylated peptide. It is firstly isolated from *Streptomyces orientalis* (Barna and Williams, 1984). It shows a bactericidal activity against Gram-positive bacteria by binding to the D-alanyl-D-alanine of the cell wall precursors. Its main mechanism is to inhibit the peptidoglycan synthesis of bacterial cell wall (Caramella et al., 2016). It also has an effect on bacterial cytoplasmic membrane permeability that may inhibit RNA synthesis.

Vancomycin has a plasma half-life of 6 hours. It was reported that 50% of vancomycin bounds to plasma proteins and diffuses into extracellular fluids in therapeutic conditions (Cevher et al., 2006). Vancomycin treatment is recommended for bloodstream infections, endocarditis, meningitis, skin infections as well as bone and joint infections. The therapeutic effect of vancomycin against osteomyelitis is also reported (Ozcan et al., 2006). The Scanning Electron Microscopy (SEM) image of Vancomycin hydrochloride is depicted in Figure 2.3.

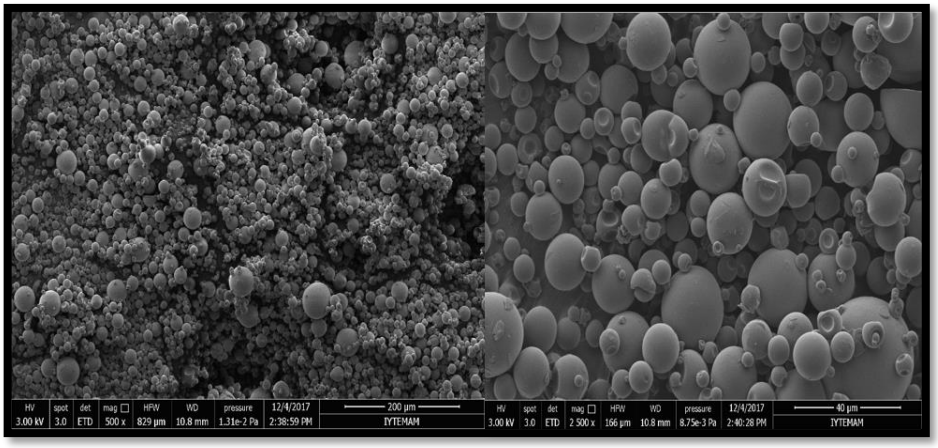

Figure 2. 2. SEM image of Gentamicin sulfate

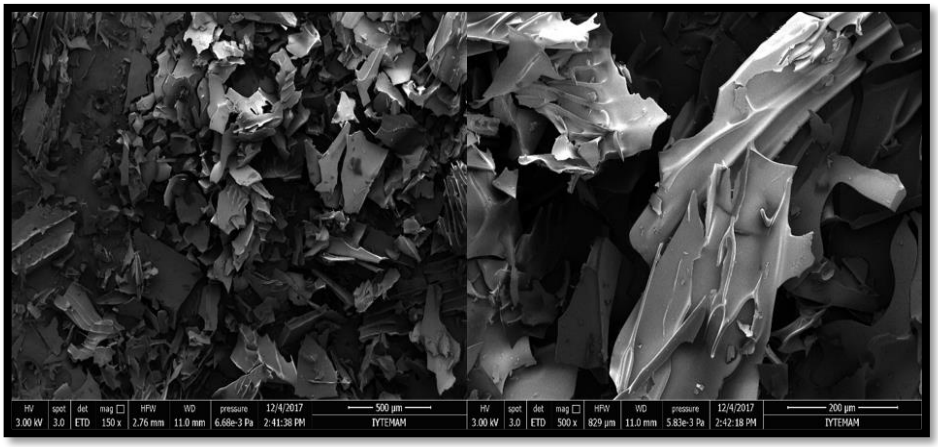

Figure 2. 3. SEM image of the Vancomycin hydrochloride

- **Amikacin**

Amikacin is a broad-spectrum antibiotic generally used for the treatment of joint infections, intraabdominal infections, urinary tract infections and sepsis. It has lower activity against Gram-positive bacteria except for *Staphylococcal* isolates. It blocks the

ribosomal subunit function of the bacteria and limits the protein synthesis. Clinical studies also showed that amikacin has a therapeutic effect on bone and joint infections (Schurman and Wheeler, 1978).

- **Tobramycin**

Tobramycin is an aminoglycosidic antibiotic firstly isolated from *Streptomyces tenebrarius* and used for the treatment of the Gram-negative bacterial infections, especially against Pseudomonas species. Tobramycin shows antimicrobial activity by binding ribosomal sides of the bacteria thus prevents protein transplantation that results in cell death. It is used for the treatment of respiratory infections, cystic fibrosis, osteomyelitis and soft tissue infections by combining with other antibiotics. It was reported that tobramycin loaded PMMA bone cement reduces the infection risk at total joint arthroplasty (Klekamp et al., 1999; Vrabec et al., 2016).

2.2. Controlled Drug Delivery Systems

The release of the drug can follow multiple roots such as absorption, distribution, and excretion to become pharmacologically available. Delivery of the active agent to target site by supporting desired concentration in desired time is called as controlled drug delivery system. The main concept of controlled drug releasing systems is to reach a therapeutic level at the defect side through the treatment period. Drug delivery systems are required to be compatible with processes in the body as well as with the drug to be delivered. In conventional drug release systems, drug concentration fluctuates in plasma according to multiple dosing to reach therapeutic level (Figure 2.4). Drug totally dissolves without the intention of an extended release profile (immediate release). However, controlled drug release systems can provide steady drug concentrations in plasma or local concentrations with the prolonged release by reducing toxicity and enhancing the bioavailability. In addition, there are also other advantages such as; better patient compliance, improvement of the intracellular penetration whilst minimizing the side effects and cost of drug usage (Kumari et al., 2010). The obstacles arising from low drug solubility, permeability, toxicity, drug degradation and bioavailability in conventional delivery methods may be easily addressed by designing a properly controlled drug delivery system with high therapeutic effect.

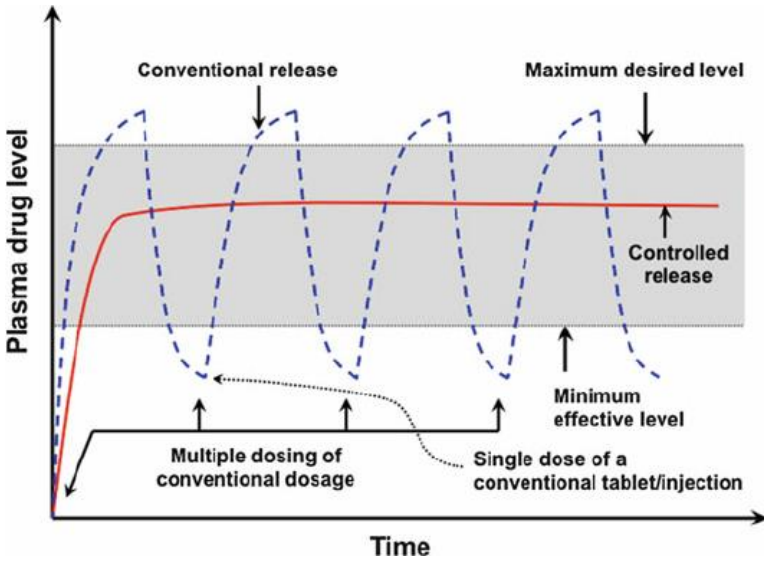

Figure 2. 4. Plasma drug concentration vs. time profile for conventional and controlled drug delivery systems (Source: Huynh and Lee, 2014)

2.2.1. Factors Affecting the Drug Release Behavior of the Material

There are many factors affecting the release profile of the active agent. Mainly, principal factors affecting the release profile of the active agent can be classified as the properties of the carrier, active agent, and the environmental conditions. The synergistic effect of these properties can result in varied release profiles. The main factors affecting the release profile can be listed as stated in Table 2.3.

Material characteristics are the key features that define the release profile of the active agent. The molecular weight, viscosity, polarity, solubility, and thermal properties of the carrier materials matrix affect the release mechanism. In literature, it is indicated that the higher molecular weight of polymer reduces the release rate of drugs (Zambaux et al., 1999). The carrier material and its degradation side-products should be compatible with the release environment and the active agent. It should successfully encapsulate the drug while resisting disintegration in release media during the therapeutic period. Surface charge and the hydrophobicity of the carrier are the criteria depending on the characteristics of the target site. In addition, the morphology and size also have an importance on release kinetics.

The drug release is also dependent on the drug properties and interactions between drug and carrier material. Physicochemical properties, pharmacokinetic and pharmacodynamic features of the drug designates the efficacy of the drug delivery.

Besides, polymer drug ratio is an important parameter in designing drug delivery device. Polymer concentration should be enough to incorporate the total amount of drug into the matrix or encapsulate it well. Higher drug to polymer ratio can be achieved with higher polymer concentration. Also, the functional groups of the molecule should allow conjugation of drug to the carrier polymer.

The drug needs to be stabilized to resist the environmental conditions of the target site. Studies proved that the temperature, pH, ionic composition of the release medium has a significant effect on drug release from polymeric microspheres (Hirota et al., 2016; Tomic et al., 2016).

Table 2. 3. Main factors affecting the drug release behavior
(Source: Langer and Chasin, 1990)

Material	**Drug**	**Environment**
Compatibility with the environment and drug	Position in carrier	pH
Extent and nature of crosslinking, denaturation, and polymerization	Molecular weight	Temperature
Size and density of the material	Pharmacokinetic, pharmacodynamic properties	Polarity
Presence of adjuvants	Polymorphic form	Presence of enzymes and ions

2.2.2. Particulate Drug Delivery Systems

Recently, most of the drug release studies have been focused on evaluating spherical/semi-spherical devices such as nanoparticles, liposomes, polymersomes, dendrimers and lipoproteins (Hadjitheodorou and Kalosakas, 2014). In particulate systems; natural and synthetic polymers, ferrofluids, quantum dots, silica-nanoparticles have been used as carrier materials for drug and gene delivery, imaging and *in vitro* diagnostics (De Jong and Borm, 2008). Among these materials, biodegradable polymeric particles are getting attendance in drug delivery applications. The side products of

biodegradable polymers can be metabolized or excreted without causing any toxic effect to the body. Biopolymeric particulate drug carrier materials can provide controlled/sustained release behavior as well as biocompatibility with tissue and cells. The drug dissolution rate can be adjusted with their large surface to volume ratio. Drugs and biomacromolecules can be delivered with the particulate systems by altering their sizes to micro-nano scales.

Drug dispersion at the target zone can be provided with nanoparticles by tailoring the material characteristics to obtain desired release profile. Nanoparticulate polymeric drug delivery systems can serve controlled release behavior according to the sensibility of polymer to temperature, pH, the presence of ions etc. The nanoparticle size distribution is a criterion to determine the interaction with the cell membrane and the penetration of the physiological drug barriers (Kumari et al., 2010). The surface charge of the particles determines the nanoparticle behavior such as clustering in the bloodstream or adhering/interacting with the cell membrane (Yin Win and Feng, 2005).

Biodegradable microspheres and microcapsules as drug delivery systems not also supply controlled release but also ensures biocompatibility with high encapsulation efficiency. These materials inhibit undesired effects such as high toxicity, low activity, compliance with pure pharmaceutical raw materials.

The active agent can be incorporated into nanosphere polymer matrix, bound to the surface or encapsulated inside polymer with a shell/core model (Figure 2.5). Depending on the method used in the formulation step, either reservoir model (nanocapsule) or monolithic (matrix system, nanosphere) drug carrier systems can be obtained. Nanocapsules carry the active acent in the core of the material while the carrier surrounds the shell. On the other hand, nanospheres are the matrix systems that includes the active agent as a dispersion in the matrix.

The drug loading into polymeric microspheres can be achieved by incorporating the drug into the polymeric solution at the production step or incubating the material in the drug solution allowing the nanoparticle to absorb the active agent. The efficiency of the route depends on the physicochemical properties of polymer and drug. Therefore, these systems should be carefully characterized in order to achieve desired release rate in desired time period.

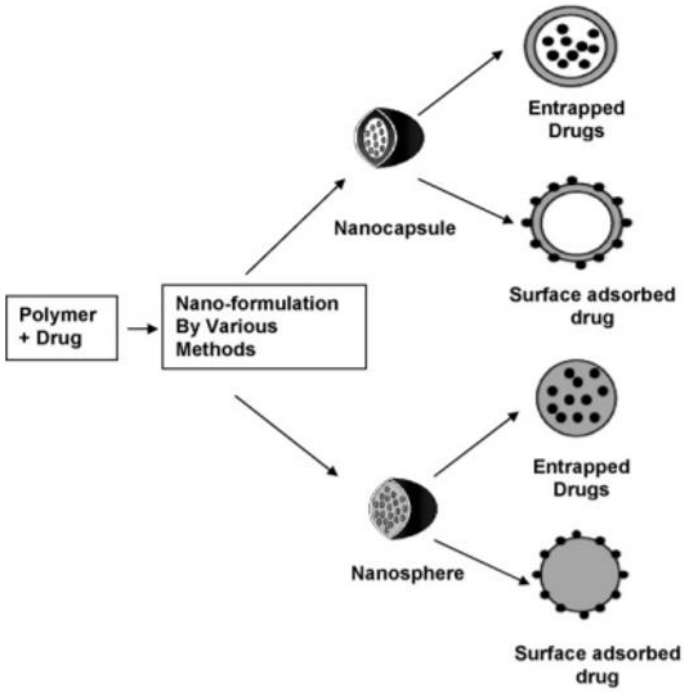

Figure 2. 5. Types of biodegradable drug releasing nanoparticles
(Source: Kumari et al., 2010)

2.2.3. Kinetic Modeling of Drug Release

It is important to understand the underlying mechanisms during the drug release process to predict the rate and avoid an excessive number of experiments. Kinetic models are utilized to explain the behavior of the drug that is dissolved in the media as a function of release time with empirical equations. The principal precept of this time-dependent phenomenon is firstly described by Noyes and Whitney equation (2.1.) as follows:

$$\frac{dM}{dt} = KS(C_s - C_t) \tag{2.1}$$

where M is the mass transfer dependent on time (t), S is the particle surface area that dissolution occurs, C_s is the solubility of the active agent at equilibrium and C_t is the concentration at time t. It was assumed that C_t that is lower than 15% of C_s has an insignificant effect on dissolution rate. According to the rule, the first-order reaction is occurring in the dissolution process.

The release rate can be predicted and optimized according to design parameters. A kinetic model that produces highest correlation coefficient (R^2) with the release profile can be selected. Besides, statistical methods like Analysis of Variance (ANOVA) and multivariate analysis of variance (MANOVA) can help to compare models and select the most suitable one. The rate can be predicted and optimized according to the design parameters.

According to mechanism-based classifications, new generation drug delivery systems (DDS) can be controlled by diffusion, dissolution, water penetration, chemical interactions or external stimulants:

Diffusion-controlled DDS: In diffusion-dominant systems, the drug is surrounded by a thin film (reservoir systems) or dissolved uniformly in a polymer matrix (monolithic systems). The release is defined by Fick's law. The release from monolithic and reservoir systems was represented in Figure 2.6. The drug concentration in non-constant drug source reservoir and monolithic system reduces with respect to time. In contrary, dissolution of drug aggregates at constant source reservoir and monolithic dispersions serves a sustained release for a prolonged time.

The diffusion-controlled DDS possess the advantage of ease of control by tailoring the physicochemical properties of the carrier. However, some carrier materials should be removed from the human body after complete drug release. The material selection is very important to obtain diffusion-controlled DDS.

Dissolution-controlled DDS: In some cases, the drug can be dispersed or entrapped in a material that dissolves slowly (Figure 2.7). Hence, the solubility and the toxicity of the degradation side products of the carrier are the key factors (Lee and Huynh, 2014). These systems do not need to be surgically removed. However, drawbacks such as the side-effects of drugs and difficulty to reach controlled release profile should be well evaluated.

Water penetration-controlled DDS: These systems can be divided into two groups including osmotically controlled and swelling controlled DDS. In osmotically controlled DDS, water penetration to membrane causes an osmotic pressure difference that controls the release. Drug solution or aggregates pass through the delivery orifices settled on the semipermeable membrane (Figure 2.8). Presence of ions, solubility, orifice sizes and permeability of the membrane are the main factors that regulate the drug release. These systems allow high drug loading but need to be surgically implanted in the body (Thakor et al., 2010). The swelling controlled systems include drug dispersion in the swellable network. The hydration of the glassy and hydrophilic matrix allows mobility for

dissolution and diffusion of the active agent through the carrier material. The physicochemical properties of the drug and the carrier material are the important factors to regulate the release rate.

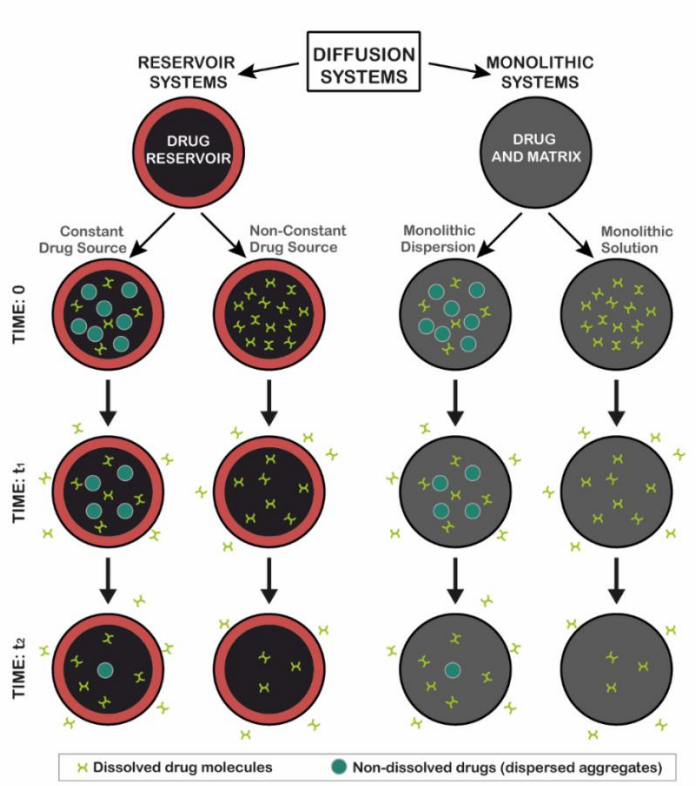

Figure 2. 6. Diffusion-controlled drug delivery: reservoir and monolithic systems

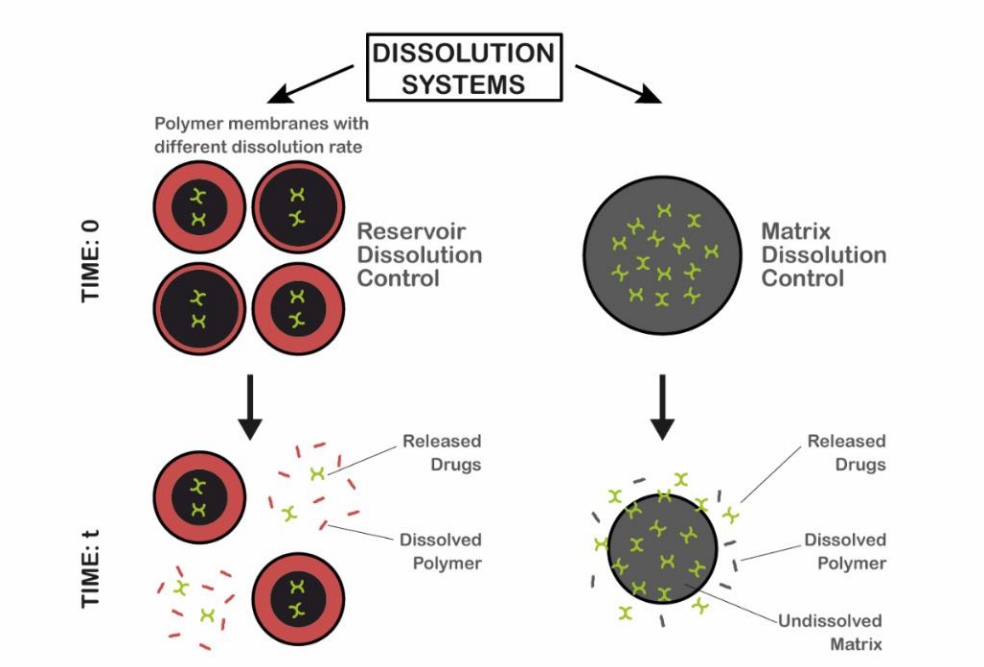

Figure 2. 7. Dissolution-controlled drug delivery: reservoir and matrix dissolution

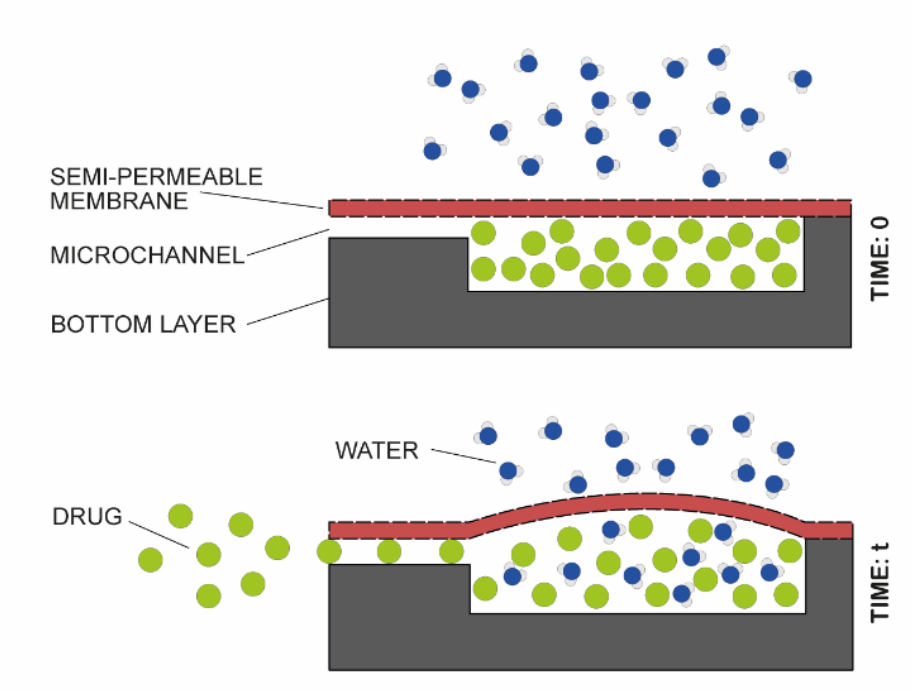

Figure 2. 8. Osmotically-controlled release system

Chemically-controlled DDS: The chemically controlled DDS includes polymer-drug conjugates and degrading/eroding monolithic devices. In polymer-drug conjugates, the active agent can be released to the media from a polymer with cleavage of the covalent or ionic bonds (Figure 2.9). Bioerodible or dissolvable polymer matrix affects the release rate with the change in device geometry. With such systems, it should be taken account that significant degradation/erosion cannot occur until drug release has been completed (Figure 2.10). These systems can allow the release of the high molecular weight drugs in a controlled manner and do not require surgical removal (Jantzen and Robinson, 2002).

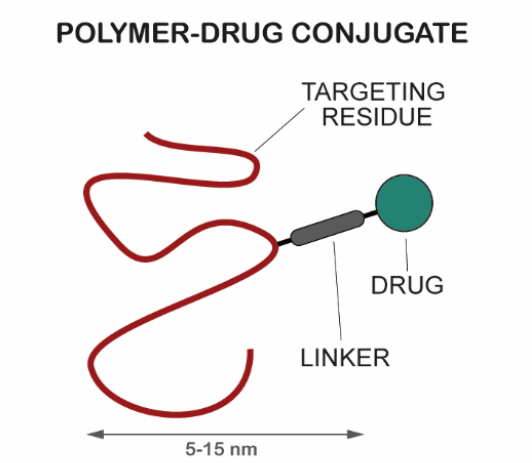

Figure 2. 9. Chemically-controlled DDS: Polymer-drug conjugates

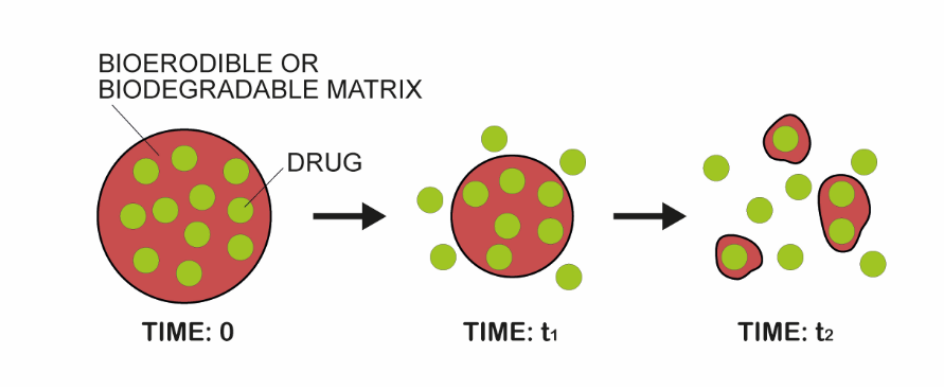

Figure 2. 10. Chemically-controlled DDS: Bioerodible/biodegradable matrix

External stimuli-responsive DDS: The "smart" polymers can supply drug release at the media by reversible conformational change under external stimulants such as pH, temperature, ultrasound, the presence of ions, electrical or mechanical signals (Figure 2.11). The control over the response to the applied stimulus is still challenging in clinical operations. These stimuli-responsive systems are promising materials as alternatives to existing delivery approaches.

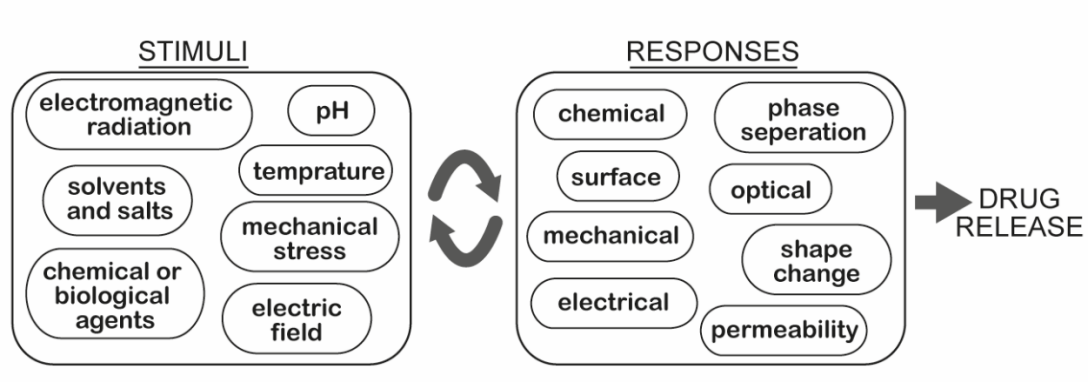

Figure 2. 11. External stimulants and responses for drug delivery
(Source: Schmaljohann, 2006)

In general, a controlled release system does not only depend on only one mechanism. However, in some cases, one mechanism becomes dominant to control the drug delivery that allows predicting the release rate with mathematical relations. The biopolymer based particulate systems generally follow three different mechanisms (Figure 2.12):

- Release from the particle surface: Drug dissolves to incubation media with an initial burst release. This type of mechanism is generally followed by a slower

rate according to the diffusion of material from the inner matrix of the micro/nanoparticle.

- The release caused by particle erosion
- Active agent diffusion through the swollen matrix: The polymer matrix swells with a water uptake and water penetrates the particle resulting in a dissolution and release of the active agent.

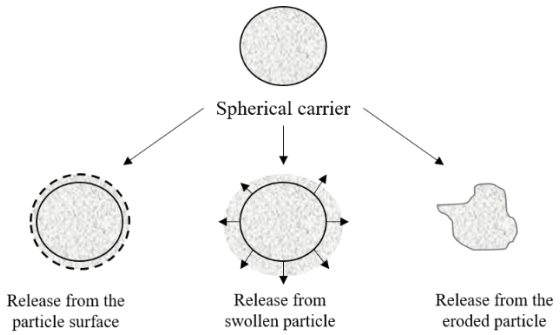

Figure 2. 12. Main mechanisms dominating the release profile

2.2.3.1. Diffusion-controlled Mechanism

Diffusion can be mainly described as the mass transfer of individual molecules by molecular motion and related to the concentration gradient (Shaikh et al., 2015). Even though erosion or dissolution is the dominant mechanism, dissolution commonly has a role in release profile.

Fick's law of diffusion describes the diffusion of the drug from polymeric matrix to release media. It indicates that the concentration gradient in steady-state conditions, diffusion flux (J), is proportional to the concentration gradient (dC_i/dx) and expressed with the equation 2.2 below;

$$J=-D\frac{dCi}{dx} \tag{2.2}$$

where D is the diffusivity constant.

The Fick's second law of diffusivity explains the concentration change with respect to time by assuming constant diffusivity constant and boundaries. It is generally represented as Equation 2.3.

$$\frac{\partial Ci}{\partial t} = -D\frac{\partial^2 Ci}{\partial x^2} \tag{2.3}$$

where C_i is drug concentration and D is diffusivity coefficient.

Several assumptions are done such as;

- One dimensional drug release
- Perfect sink conditions
- Negligible surface resistance
- Constant viscosity and the temperature
- Constant diffusion coefficient
- No chemical reactions

It is known that the release profile depends on the matrix architecture. Therefore, Crank rearranged the equation for spherical matrix systems as follows (Crank, 1975):

$$\frac{M_t}{M_0} = 1 - \frac{6}{\pi^2}\sum_{n=1}^{\infty}\frac{1}{n^2}\exp\left(-\frac{Dn^2\pi^2 t}{R^2}\right) \tag{2.4}$$

where M_t is the cumulative drug release at time t, M_0 is the initial drug loading, D is the diffusion coefficient of drug and R is the radius of the sphere. The summation term goes to zero in short-time release systems and is negligible. Therefore, the equation can be simplified for the short-term release if the M_t/M_0 value is smaller than 0.3,

$$\frac{M_t}{M_0} = \frac{6}{\sqrt{\pi}}\sqrt{\frac{Dt}{r^2}} \tag{2.5}$$

In the long-term region, where the M_t/M_0 is higher than 0.3, the equation is rearranged as:

$$\frac{M_t}{M_0} = 1 - \frac{6}{\pi^2}\exp\left(-\frac{Dn^2\pi^2 t}{R^2}\right) \tag{2.6}$$

Several empirical/semi-empirical models are developed to predict the drug release mechanism. These models can give an indication of drug release mechanism under

specific conditions. Mathematical models that define the dominant mechanism as diffusion can be listed as follows:

Zero-order kinetic model: This model is used for systems where drug release is not dependent on drug concentration. The ideal drug release system can be expressed by zero-order release kinetics, where the release rate remains constant over time and independent of the drug concentration in the system. It can be described as:

$$M_t = M_0 + K_0 t \tag{2.7}$$

where M is the released drug amount at a certain time, t; M_o is the initial amount of drug (mostly equals to 0); K_o: zero-order rate constant. Cumulative percentage of drug release versus time is plotted to study the zero-order release model.

First order kinetic model: According to the first order release model, the drug release is dependent on concentration. It was assumed that the surface area remains constant during the dissolution. The release is described as:

$$M_t = M_0 e^{-K_1 t} \tag{2.8}$$

$$logM_t = logM_0 - \frac{K_1 t}{2.303} \tag{2.9}$$

The logarithmic (Cumulative percentage drug remained) versus time graph can be used to find slope (k/2.303) value.

Higuchi model: Higuchi model is the most used release model in polymer matrix release systems and it is applicable for various architectures. There are several assumptions as follows (Peppas and Narasimhan, 2014):

- Pseudo-steady approach (Initial drug concentration is higher than the solubility of the drug).
- Edges are negligible (Uni-dimensional diffusion)
- Drug particles are smaller than the thickness of the carrier.
- Dissolution and the swelling behavior of the polymer matrix are neglected.

The simplified form of the Higuchi model is represented as follows:

$$\frac{M_t}{M_0} = K_H t^{1/2} \tag{2.10}$$

where K_H is the Higuchi dissolution constant. The slope of the cumulative percentage of drug release versus square-root of time plot gives the K_H value.

Baker-Lonsdale model: It is a model derived from Higuchi model originally and used to describe the release from the spherical matrix. It is represented by the following equation:

$$\frac{3}{2}\left[1-\left(1-\frac{M_t}{M_\infty}\right)^{2/3}\right]-\frac{M_t}{M_\infty}=\frac{3D_mC_{ms}}{r_0^2C_0}t \tag{2.11}$$

where M_t is the released drug at time t, M_∞ is the drug released at the infinite time, D_m is the diffusion coefficient, C_{ms} is the solubility of the drug in the matrix and C_0 is the initial concentration. The equation is rearranged by assuming the initial porosity of the matrix is negligible and defined as:

$$\frac{3}{2}\left[1-\left(1-\frac{M_t}{M_\infty}\right)^{2/3}\right]-\frac{M_t}{M_\infty}=kt \tag{2.12}$$

where the k corresponds the release constant.

Korsmeyer-Peppas model (the power law): It is a semi-empirical model which assumes that the diffusion is the main mechanism that controls the release profile from the polymeric systems. In general, this model is applied by fitting the first 60% of the cumulative release in the model.

$$\frac{\mathrm{M_t}}{\mathrm{M_\infty}}=Kt^n \tag{2.13}$$

where n is the release constant that defines the mechanism and K is the release constant. M_t and M_∞ are the released drug amount at time t and at equilibrium. (Gierszewska and Ostrowska-Czubenko, 2016).

The slope of the graph $\log(M_t/M_\infty)$ versus log time gives n, that indicates the release mechanism for thin film, spherical and cylindrical architectures. For spherical coordinates; $n \leq 0.45$ corresponds to a Fickian diffusion, $0.43<n<0.85$ indicates the non-Fickian and $n \geq 0.85$ reveals Case-II transport as seen in Table 2.4. Molecular diffusion of the active agent is controlled by a chemical potential gradient in Fickian diffusional release (Singhvi and Singh, 2011). The Korsmeyer-Peppas model is not only applicable

to the Fickian diffusion-controlled system. In anomalous diffusion dominant model, there is more than one mechanism that conducts the release rate. Case-2 relaxation is the polymer swelling, disentanglement, chain relaxation, followed by erosion of the matrix.

Table 2. 4. Release exponent ranges to determine the mechanism (The power law) (Source: Siepmann, 2008)

Release Exponent (n)			**Release mechanism**
Thin film	**Sphere**	**Cylinder**	
n ≤ 0.5	n ≤ 0.45	n ≤ 0.43	Fickian diffusion
0.5<n<0.1	0.45<n<0.89	0.43<n<0.85	Anomalous diffusion or non-Fickian diffusion
n ≥1	n ≥0.89	n ≥0.85	Case-II transport

Weibull model: Weibull model is applicable for dissolution of the pharmaceutical dosage form and it is expressed as drug accumulation:

$$\frac{M_t}{M_\infty} = 1 - e^{-\frac{(t-T)^b}{a}} \tag{2.14}$$

where M_t and M_∞ are the cumulative releases at the specified and infinite time, T is the lag time and a is the time scale parameter. The term "b" describes the dissolution curve shape. Exponential profile when the b value is equal to 1 can be simplified by taking k as 1/a and shown as:

$$\frac{M_t}{M_\infty} = 1 - e^{-k(t-T)} \tag{2.15}$$

2.2.3.2. Erosion Controlled Mechanism

Hixon-Crowell model: Model is evaluated by Hixon and Crowell for materials that do not keep its surface and diameter during the release period (Hixson and Crowell, 1931).

Hixson-Crowell model assumes that the erosion controls the release profile and described in Eq. 2.16.

$$M_0^{\frac{1}{3}} - M_t^{\frac{1}{3}} = K_{hc}t \tag{2.16}$$

where K_{HC} is the constant considering surface-volume relations during the erosion. The cubic root of the remaining fraction of drug versus time graph will be linear if the release profile obeys the Hixson-Crowell model.

Hopfenberg model: The model is used for the release from eroding the surface of polymers by maintaining the initial surface area. It displays the release depending on heterogeneous erosion as:

$$\frac{M_t}{M_\infty} = 1 - \left[1 - \frac{k_0 t}{C_0 a_0}\right]^n \quad (2.17)$$

where k_0 is indicating the erosion rate constant, C_0 is the initial drug concentration, a_0 is the radius of the spherical matrix and n is the shape factor. The Hopfenberg model is generally applied for oil-carrier spheres (Sibanda et al., 2004).

Kopcha Model: The Kopcha model can be used to quantify the relative contributions of diffusion and erosion to drug release.

$$M=A\sqrt{t+Bt} \quad (2.18)$$

where, M: Cumulative released drug at a time, t; A: Diffusional constant; B: Erosion constant. According to the equation, the ratio of diffusion to erosion eradicates the controlling mechanism. If diffusion/erosion ratio A/B=1, the release mechanism is equally controlled by both diffusion and erosion mechanism. If A/B>1, diffusion prevails and if A/B<1 erosion predominates. To determine the coefficients, A and B, the data can be drawn as M/t versus $1/\sqrt{t}$ graph. Slope gives A value and the intercept gives B value (Chevalier et al., 2009).

2.2.3.3. Swelling Controlled Mechanism

Sequential layer model: The model is generally about the swelling-controlled release from hydrophilic tablets by assuming the swelling occurs layer by layer. In addition, hydrogels are the main materials that swelling dominates the release mechanism by ensuring material stability while uptaking the biological fluid.

2.3. Chitosan-based Materials in Drug Delivery Applications

2.3.1. Sources, Physical and Biological Properties of Chitosan

Chitin is the most abundant polymer after cellulose in nature. It is the principal component of the crustacean exoskeleton. It has many favored physical, chemical and biological properties that result with peculiarities over other biopolymers (Table 2.5). It can also be found at the cell walls of some fungi and bacteria species. The usage of chitin itself is limited because of its poor solubility, therefore, it has to be chemically modified. The partial deacetylation of the N-acetyl-2-amino-2-deoxy-D-glucose repeating units of chitin results with the chitosan formation. The deacetylation of chitin to chitosan is illustrated in Figure 2.13. Chitosan is more reactive than chitin and can be tailored to a variety of morphology. The ratio of D-glucosamine to the summation of D-glucosamine and N-acetyl D-glucosamine structural units is the deacetylation degree (DD%) of the chitosan that gives information about the number of amino groups along the chains.

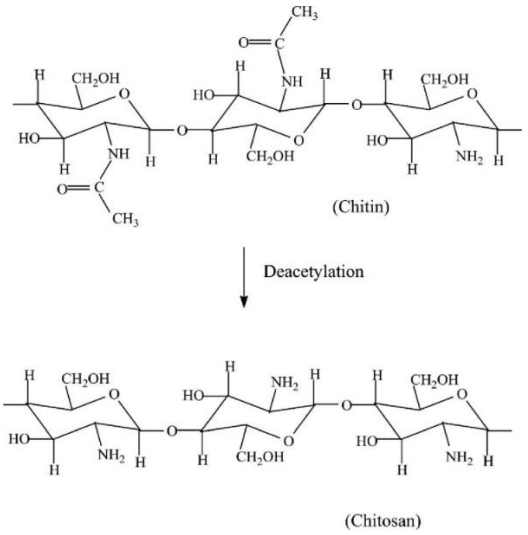

Figure 2. 13. Deacetylation of chitin to form chitosan
(Source: Gomathysankar et al., 2014)

Deacetylation degree of chitosan is a crucial factor for physicochemical and biological characteristics of chitosan. It is a semi-crystalline polymer and the crystallinity degree is related to the deacetylation degree (Ehrlich et al., 2006). The maximum crystallinity is achieved in both chitin and 100% deacetylated chitosan. Since chitosan

has a crystalline structure, it is insoluble in solutions that have a pH value of more than 7. The dilute acidic solutions with a pH below 5 can pave the way for protonation of free amino groups of chitosan and fully dissolves it. Moreover, its molecular weight, viscosity, and crystallinity give information about the chitosan characteristics. Chitosan exhibits many remarkable features with its structural properties. It can form polyelectrolyte complexes with a variety of anionic species. The complex formation can be achieved with natural polyanions such as alginate, Na-carboxymethylcellulose and glycosamine glycans.

Table 2. 5. Physical, chemical and biological properties of chitosan

Physical and Chemical Properties	**Biological Properties**
Polycationic nature	Biocompatible
Semi-crystalline	Non-toxic
Free amine groups (ready for crosslinking)	Biodegradable
Hydrophilic surface	Hemostatic
Ability to chelate transition metal ions	Antibacterial, Fungistatic, Antitumoral

2.3.2. Chitosan in Biomedical Applications

Chitosan is the only positively charged natural polysaccharide that leads many peculiar advantages in biomedical applications. The positive charges on the backbone give chitosan hemostatic property. The cationic nature of the chitosan promotes the cell interaction with the material and supports the rate of internalization. The negatively charged parts of the cell membrane can easily interact with chitosan (Kumari et al., 2010; Croisier and Jérôme, 2013). It is widely preferred polymer in biomedical applications with its low toxicity and hydrophilic property.

Chitosan associates with anions of the bacterial cell wall and hinders the mass transport that induces the death. Hence, it is preferred in biomedical applications with its antibacterial property (Di Martino et al., 2005). In addition, chitosan can be sterilized by various methods such as radiation, heating, steam and chemical methods (Agnihotri et al., 2004).

N-acetyl-β-D-glucosamine, the degradation side product of chitosan, stimulates wound healing by stimulating fibroblast proliferation. Also, chitosan-based wound dressings help exudate absorption and oxygen transfer to the defect region (Pillai et al., 2009).

The chitosan-based structures can be processed in diverse morphologies such as film, micro/nanoparticle, sponge or tablet according to the end purpose. Chitosan is employed in drug delivery systems, wound healing applications, scaffolds for tissue regeneration, injectable systems, tables, surgical dressing etc.

The usage of chitosan in wound dressing applications was approved by Food and Drug Administration (FDA) (Wedmore et al., 2006). Researchers have examined the chitosan-based materials in different forms such as bone substitutes/fillers, implant coatings or delivery agents. A literature survey based on chitosan based biomaterials was tabulated in Table 2.6.

Chitosan is the most common biopolymer that is used in bone tissue engineering applications. The remarkable point of the chitosan is its similarity to glycosaminoglycan (GAG) groups of the extracellular matrix (ECM). It is preferred as scaffolding material since the degradation side-products of chitosan are harmless oligosaccharides that can be completely absorbed by the human body (Dash et al., 2011).

In literature, it was found that chitosan promotes the osteoblast growth and mineral deposition (Kim et al., 2008). Moreover, chitosan-based materials showed enhancement in blood coagulation and prevented the abnormal fibroblastic reactivities (Cha and Pitt, 1988).

Chitosan powder can be used to develop the characteristics of conventional bone cement. Kim et al. (2004) fabricated a chitosan and hydroxyapatite powder doped polymethylmethacrylate (PMMA) bone cement. According to the *in vitro* studies, they obtained better results regarding osteoconductivity and biocompatibility when compared to pure PMMA cement.

Table 2. 6. Chitosan-based biomaterials in bone tissue engineering applications

Form	**Purpose**	**Reference**
Scaffold	Scaffold for bone regeneration, drug/growth factor release	Jeong Park et al., 2000
Fiber	Bone regeneration	Zhang et al., 2008

(Cont. on next page)

Table 2.6. (cont.)

Film	Implant covering, protein delivery	Abarrategi et al., 2008
Bar	Bone infection treatment	Aimin et al., 1999
Hydrogel	*In situ* forming scaffold	Niranjan et al., 2013
Micro/Nanoparticle	Drug delivery; Implant coating	Mitra et al., 2001; Wang et al., 2004
Micro/Nanosphere	Drug delivery; bone filling material	Sunny et al., 2002; Arya et al., 2009
Film	Implant covering, protein delivery	Abarrategi et al., 2008

2.3.2.1. Chitosan Micro/Nanospheres in Bone Tissue Engineering Applications

Chitosan has many advantages particularly in the development of nanoparticle/sphere. These may be generally classified as:

- Ability to reduce the morphology in nano-scales.
- Very low toxicity. The study with laboratory mice confirmed that LD_{50} of chitosan is 16 g/kg body weight, which is close to sugar or salt (Burg et al., 2000).
- Easy to sterilize for clinical applications.
- Contains free amine groups available for crosslinking.
- Solubility in aqueous acidic media, no need to use hazardous organic solvent.

Among different system morphologies, the chitosan nanoparticulate systems, having optimized physicochemical and biological properties, have been referred as promising materials for replacing conventional methods for drug delivery applications. Active agents, proteins, enzymes or drugs can be absorbed or conjugated onto the particle surface, encapsulated or dissolved in particle matrix to form drug releasing nanoparticles. Noticeably, the undesired effects can be eliminated by the tailored material properties.

Chitosan-based spherical carriers can be physically characterized regarding their morphology, size and size distribution, surface charge, entrapment/encapsulation efficiency, swelling and degradation behavior and thermal properties.

Numerous studies have focused on controlled delivery with chitosan-based micro/nanospheres. The *in vivo* study of Cho et al. (2004) evidenced that human growth hormone encapsulated chitosan microspheres were effective in early bone consolidation in distraction osteogenesis. Gumusderelioglu et al. (2015) fabricated boron doped chitosan nanoparticles as an osteoinductive agent to be attached into chitosan scaffolds and observed the supporting effect of controlled boron release on proliferation and differentiation of preosteoblastic cells. Zhou et al. (2017) prepared bone morphogenetic protein 2 (BMP-2) loaded chitosan and O-carboxymethyl chitosan microspheres by emulsification cross-linking method using vanillin as a cross-linker. Good biocompatibility and release profiles suggested that both groups have a potential for bone regeneration. Bastami et al. (2017) developed gelatin/β-tricalcium-phosphate composite scaffolds containing chitosan-based nanoparticles for controlled release of bone morphogenetic protein-2 (BMP2) for reconstruction of critical-sized bone defects. It was indicated that chitosan nanoparticles successfully encapsulated BMP2 with a loading efficiency up to 80%.

Chitosan in particulate morphology was mostly selected as a drug-carrier system in bone tissue engineering applications. The drug loading to the particles can be achieved by incorporating the drug in particle-forming solution or adsorption of the drug after the particle fabrication. However, maximum efficiency is achieved by drug incorporation into the matrix during material formation.

To eradicate the bone infection, many studies have been performed by incorporating the drugs into these chitosan-based materials and listed in Table 2.7. These materials have been used to eradicate the bone tissue infection at post transplantation period.

Table 2. 7. Chitosan-based DDS for bone infection treatment

Components	**Drug**	**Method**	**References**
Chitosan	Gentamicin	Crosslinking-Solvent evaporation	Aimin et al., 1999
Chitosan	Vancomycin	Spray Drying	Cevher et al., 2006
Chitosan/Borate glass composite	Teicoplanin	Quenching-Crushing-Sieving	Jia et al., 2010
Chitosan	Ciprofloxacin	Spray Drying	Orhan, 2006

(Cont. on next page)

Table 2.7 (cont.)

Hydroxyapatite/ Chitosan Composite	Fluorescein	Ultrasound-assisted sequential precipitation	Uskoković and Desai, 2014
Chitosan/Nano-hydroxyapatite/ Ethylcellulose	Gentamicin	Complex coacervation and freeze drying	Shi et al., 2010

The biodegradable microspheres as an example to particulate carriers can supply the transport of the antibiotics to the bacteria-infected intracellular sites with a sustained manner, therefore decrease the drug toxicity (Blanco-Príeto et al., 2002). Since chitosan itself has antibacterial and non-toxic properties with efficient physicochemical characteristics, it is getting attention in controlled delivery systems in recent studies.

2.3.3. Chitosan Micro/Nanosphere Production Techniques

Chitosan-based drug delivery systems utilizing different methods have been developed for the release of various kinds of drugs. The drug delivery system can be fabricated in various forms such as tablet, sphere/particle, film, gel or capsules. Among these systems, the micro/nanospheres have many advantages by improving the entrapment efficiency, surface area, non-toxicity.

Chitosan as a nanoparticulate form was firstly prepared for intravenous anticancer drug delivery with emulsification method. Furthermore, several methods have been evaluated to prepare chitosan micro/nanoparticulate systems (Ohya et al., 1993). The method selection is dependent on desired particle size, thermal/chemical stability of the final product, the nature of the active molecules and the toxicity of the material and its degradation side-products (Agnihotri et al., 2004).

The micro/nanospheres can be obtained with chemical, physicochemical or physical processes. Emulsion crosslinking, coacervation, ionic gelation, spray drying and electrospraying are the most commonly used production methods for micro/nanosphere production. These techniques have some superiorities and disfavor when compared to each other (Table 2.8). Therefore, the fabrication method should be well evaluated by considering each point.

Table 2. 8. Comparison of chitosan micro/nanospheres production techniques

Method	Advantages	Disadvantages
Emulsion cross-linking	Highly stabilized spheres	Exposure to chemicals, impurities Loss of bioactivity
Coacervation and precipitation	High encapsulation efficiency of unstable agents	Deviation from sphericity High cost
Ionic gelation	Single stage and simple method	Low product yield Deviation from sphericity
Spray drying	- Rapid drying - Continuous operation	Degeneration of temperature sensitive agents
Electrospraying	- One step technique - High yield	Disability of size control

- **Emulsion cross-linking**

Emulsion method is one of the most popular techniques of nanoparticle fabrication. The main purpose is to take the advantage of the functionality of amine groups to crosslink with a cross-linking agent. The chitosan solution (dispersed phase) is contacted with a non-aqueous emulsifier and form water-in-oil (w/o) emulsion, followed by emulsification and drying to remove solvents. Ionotropic gelation can be applied in between steps to improve the stability. The emulsion cross-linking of chitosan particulate systems is schematically represented in Figure 2.14.

The nanospheres formed with this technique has improved stability. However, the emulsifiers can cause a diminution in bioactivity. Besides, the incomplete removal of cross-linking agent can cause impurities.

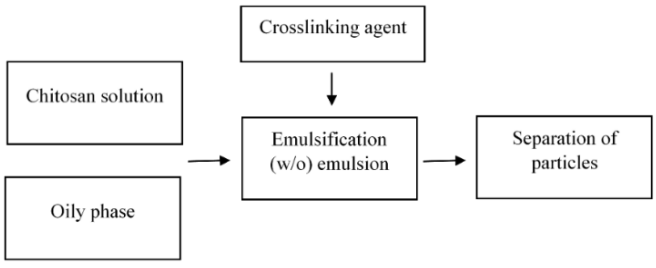

Figure 2. 14. Emulsion cross-linking method

- **Coacervation/precipitation**

Coacervation, followed by precipitation can be simply defined as polymer solubilization and adding an insolubilizing solute to precipitate polymer particles (Figure 2.15). Chitosan particulates can be fabricated with this method by taking advantage of its insolubility in alkaline pH. The particles formed in the insolubilizing agent can be centrifuged, washed and filtrated.

Complex coacervation is the usage of another oppositely charged polymer. The parameters of the fabrication method can be listed as pH, ionic strength, molecular weight, temperature and the concentration of the polymeric solution.

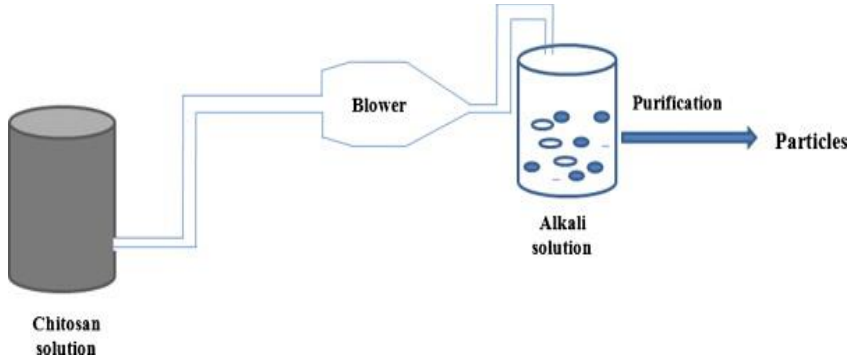

Figure 2. 15. Coacervation and precipitation method (Source: Sinha et al., 2004)

- **Spray drying**

Spray drying is a rapid, one-step technique to obtain micro/nanoparticles by atomizing the solution in a stream of hot air. Atomized particles are directly exposed to solvent evaporation that leads to the formation of freely flowing particles.

The desired particle morphology and drug loading efficiency can be obtained by tailoring the process parameters of spray drying such as nozzle size, pressure, flow rate and operating temperature. The schematic representation of spray drying method to form chitosan particles is described in Figure 2.16.

- **Ionic gelation**

The ionic cross-linking of chitosan can be simply obtained with its counterions. The ionic gelation method is simply described in Figure 2.17. The counterion can be selected by considering its ionic strength, molecular weight or hydrophobicity. The cationic chitosan solution is fed into the counterion solution dropwise and stirred continuously. The complex products are filtered, washed and dried. The technique is preferable according to the abstain from the toxicity of organic solvents.

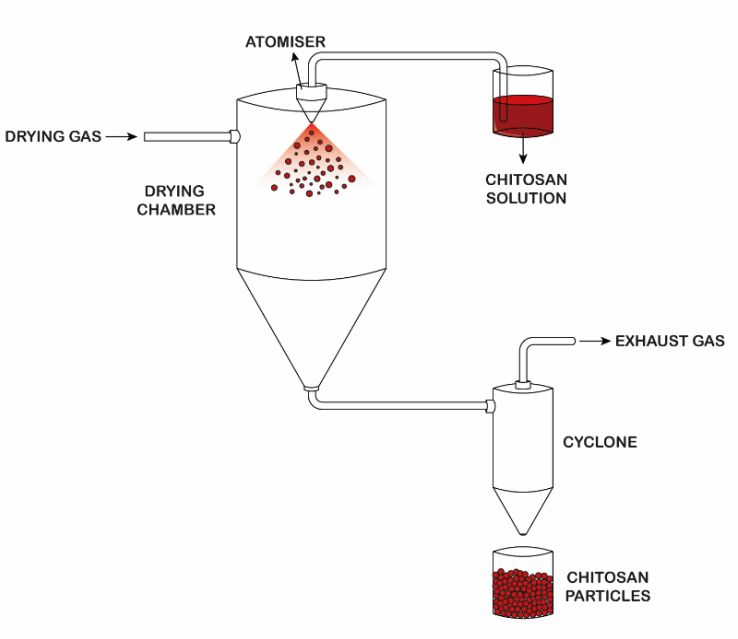

Figure 2. 16. Spray drying method

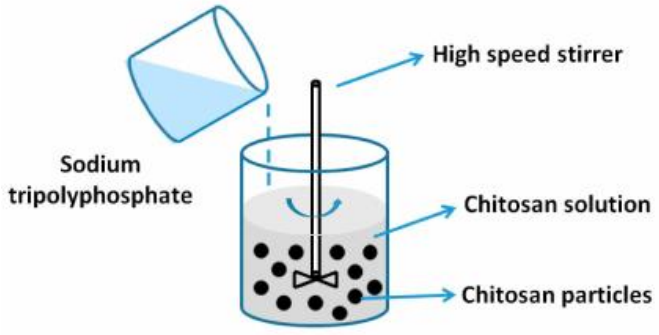

Figure 2. 17. Ionic gelation method

- **Electrospraying**

Conventional methods include major drawbacks such as lower loading efficacy, larger particle sizes, degradation of drugs according to the organic solvent usage. On the other hand, electrospraying is a one-step technique that can be applied in several applications such as microencapsulation, fine powder production, thin film deposition and controlled delivery. The schematic diagram of the simple vertical electrospraying unit is illustrated in Figure 2.18.

In electrospraying process, the polymeric solution is fed to a system with a controlled rate and subjected to an electric field which leads to elongation of the meniscus to form a jet. When the electrostatic forces overcome the surface tension of the droplet, the particles are atomized on the collector surface with radial dispersion. Applied shear

stress with high electric potential makes the liquid more unstable and causes droplets to repel each other.

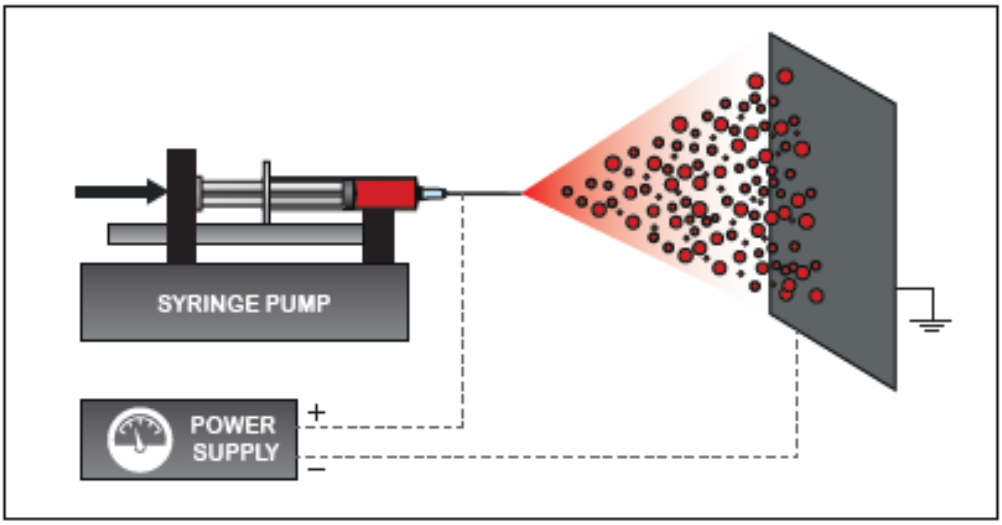

Figure 2. 18. Schematic diagram of the electrospraying unit

The dispersion of liquid into micro/nano-sized droplets occurs when it cannot resist electrical charge more. The solution droplets are forced to evaporate, split up and deposited on a collector surface. Droplets rapidly sprayed on the collector surface since collector is subjected to the opposite charge of the needle. Particle coagulation is prohibited and dispersion is supported according to high voltage supplement to the system. These electrospraying steps are illustrated in Figure 2.19.

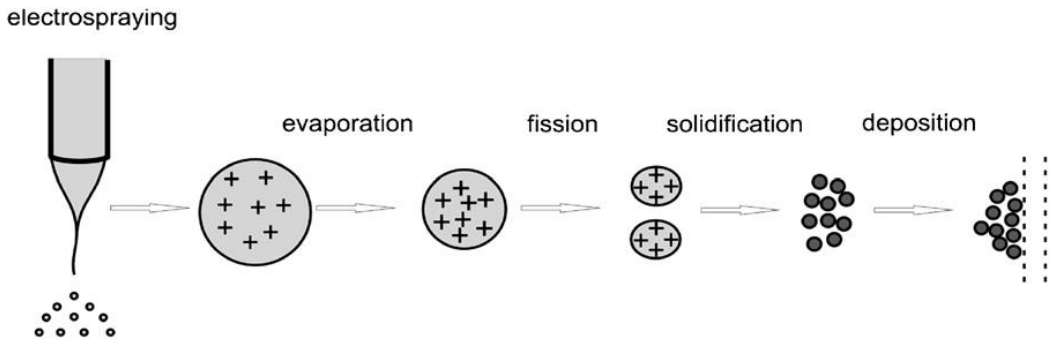

Figure 2. 19. Micro- and nanoparticle production steps via electrospraying (Source: Jaworek and Sobczyk, 2008)

The instability of the excessively charged droplet was firstly described by Rayleigh in 1882 (Salata, 2005). When the repulsive forces between the charges on the droplet surface overcome surface tension (σ), charged droplets tend to erupt and form

smaller particles. The minimum limit to exceed surface tension is called as Rayleigh limit. The ratio of these forces is called as fissility (X) and represented in Eq. 2.19.:

$$X = \frac{q^2}{64\pi^2\sigma\varepsilon_o R^3} \tag{2.19}$$

where q is surface charge density, σ is surface tension of the liquid, ε_o is permittivity of the free space and R is the radius.

Rayleigh demonstrated that the fissility should be smaller than 1. This fact is well explained by Konermann (2009); the spherical shape has the lowest surface area, leading to lowest surface energy for a given volume. The shape instability increases and the morphology is more like ellipsoids when the X value becomes closer to 1.

Several relations have been evaluated to predict the electrosprayed particle size. The radius of the electrosprayed particles (R) is evaluated as a function of liquid density, liquid flowrate (V_F) and the surface tension (γ) (Salata, 2005).

$$R \propto (\rho V_F^2 \gamma)^{1/3} \tag{2.20}$$

The flow and the deformation of the induced droplet is called as Taylor cone-jet. In this mode, the surface stresses act against electrodynamic stress, the pressure differential across the jet-air interface, liquid dynamic viscosity and inertia stresses. In order to predict the diameter of the particles (d) in cone-jet mode, following equation is derived as (Jaworek and Sobczyk, 2008):

$$d = \alpha \frac{Q^{aQ}\varepsilon_0^{a\varepsilon}\rho_1^{a\rho}}{\sigma_1^{a\sigma}\gamma_1^{a\gamma}} \tag{2.21}$$

where the α is a constant depending on the liquid permittivity, Q: volumetric flowrate, ε: permittivity of the free space, ρ: solution density, σ: solution surface tension and γ is the solution bulk conductivity.

As it is indicated, properties of the solution and environment, as well as processing parameters should be well optimized to obtain monodispersed particles. The parameters affecting the efficacy of the system is tabulated in Table 2.9. Although electrospraying is a one-step technique, these factors should be tailored to achieve high loading capacity

and minimum active agent usage in drug delivery applications. Furthermore, fabricated spheres should be characterized regarding their physicochemical, biological properties and *in vitro* release profiles.

Table 2. 9. Electrospraying parameters

Material Parameters	**Processing Parameters**	**Ambient Parameters**
Solution properties (Molecular weight, viscosity, concentration, the electric conductivity of the solution)	Size of the capillary	Humidity
Solvent properties (Surface tension, permittivity, the vapor pressure of the solvent)	Flowrate	Temperature
Organic/aqueous ratio	Distance	Pressure
Swelling and degradation behavior	Voltage	

The polymer concentration strongly affects the morphology of the product. In this thesis study, 90% v/v acetic acid solution is selected as a solvent and the chitosan concentration was kept constant (2% w/v) according to the previous literature findings (Arya et al., 2009). During the process, acetic acid ionizes into acetate and hydrogen ions that increases the electric force applied to the jet. Therefore, the adequate concentration must be applied to provide required conditions.

The size of the droplets can be controlled by adjusting voltage, working distance, solution flow rate and nozzle diameter. In a study, it was reported that highly conductive liquids should be electrosprayed with smaller capillaries for stable jet formation (Hayati et al., 1987). In addition, the voltage change has a vital role since it is the driving force of the electrospraying. It is expected that lower voltage causes the formation of large beads whereas high voltage application results with the formation of narrowly distributed smaller spheres and fibers (Hayati et al., 1987; Doshi and Reneker, 1993).

The droplets tend to split and their sizes are reduced as the distance between syringe and collector increases. However, significant particle loss to the surroundings may occur if the distance is very large. In contrary, the distance below optimal range may

lead to electric discharges. By changing the solution and the production parameters, electrospinning micro/nanofiber formation can be achieved at the collector that is called as electrospinning (Figure 2.20).

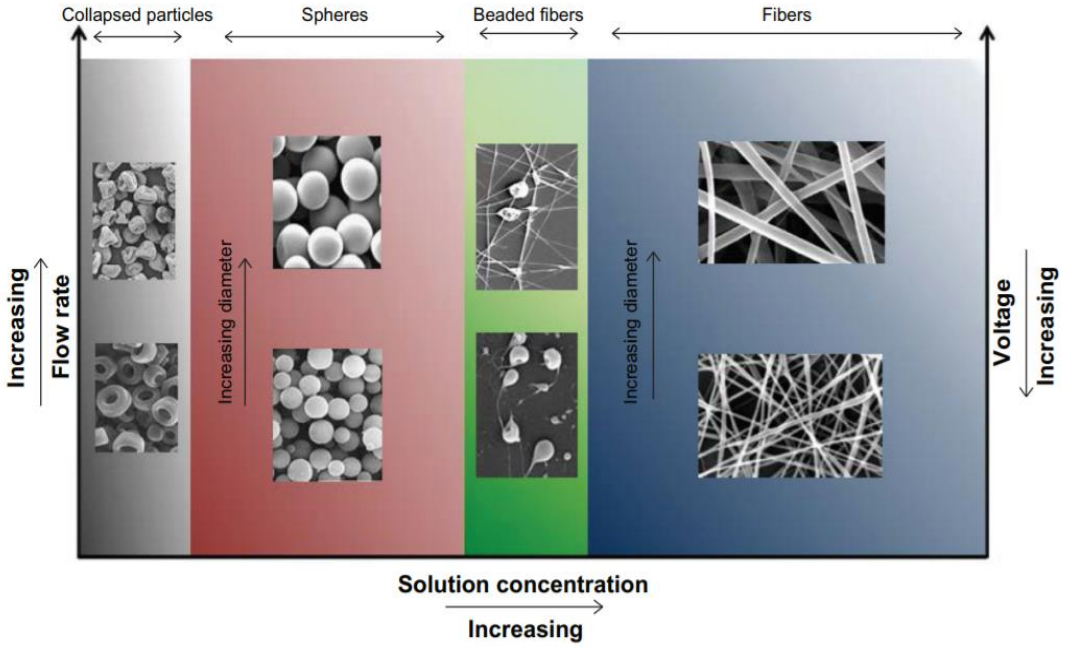

Figure 2. 20. Effect of concentration, flow rate and the voltage on electrospraying parameters (Source: Zamani et al., 2013)

Electrospraying is widely selected technique to produce spherically shaped drug carriers for controlled release applications. It allows encapsulation or incorporation of various active agents such as hydrophobic/hydrophilic drugs and phytochemical extracts. It was reported that electrospray method is applicable for synthetic polymers, natural polymers and polymer composites (Jayaraman et al., 2015). According to the literature survey given in Table 2.10, electrospraying technique provides encapsulation of varied drugs with high loading efficiency. Therefore, in this thesis, electrospraying method was selected for chitosan-based nanosphere formation according to its favorable properties and promising results in drug delivery operations with natural polymer-based materials. The processing parameters (voltage, distance and flowrate) were optimized to achieve desired morphology and uniform size distribution. The spherical and nanoscale particles were aimed to fabricate in order to ensure controlled drug release with homogeneous morphological properties. The main effects and their two-way interactions were determined according to achieve optimum nanoparticle morphology.

Table 2. 10. Literature survey on electrosprayed particles for controlled drug release

Polymer	Drug	Purpose	Major outcomes	Reference
PLGA	Simvastatin	Bone regeneration	- Encapsulation efficiency: 90% - The continuous release was supplied for 3 weeks.	Nath et al., 2013
PLGA	Metronidazole	Periodontal regeneration	- The sustained release was achieved for 41 days. - The release profile was fit to Korsmeyer-Peppas model.	Prabhakaran et al., 2015
PLGA	Budesonide and EGCG	Lung cancer treatment/Antitumor drug release	- Lipophilic and hydrophilic drugs were successfully encapsulated with electrospraying method. - Sustained release with prolonged time was achieved with electrospraying when compared to emulsion method.	Lee et al., 2010
Polycaprolactone	Budesonide	Inflammatory disorder treatment	- Encapsulation efficiency: 75% - Biphasic release pattern was observed due to drug dissolution followed by polymer degradation.	Midhun et al., 2011
Chitosan	Doxorubicin	Cancer therapy	- Encapsulation efficiency: 63-67% - The prolonged release was assured when compared to another production techniques.	Songsurang et al., 2011

(Cont. on next page)

Table 2.10 (cont.)

Chitosan	Ampicillin	Bacterial infection treatment	- Morphology and particle sizes were adjusted by changing the electrospray parameters. - Release mechanism was defined as diffusion followed by polymer degradation.	Arya et al., 2009
Alginate	Paclitaxel	Cancer therapy	- Encapsulation efficiency: 82% - Zero-order kinetics was nearly achieved, the release was prolonged up to 60 days.	Ranganath et al., 2009
Alginate	*Ganoderma lucidum* spores	Diabetes treatment	- Electrospray parametric optimization was successfully performed to obtain uniformly sized spheres. - Release profile was tuned according to the drying method.	Zhao et al., 2016
Eudragit L 100-55	Omeprazole	Peptic ulcer and gastroesophageal reflux treatment	- Voltage, nozzle diameter and flowrate were optimized to adjust the particle morphology. - the pH-dependent release was reached for the oral delivery.	Hao et al., 2013

2.3.4. Chitosan-MMT Nanoclay Composites

Despite the advantages of using chitosan in biomedical applications, chitosan-based nanomaterials should be stabilized for sustained long-term drug release. The low stability of chitosan must be compensated by using crosslinkers, negatively charged polymers or reinforcement agents. The strengthened structure ensures improved mechanical properties and slower release behavior. However, chemical crosslinkers such as glutaraldehyde or tripolyphosphate (TPP) can cause a loss of bioactivity and provoke some side effects due to their toxicity if they cannot be totally removed.

Polymers such as carboxymethyl cellulose, alginate, dextran sulfate are negatively charged; which allows them to form complexes with chitosan. These polyelectrolyte complexes have increased stability due to the intermolecular electrostatic interactions.

Chitosan nanocomposites that fabricated with a dispersion of nanosized inorganic fillers serve as an alternative to overcome the initial burst problems of drug carriers. In recent studies, these polymeric nano-biocomposites are used in various biomedical applications such as biosensors, drug and gene delivery, tissue regeneration and surface modification (Kong et al., 2005; Kaushik et al., 2008; Kang et al., 2009; Bao et al., 2011). The nanocomposites can combine the advantages of polymer and filler material in biological, chemical and physical point of view. Nano-silicate particles are preferred as inorganic fillers in both natural and synthetic polymer matrix in order to improve the mechanical properties. Nanoclay layers that stacked together with weak van der Waals forces can be dispersed in the polymer matrix and tailored to obtain desired nanocomposite structure (Gao, 2004). The physical crosslinking between polymer chains and silicate nanoparticles improves the physical properties of the materials. Slower degradation rates can be achieved with stabilized morphologies of the nanocomposite materials.

In literature, it was proven that nanoclay/polymer composites have enhanced mechanical and thermal properties when compared to pure polymer materials (Günister et al., 2007).

The homogeneous dispersion of nanoclay layers in the polymer matrix is substantial to improve material characteristics. The nanocomposite structure is dependent on clay dispersion level which can be classified as flocculated, intercalated and

exfoliated/delaminated (Wang et al., 2005) (Figure 2.21). When the polymer cannot penetrate into clay layers, the structure can be named as phase separated; where the clay particles formed aggregates in the polymer matrix. The clay inclusion in polymer matrix causes an increase in layer spacings. If the layers are not completely dispersed in the matrix but still has an ordered morphology, the structure is referred as intercalated. If the clay layers are completely separated according to the perfect dispersion, exfoliated nanocomposite formation occurs. The exfoliated structure causes reinforcement effect on physicochemical properties of the material. The largest interfacial area is achieved between polymer and clay. The reinforced matrix structure can be achieved with the stacks of parallel nanoclay sheets or exfoliated sheets. This structure can be better achieved with the addition of a small amount of nanoclay (Khlibsuwan and Pongjanyakul, 2016).

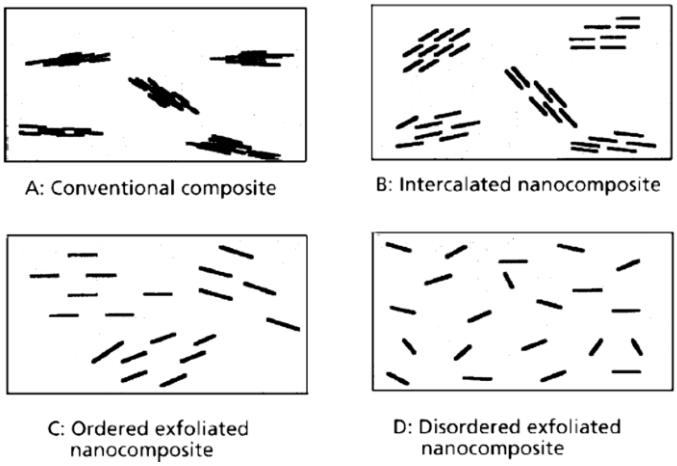

Figure 2. 21. Dispersion of clay platelet in a polymeric matrix (Source: Utracki, 2010)

Among natural clays, montmorillonite (MMT) has a major interest, especially in drug delivery systems. It belongs to the smectite group of minerals and composed of the multi-layered sandwich structure with two tetrahedron sheets and edge-bridged octahedral sheet (2:1 type) (Figure 2.22). It is negatively charged due to the imperfection of the crystal lattice and isomorphous substitution (Kevadiya et al., 2009). The cation exchange capacity of MMT depends on the extraction site and ranges between 70 and 120 meq/100 g clay (Thomas et al., 1999). The slack bonds between individual clay crystals lead to water interpenetration and swelling.

The material characteristics can be improved in terms of their mechanical and thermal properties with MMT reinforcement. In addition, the biological properties of

MMT such as antimicrobial activity and cytotoxicity provide various opportunities for further development in biomedical applications.

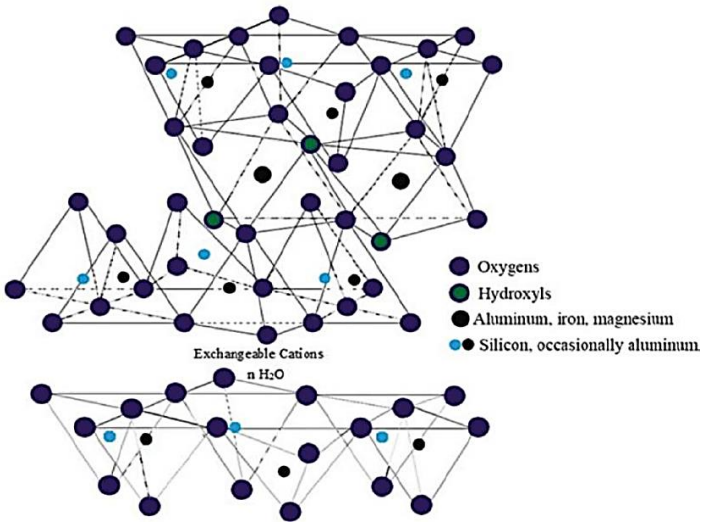

Figure 2. 22. The structure of the MMT (Source: Maina et al., 2016)

Recently, MMT nanoclay have been utilized as a carrier for controlled and sustained drug delivery because it can entrap the cationic drug molecules into its layers via intercalation (Yang et al., 2016). In a study, it was revealed that the MMT nanoclay showed the most retarded release profile when compared with other smectite clays as saponite and laponite (Park et al., 2008). This fact was attributed to the strong electrostatic interactions between MMT and model drug, donepezil.

Joshi et al. (2009) attempted to intercalate timolol maleate (TM), a drug against hypertension and myocardial infarction, into MMT to prepare hybrid system providing a controlled release under different pH and initial drug concentration. Intercalation is successfully provided in a short time. The TM release based on ion-exchange showed a slow and persistent profile in pH 1.2 and 7.4. However, 100% of the TM could not be released according to the ionic equilibrium in media. Results demonstrated that MMT-TM hybrids could be a potential oral delivery system.

As another example of MMT hybrids, Chen et al. (2010) intercalated tramadol hydrochloride (TM), a drug that lessens the physical pain, to avoid its side effects and ensure the effective plasma concentration. The TM release from MMT interlayers showed a good fit to Bhaskar and Korsmeyer-Peppas empirical models. Controlled drug release was achieved up to 6 hours of immersion in simulated intestinal fluid (pH=7.4).

The MMT intercalated antibiotic drug, metronidazole drug (MNE), showed promising release profile when compared to commercially available tablets (Calabrese et al., 2013). The intercalation did not change the chemical nature of the antibiotics but also lowered the burst release effect. In stomach fluid, zero-order release was observed. The hybrid in intestinal fluid (pH=7.4) showed a good fit to the first-order model with the derived formulation of MNE-MMT hybrids.

MMT layered structure could encapsulate various kinds of active agents. In a study, vitamin B_1 was intercalated into MMT. The release profile was investigated in simulated gastric (pH=1.2) and intestinal fluid (pH=7.4). Results showed that the release profile was dominated by diffusion and followed the Higuchi model (Joshi et al., 2009).

The major drawback of the MMT/drug hybrid system when compared to conventional composites is the difficulty to reach long-term controlled drug release. Albalawi et al. (2016) studied the loading and delivery of Platinol from MMT and Chitosan/MMT nanocomposite as therapy to be employed as bladder and testicular cancer. According to the results, it was concluded that drug release was prolonged and achieved in a controlled manner with Chitosan/MMT composites.

The Chitosan/MMT bionanocomposite can be formed by the cationic exchange and hydrogen bonding. The cationic nature of the chitosan enables intercalation with ionic exchange into negatively charged MMT interlayers (Darder et al., 2005). The schematically representation of MMT layer spacing opening due to intercalation with chitosan polymer is depicted in Figure 2.23. Nanocomposite formation with chitosan and MMT nanoclay can be depicted with some characterization tests. Characterization of nanocomposites has been mainly done by X-Ray diffraction (XRD) and transmission electron microscopy (TEM) techniques to determine the distribution of clay platelets into chitosan matrix. XRD technique is generally used in combination with TEM by monitoring the position, shape and intensity of the basal reflections from the distributed clay layers. The characteristic peaks of clay shift to a smaller two-theta degree indicating intercalated polymer-clay nanocomposites due to insertion of polymer layers into the clay galleries (Wang et al., 2005). In exfoliated structure, the characteristic clay peak disappears in the XRD pattern which is desirable for improved properties because of the perfect homogenization conditions (Fu and Qutubuddin, 2001).

Transmission Electron Microscopy (TEM) is used to understand the real picture of the nanostructure of the composites. It can give spatial distribution and dispersion of the nanoparticles within the polymer matrix.

In addition, Fourier Transform Infrared Spectroscopy (FT-IR) technique is used to determine the molecular interactions between the polymer matrix and the nanoclay, as well as structural changes, occurred due to exfoliation/intercalation of layered clays.

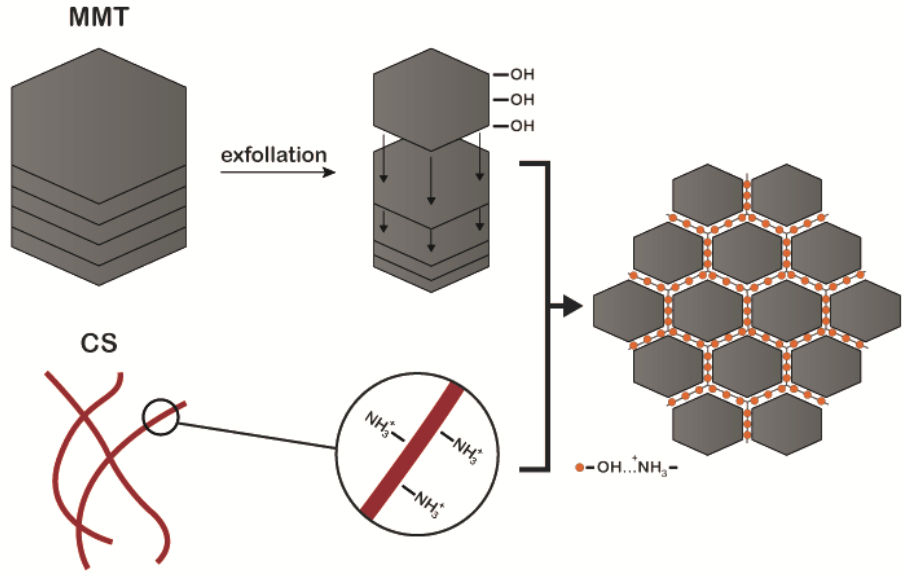

Figure 2. 23. Schematical representation of Chitosan/MMT nanocomposite formation

Chitosan/nanoclay composite systems have gained a great interest in various application areas such as packaging, sensor coating, drug delivery and enzyme immobilization. Several studies related to chitosan/nanoclay composites and their major outcomes were briefly described in Table 2.11.

The nanoclay loading is widely preferred in packaging applications since it provides a tortuous pathway, followed by improvement in water vapor and oxygen barrier properties. Lavorgna et al. (2010) indicated that MMT addition on chitosan film forming solution affected the thermal, mechanical and barrier properties. The barrier and mechanical properties were improved due to the intercalated structure of the chitosan/MMT nanocomposites.

Recently, the use of Chitosan/silicate clay minerals as DDS is getting attention in particularly long-term drug release applications. Many different forms of drug release carrier systems have been prepared for Chitosan/MMT composite system according to application/target purpose. The main advantages of Chitosan/MMT composites in drug delivery applications are (Kevadiya et al., 2010; Salcedo et al., 2012):

- Anionic-cationic interaction preventing the burst release
- Slower degradation profile

- Improved structural and functional properties
- High antimicrobial activity
- Inertness
- Biocompatibility

Recent studies regarding Chitosan/MMT drug delivery systems were depicted in Table 2.12. Liu et al. (2008) developed electrostimulation controlled release of Vitamin B_{12} from Chitosan/MMT composites. The exfoliated structure was successfully achieved with a small amount of MMT addition (1% w/v). As MMT concentration was increased, the antifatigue behavior of the system was considerably increased. However, response to electrostimulation was decreased. The release rate followed the pseudo-zero order model.

Depan et al. (2009) fabricated Ibuprofen loaded Chitosan/MMT composite films and observed enhanced mechanical properties when compared to neat chitosan. The release rate was reduced with MMT addition in the polymer matrix. Fabricated films were found biocompatible with fibroblast cells.

In another study based on Chitosan/MMT hydrogel, Hua et al. (2010) prepared TPP crosslinked MMT/Chitosan hydrogel beads in the purpose of ofloxacin release and found that MMT incorporation increased the drug loading efficiency from 31.2% up to 83.5% while reducing the release rate significantly. Hence, MMT incorporation ensured an increase in stability when compared to pure chitosan beads.

In a study, glutaraldehyde crosslinked Chitosan/MMT hydrogels in the purpose of the controlled release of various drugs (Cojocariu et al., 2012). It was observed that MMT concentration significantly affect the release model. The kinetic constant, k, decreased with increasing MMT content.

Salcedo et al., (2014) evaluated oxytetracycline (OXT) releasing Chitosan/MMT nanoparticles. OXT loaded particles occurred in cell substrates and the drug permeation was increased with nanocomposite formation.

In a study, chitosan/MMT microparticulate system was fabricated for controlled delivery of water-soluble Propranolol HCl with spray drying method. It was observed that particle sizes were decreased when compared to neat chitosan microparticles. However, the hardness of the tablets was increased according to the nanocomposite formation. Results indicated that the release in acidic and neutral media was perfectly fit zero-order model (R^2=0.977-0.999) (Khlibsuwan and Pongjanyakul, 2016).

Although there are various studies related to Chitosan/MMT, there are few studies about naturally modified MMT as a nanofiller in drug delivery systems. Modified

nanoclays differ in their counter ions and cation exchange capacities. Studies showed that clays modified with cationic surfactants have strong antimicrobial activity against *E. coli* and *S. aureus* bacteria (Nigmatullin et al., 2008). In a study, Roul et al. (2006) showed that modified MMT (Cloisite 10A) incorporation enhanced the Diclofenac sodium loading capacity and provided a better-controlled release profile for chitosan nanoparticles. In addition, results demonstrated that MMT addition improved the antimicrobial activity against both gram-positive and gram-negative bacteria.

Similarly, in this thesis work, Cloisite 10A (surface-modified natural MMT with benzyl(hydrogenated tallow alkyl) dimethyl) was used to prepare Chitosan/MMT nanocomposite systems.

2.3.4.1. Homogenization in Nanocomposite Formation

Nanoscale fillers that are mostly used for composite formation tend to agglomerate and form clusters. This yields to non-uniformity of material characteristics. Several homogenization methods are applied to the polymer-nanofiller suspension to spread particles in the polymer matrix. Homogenization for nanocomposite formation can be achieved with an ultrasonic method, mechanical shearing or micro-scale techniques.

Ultrasonication is widely used for intercalation and distribution of nanofillers in natural polymer-based solutions. This technique also decreases the particle size and induces homogeneous particle size distribution. However, the usage of the ultrasonic method is decreased in biomedical applications due to the contamination caused by erosion of metal ions on sonicator probe. Mechanical shearing can be alternative but the homogenization efficiency is low when compared to other methods.

Micro-scale methods can be served as an alternative to conventional methods with their properties such as easy processability and low energy consumption. Microfluidizer (MF) is a high-pressure homogenization technique that exposes the solution to high shear stress in microchannels. The schematic representation of high-pressure homogenization is depicted in Figure 2.24. Product enters the MF via inlet reservoir and forced to pass through microchannels by a high-pressure pump into the interaction chamber. A condenser pump inside provides the desired pressure to the product along the microchannels in the interaction chamber. The solution is passed through the

microchannels several times to obtain desired homogenization. The velocity in microchannels can increase up to 500 m/s (Panagiotou et al., 2008).

The physicochemical properties of the polymeric solution can be altered by changing the pressure and the pass number. It has been used in various applications such as nano-emulsion and liposome production, high-pressure homogenization and polymer degradation (Mahdi Jafari et al., 2006; Perdones et al., 2012; J. Chen et al., 2012).

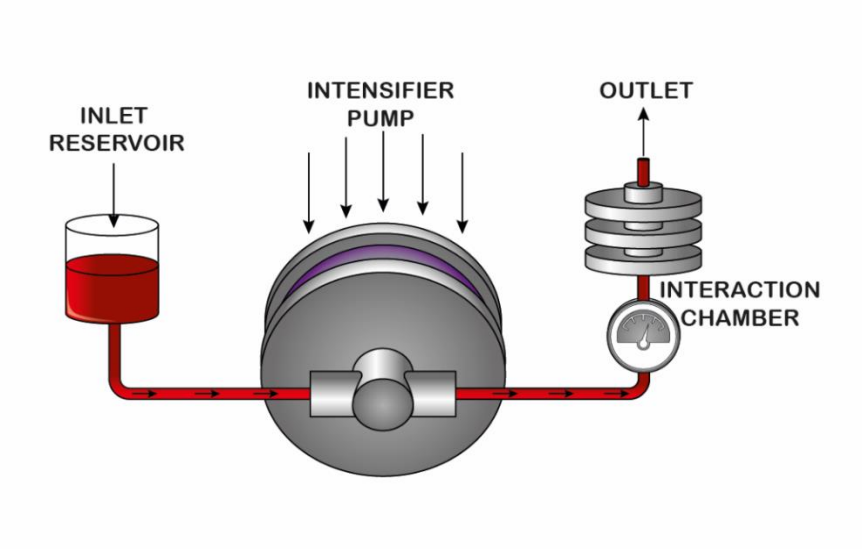

Figure 2. 24. A microfluidizer unit

In literature, the effect of homogenization techniques on the molecular weights of chitosan and pectin biopolymers was studied. It was reported that the molecular weight of chitosan decreased drastically due to the breakdown of covalent bonds in the macromolecule chain with MF treatment in operating conditions of 82.7 and 117.2 MPa for 5-25 passes, when compared to mechanical shearing and ultrasonication (Chen et al., 2011). In another study, (Chen et al., 2012) studied the degradation of pectin due to MF application with 40-200 MPa for 5 passes. Viscosity, molecular weight and particle size of the microfluidized pectin showed that pressure is a significant factor in the extent of degradation. However, the mechanism of pectin degradation still could not be clarified.

However, a few studies have been conducted that dealt with microfluidizer technology as a homogenization technique for nanocomposite formation. In a study, microfluidizer processor was used to decrease the size of the cellulose fibers that will be used as a nanofiller in HPMC films. It was observed that pass number and pressure significantly reduces the microfiber size (De Moura et al., 2011).

Table 2. 11. Studies related to chitosan/nanoclay nanocomposites

System	Purpose	Major outcomes according to the composite formation	References
Film	Packaging	Improved mechanical and barrier properties were achieved by increasing the clay concentration	Casariego et al., 2009; Oguzlu and Tihminlioglu, 2010
Tablet	Controlled drug delivery	Nanoclay filler promoted controlled release profile and water uptake capacity of the tablets	Khlibsuwan and Pongjanyakul, 2016
Particle	Controlled drug delivery	Nanofiller addition lowered the particle degradation in acidic media.	Yuan et al., 2010; Salcedo et al., 2012
Sponge	Controlled drug delivery/Wound healing	The exfoliated structure was achieved with the lower nanoclay concentrations results with higher drug loading.	Sandri et al., 2014
Disc	Electrochemical sensor	Potentiometric anion detection was supplied with high durability and elevated stability according to nanoclay-chitosan modification of the surface.	Darder et al., 2005
Sphere	Enzyme immobilization support	Phenol removal from aqueous solutions was supported with nanocomposite beads due to favored adsorption of tyrosinase on the clay surface	Dinçer et al., 2012
Hydrogel	Electrostimulated drug release	Responsiveness and reversibility of the cyclic electrostimulation were ensured with MMT addition, resulted in a desirable release profile	Liu et al., 2008

Table 2. 12. Chitosan/MMT nanocomposite delivery systems

Model drug	Material morphology	Major outcomes	References
Diclofenac sodium	Nanoparticle	- Enhanced drug loading capacity and antimicrobial activity was achieved by increasing MMT concentration	Roul et al., 2006
Vitamin B_{12}	Hydrogel	Exfoliated structure Pseudo-zero order release Excellent anti-fatigue behavior	Liu et al., 2008
Ibuprofen	Film	Intercalated structure Reduced release with MMT incorporation Biocompatible with fibroblast cells	Depan et al., 2009
Ofloxacin	Hydrogel	Intercalated structure Encapsulation efficiency: up to 83.5% Controlled release up to 10 hours	Hua et al., 2010
Theophylline, Paracetamol, Xanthine derivatives and nitric oxide donor compounds	Hydrogel	Intercalated structure Burst effect was significantly reduced Release model changed with MMT concentration	Cojocariu et al., 2012
Oxytetracycline	Nanoparticle	Enhanced cellular drug uptake Non-toxic to Caco-2 cell line	Salcedo et al., 2014
Propranolol HCl	Tablet	Sustained release in both acidic/neutral medium Zero-order release	Khlibsuwan and Pongjanyakul, 2016

In a study, microfluidizer was used for dispersion of cellulose nanocrystals to obtain chitosan-cellulose nanocomposite films. Effect of microfluidization pressure (5000-15000 psi) and pass number (2-10) was investigated in terms of mechanical properties of the prepared films. It was reported that the aggregation was perfectly enhanced and mechanical properties are ameliorated by the aid of homogeneously distributed nanocrystals (Khan et al., 2014). In another study, carbon nanotubes were perfectly dispersed in epoxy resin by this technique at 158 MPa and the nanocomposite structure was achieved even with a single pass (Panagiotou et al., 2008). However, in these studies, the effect of high-pressure application on polymer characteristics has not been completely evaluated.

In summary, the processing parameters (pressure and pass number) in MF technology should be optimized to obtain good dispersion of particles in the polymer matrix as well as avoid degradation of the polymer structure, especially in biopolymer degradation.

In this thesis work, microfluidization homogenization was selected to distribute nanoclay particles in chitosan matrix homogenously. A parametric study was performed regarding molecular weight, rheological behavior and deacetylation degree of chitosan by altering pressure and the pass number of the microfluidization.

CHAPTER 3

MATERIALS AND METHODS

3.1. Materials

High molecular weight chitosan (CS) was purchased from Sigma-Aldrich (Germany, Cat. No. 419419) to produce chitosan nanospheres. The organically modified montmorillonite (MMT) (Cloisite 10A, Southern Clay Products Inc.) was used as an inorganic filler. Glacial acetic acid (Analytical grade, Merck) was used as a solvent to dissolve the polymer solution homogeneously.

Gentamicin (Genta, IE Ulagay) and vancomycin (Anko-L, Mustafa Nevzat) were selected antibiotics to be entrapped in nanospheres. Ammonium acetate (Sigma-Aldrich, >99%) was used for solvent system preparation in intrinsic viscosity measurements. Phosphate buffer saline (PBS) solution (pH=7.4, Sigma-Aldrich) was used for *in vitro* drug release, DLS and zeta potential studies.

The WST-1 assay was purchased from Biovision Inc. for *in vitro* cytotoxicity tests. Dulbecco's Modified Eagle Medium (DMEM, Capricorn), penicillin and streptomycin antibiotic solution (Capricorn), fetal bovine serum (FBS, Capricorn) were used for the culture of NIH/3T3 and SaOS-2 cell lines.

3.2. Optimization of High-Pressure Homogenization Parameters

3.2.1. Intrinsic Viscosity Measurement

The intrinsic viscosity was examined with a capillary viscometer (SI Analytics, Typ 513 10, App. Nr. 1067 23) to observe the effect of microfluidizer treatment on the molecular weight of chitosan. The chitosan solutions were prepared with 0.15M Ammonium Acetate and 0.2M Acetic Acid solution at 25°C and stirred vigorously. Then, high molecular weight chitosan solutions were treated with microfluidizer. The pressure

and pass number were altered as 10,000 and 20,000 psi (68.95 MPa, 137.89 MPa) and 3, 5, 10 passes, respectively. The samples were fed to the capillary viscometer and the experiments were conducted at 25°C. The flow time of the solvent and the chitosan solutions were recorded and the following viscosities were determined with the equations below:

Relative viscosity: $$\eta_{rel} = t/t_s \quad (3.1)$$

Specific viscosity: $$\eta_{sp} = (t/t_s) - 1 \quad (3.2)$$

Reduced viscosity: $$\eta_{red} = \eta_{sp}/c \quad (3.3)$$

where t_s is the solvent flow time and c is the concentration of chitosan solution.

Experiments were performed as triplicates. The reduced viscosity versus chitosan concentration was plotted and the extrapolation of reduced viscosity to zero concentration was recorded as the intrinsic viscosity. Finally, the viscosity-average molecular weight was calculated according to Mark-Houwink-Sakurada equation below:

$$\eta = KM^{\alpha} \quad (3.4)$$

where K and α are constants specific to polymer, solvent and temperature system. The viscosity average molecular weight was calculated from the equation where $K=9.66x10^{-5}$ (dm^3/g) and α=0.742 in 0.15M Ammonium acetate and 0.2M Acetic acid solution at 25°C (Yacob et al., 2013).

3.2.2. The Rheological Properties of Chitosan Solutions

Chitosan solutions were prepared with a concentration of 2% (w/v) in 90% (w/v) acetic acid solution and magnetically stirred for 1 day to obtain a homogeneous solution and filtered using Whatman paper no 4. The solution samples (chitosan solutions treated with a pressure of 10,000 and 20,000 and pass number of 3, 5, 10) were prepared. High shear homogenization (Microfluidizer) induces temperature increase. Therefore, samples were cooled to a controlled temperature of 25°C. The rheological properties of the chitosan solution treated with high-pressure homogenization were determined with a rotational rheometer (Haake Mars II, Advanced Rheometer System) with a sensor system

of cone and plate (with a 35mm diameter and 2° of angle). The shear stress (σ) was obtained as a function of shear rates (γ) between 0 and 10 s^{-1}. The average of five measurements was reported. The power law model was applied to find the consistency index (K) and the flow behavior index (n) of the chitosan solution.

$$\sigma = K.\gamma^{n} \quad (3.5)$$

where the "n" value indicates the rheology of the solution.

if n=0, the fluid is Newtonian

if n<1, the fluid is shear thinning,

if n>1, the fluid is shear thickening (Geankoplis, 2003).

3.2.3. X-ray Diffraction (XRD) Analysis

XRD analysis was performed to observe nanoclay dispersion in chitosan matrix. Prepared samples were prefreezed and lyophilized and analyzed with Philips X'PertPro MRD. X-ray diffraction patterns were determined at a voltage of 40kV using Cu-Kα radiation (λ=1.54Å). Intensities were recorded in a range of 2-30° (2θ) with a scanning rate of 0.139°/sec. The d-spacing value that indicates the distance between the nanoclay silicate layers was calculated with the Bragg's law:

$$\lambda = 2dsin\theta \quad (3.8)$$

where λ indicates the incident beam wavelength, θ is the diffraction angle and d is the d-spacing.

3.3. Preparation of Drug Loaded Nanospheres

Briefly, 2% (w/v) high molecular weight chitosan was dissolved in 90% (v/v) acetic acid solution and stirred overnight. MMT nanoclay with a concentration of 3% w/w was dispersed in distilled water and stirred for 24h at room temperature. Finally, nanoclay was added to polymer solution dropwise, followed by a continuous stirring. Gentamicin

and vancomycin were added to the solution and integrated to the polymer matrix. The solution was obtained with a polymer to drug ratio of 4:1, 8:1 and 10:1,20:1 for vancomycin and gentamycin antibiotics, respectively. Prepared chitosan/clay-GS solution was injected to Z type interaction chamber of the microfluidizer (Microfluidics LV1, USA) to obtain homogeneous polymer-drug dispersion and intercalation of clay in chitosan matrix. The homogenization parameters were determined as 10,000 psi and 5 passes according to the molecular weight, rheological properties and deacetylation degree change.

In the study, electrospraying was selected for preparation of drug loaded chitosan nanocomposite spheres due to its advantages such as higher loading efficiency, narrow size distribution and elimination of the need for toxic solvents as explained in detail in section 2.3.2.2. The voltage, distance and the solution flowrate were optimized with Minitab software to achieve ideal nanosphere morphology. The effect of process parameters was investigated by altering voltage (10 and 20 kV), distance (5 and 10 cm) and the flowrate of the polymeric solution (5 and 10 ml/h). Optimum electrospray conditions were determined according to the particle size and morphology of the nanospheres.

3.4. Characterization Tests

3.4.1. Morphology and Surface Characterization

SEM analysis was performed in order to observe the morphology and the sphericity of the nanospheres. Before the analysis, samples were coated with a thin gold layer under argon gas (Emitech K550X). Then, SEM analysis was performed with Quanta FEG 250 (at $7x10^{-2}$ mbar and 15 mA). The optimization of electrospray process parameters was done according to the morphology of nanospheres by considering SEM micrographs.

Additionally, the surface and the morphology of the nanospheres were characterized with tapping mode atomic force microscopy (AFM). The analysis was performed with 1.5 μm x 1.5 μm scan sizes. The 3D surface topography images were analyzed with the Nanoscope software.

3.4.2. Fourier Transform Infrared Spectroscopy (FT-IR) Analysis

The effect of high-pressure homogenization on deacetylation degree (DD %) of chitosan was determined with FT-IR analysis. 2% (w/v) high molecular weight chitosan solutions in 90% (v/v) acetic acid solutions were prepared and stirred overnight. Microfluidizer homogenization was applied to the solutions with a pass number of 3,5 and 10 with a pressure of 10,000 and 20,000 psi. Solution samples were prefreezed at -20°C for a day, lyophilized and dehumidified under vacuum at 35°C.

The deacetylation degree of chitosan was determined with FT-IR (Shimadzu FTIR-8400S) by KBr pellet technique (Zhang et al., 2005). The relation comprising the amide I bond (1655cm^{-1}) and hydroxyl peak (3450^{-1}) were used to determine the DD (%) of chitosan (Equation 3.7):

$$DD\ (\%) = \left[1 - \left(\frac{\frac{A_{1655}}{A_{3450}}}{1.33}\right)\right] \times 100 \qquad (3.7)$$

The peak heights were determined with IR Solution (Shimadzu) software. Besides, the interactions between chitosan and clay, drug and chitosan-clay were also determined with FT-IR analysis at wavelengths ranging from 4000 to 400 to cm^{-1} at a resolution of 4 cm^{-1}.

3.4.3. Size Distribution of Nanospheres

The hydrodynamic size distribution of the chitosan-clay composite nanospheres was determined with the Dynamic Light Scattering (DLS) analysis. The samples were suspended in 5 ml of 1x PBS (pH=7.4) at 25°C, sonicated for 5 minutes to prevent aggregation, decanted into a glass scintillation vial and analyzed by Malvern Zetasizer Nano-Zs. The data were acquired in automatic mode.

The particle size distribution and mean hydrodynamic diameters were analyzed as intensity averaged distributions. The experiments were conducted as three replicates and the results were given as the average of 3 runs and 100 scans for each run.

3.4.4. Zeta Potential

The surface charges of chitosan-clay composite nanospheres were analyzed with Malvern Zetasizer Nano-Zs. Samples were dispersed in 1x PBS (pH=7.4) at 25°C, vortexed and sonicated for 5 minutes to prevent agglomeration. The samples (n=3) were analyzed with 3 runs and 100 scans for each run. The point of zero charge of MMT nanoclay dispersion in 1x PBS was determined by altering the pH between 3-12. The pH of the nanoclay dispersion was adjusted by using buffer solutions of 0.1M HCl and 0.1M NaOH.

3.5. Antimicrobial Activity

The antimicrobial activity of drug release media of chitosan nanospheres was evaluated with disc diffusion method. Gram-positive *Staphylococcus aureus* (RSKK 1009 strain) and gram-negative *Escherichia coli* (ATCC® 25922) was used as model bacteria. The frozen bacteria stocks were activated at 37ºC for overnight. The turbidity of cultured microorganisms in peptone solution was adjusted to 0.5 McFarland.

Firstly, in order the observe whether the concentration of released antibiotic is sufficient to prevent the bacteria colonization, the bacteria culture was incubated with serially diluted antibiotic concentrations for 24 h of incubation in 6-well plate in an orbital shaker at 55 rpm and 37°C. Then, the bacteria solution containing antibiotic were placed on agar and incubated at 37°C for 24 h. The minimum required drug concentration was determined by observation of bacteria colonization on Petri dishes.

The agar diffusion method was applied to verify the antimicrobial activity of the released media. Discs were sterilized under UV cabinet for 30min. $3.4x10^7$ cfu ml^{-1} of early mid-log phase culture of *S. aureus* in tryptic soy broth and $2.5x10^7$ cfu ml^{-1} of *E. coli* in nutrient agar were incubated at 37°C for 24 h. The discs gently put on the surface of inoculated agar with *S. aureus* and *E. coli*. 10 µl of drug release media taken at specified time intervals (6 hours, 24 hours and 25 days) were dropped on antimicrobial susceptibility discs (Oxoid™). Vancomycin and amoxicillin antibiotic discs were used as positive control groups. The blank disk was used as a negative control. Petri dishes were incubated at 37°C overnight and the clear zones around the discs were recorded as

inhibition zone which indicates the antimicrobial activity. Experiments were carried out in triplicate (n=3).

3.6. Encapsulation Efficiency and *In vitro* Drug Release Profile

Drug loaded nanocomposite spheres were dissolved in 5 ml of 1x PBS and disrupted in an ultrasonic bath for 30 minutes. The solution was filtered and the amount of drug entrapped by polymer-clay matrix was determined by UV-Vis spectroscopy (Varioskan). The absorbances of the samples were measured at 256 and 282nm for gentamicin and vancomycin, respectively. Encapsulation efficiency of CS/MMT nanospheres was calculated according to Equation 3.9.

$$\text{EE}\ (\%) = \frac{\text{Amount of drug loaded}}{\text{The theoretical amount of drug loading}} \times 100 \qquad (3.9)$$

In vitro vancomycin and gentamicin release from CS/MMT nanocomposite spheres was determined under immersion conditions. The aluminum foil coated with nanospheres were cut in dimensions of 1 cm x 1 cm and placed in 1 ml of phosphate-buffered saline solution (PBS, pH=7.4). The specimens (n=3) were incubated in an orbital shaker at 75 rpm and temperature of 37°C (Thermoshake, Gerhardt). Samples were collected at predetermined time intervals. The release rate was determined with absorbance data taken by UV-VIS spectroscopy (Varioskan). The collected media was replaced with the fresh PBS and the volume of incubation medium was kept constant. The rate of the drug release was fitted into mathematical release kinetic models.

3.7. *In vitro* Cytotoxicity

The cytotoxicity behavior of the composite nanospheres was defined with the WST-1 [4-3-(4-Iodophenyl-2-(4-Nitrophenyl)-2H-5-Tetrazolio]-1,3-Benzene Disulfonate] assay. The amount of formazan dye is correlated with the glycolytic production of NAD(P)H in metabolically active cells (Berridge et al., 2005). Hence, the assay is based on the conversion of the stable tetrazolium to a soluble formazan dye on

the viable cell surface. The % viability of the NIH/3T3 fibroblast and SaOS-2 bone osteosarcoma cell lines were found by indirect extraction method according to the ISO 10993 standards. Nanospheres were extracted for 24h in Dulbecco's Modified Eagle Medium (DMEM) supplemented with 10% fetal bovine serum (FBS), 100 µg/ml streptomycin and 100 µg/ml penicillin in an atmosphere of 5% CO_2 at 37°C. Cell seeding was carried out at 10^5 cell/ml cell density and incubated on 96-well plates with 100 µl extraction medium for 72 hours. The cytotoxicity of the nanospheres was measured at specified incubation periods (24 h, 48 h and 96 h) by spectrophotometrically at 440 nm. The cell viability % was determined by normalizing the absorbance data of the viable cell medium with a negative control which includes fresh medium. The viability of the cells was calculated with the Equation 3.10.

$$\text{Cell viability } \% = (\text{ABS of sample}/\text{ABS of NC}) \times 100 \qquad (3.10)$$

where ABS is the average absorbance value and NC is the negative control

3.8. Statistical Analysis

The significance of the differences between the results was evaluated by one-way and two-way analysis of variance (ANOVA) with Minitab software. The results were expressed as a mean ± standard error.

CHAPTER 4

RESULTS AND DISCUSSIONS

4.1. The Optimization of Microfluidizer Process Parameters

Chitosan can be mainly characterized in terms of three properties: viscosity, molecular weight and deacetylation degree. Therefore, the effect of microfluidizer (MF) on chitosan properties was determined with rheology, viscosity, molecular weight, deacetylation degree and X-Ray Diffraction (XRD) analysis.

4.1.1. Rheological Behavior

The effect of microfluidizer pressure and pass number on rheological properties of chitosan solution was investigated with a rotational rheometer. Figure 4.1 and 4.2 represent the flow and viscosity curves of MF treated chitosan solutions, respectively. It was observed that viscosity is decreasing with increasing shear rate. The experimental viscosity versus shear rate data in Figure 4.2 showed a good fit to the power law with the high regression coefficients (R^2>0.99). The rheological parameters together with the apparent viscosity and shear stress values were shown in Table 4.1. Apparent viscosities were calculated at the shear rate of 10 s^{-1}. The flow behavior index indicates the solution shows pseudo-plastic (Shear thinning) properties since n is smaller than 1, as generally found in polymeric solutions (Geankoplis, 2003).

The shear stress and apparent viscosity data implies that MF caused a change in rheologic properties of chitosan solution. The solution becomes more Newtonian with the MF application. It was found that pressure change was more effective on solution viscosity when compared with pass number. Groups with a pass number of 3 and 5 at constant pressure (10,000 psi) showed similar rheological properties as seen in Table 4.1.

Increasing the pressure from 10,000 to 20,000 psi significantly affected the solution characteristics. The significant decrease in viscosity impeded the sprayability of

the solution at 20,000 psi. Therefore, groups treated with 20,000 psi pressure could not be used for nanosphere fabrication. Hence, exfoliated nanocomposite structure were tried to obtain with a pressure of 10,000 psi.

The decrease in viscosity can be attributed to polymer chain degradation, conformational change and decrease in the molecular weight. Kasaai et al. (2003) implied that the molecular weight of chitosan decreases with microfludization treatment. In literature, similar findings were found with microfluidization of chitosan solutions (Vargas et al., 2011; Bonilla et al., 2012).

Perdones et al. (2012) found that the apparent viscosity of the chitosan solution containing lemongrass essential oil has been significantly reduced with high-pressure homogenization. The fact can be explained by fragmentation of polymer chains with high pressure. Our findings are in good agreement with the literature. Additionally, literature involves some other studies performed with other biopolymers such as alginate and xanthan gum revealing MF treatment causes a decrease in molecular weight for biopolymers (Lagoueyte and Paquin, 1998; Villay et al., 2012; Salvia-Trujillo et al., 2015).

Table 4. 1. Power law parameters; shear stress and viscosity values for chitosan solutions homogenized with microfluidizer (Shear rates were taken as 10 s^{-1})

Groups	**K**	**n**	**R^2**	**Predicted Shear Stress (Pa)**	**Predicted Viscosity (Pa.s)**
w/o MF	4.46	0.70	0.99	22.14	2.21
10,000 psi 3 pass	2.76	0.71	0.99	14.11	1.41
10,000 psi 5pass	2.56	0.79	0.99	15.75	1.57
10,000 psi 10 pass	1.64	0.86	0.99	11.47	1.14
20,000 psi 5 pass	0.84	0.94	1.00	7.39	0.74
20,000 psi 10 pass	0.56	0.97	1.00	5.26	0.53

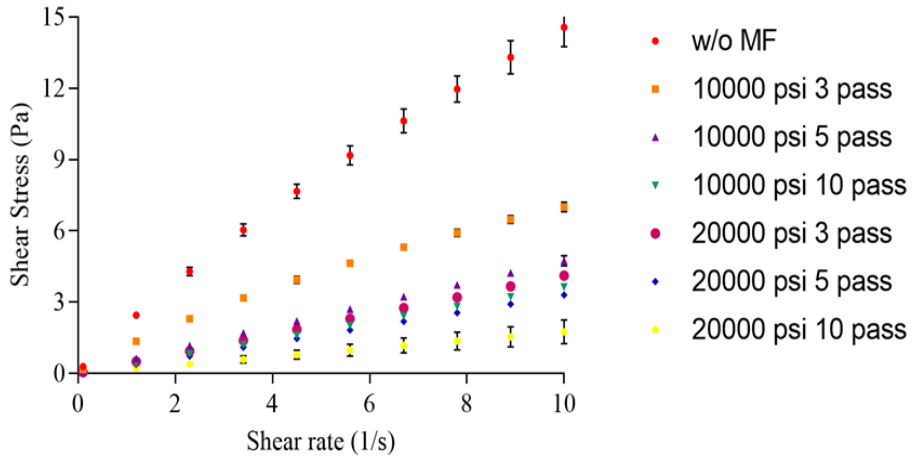

Figure 4. 1. Flow curve of chitosan solution treated with different microfluidizer parameters

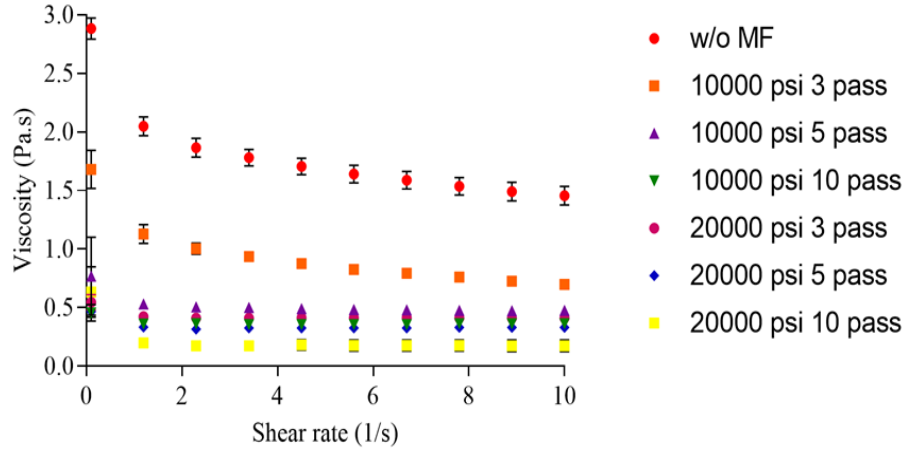

Figure 4. 2. Viscosity curve of chitosan solution treated with different microfluidizer parameters

4.1.2. Viscosity and Molecular Weight

According to the rheology study, high shear homogenization of chitosan solution caused a decrease in the viscosity. Therefore, the effect of viscosity change on the viscosity average MW of the chitosan was determined at various MF conditions. In this study, intrinsic viscosities of the dilute chitosan solutions treated with microfluidizer pressure of 10,000 psi at various pass numbers were measured with Oswald viscometer. Intrinsic viscosity is a simple and one step technique to find the viscosity average molecular weight of a dilute polymeric solution. Solutions were allowed to flow through capillary of viscometer under the action of pressure drop and time taken through a specified length is measured. Relative viscosities of the chitosan solutions were defined

as flow time of the polymeric solution over flow time of the pure solvent system (Eq. 3.1). Reduced viscosity values were found by using the Eq. 3.3 that is specific viscosity over concentration. Reduced viscosity over concentration graph was plotted and the intrinsic viscosity values of the chitosan solutions were found by extrapolation to infinite dilution (Figure 4.3). The flow time, relative viscosity and the specific viscosity values for each concentration and treatment method were given in Appendix A. Linear regression for each group was performed with GraphPad Prism Software Linear Regression of Data tool. Linear regression equations and correlation coefficients of each group were represented in Table 2.

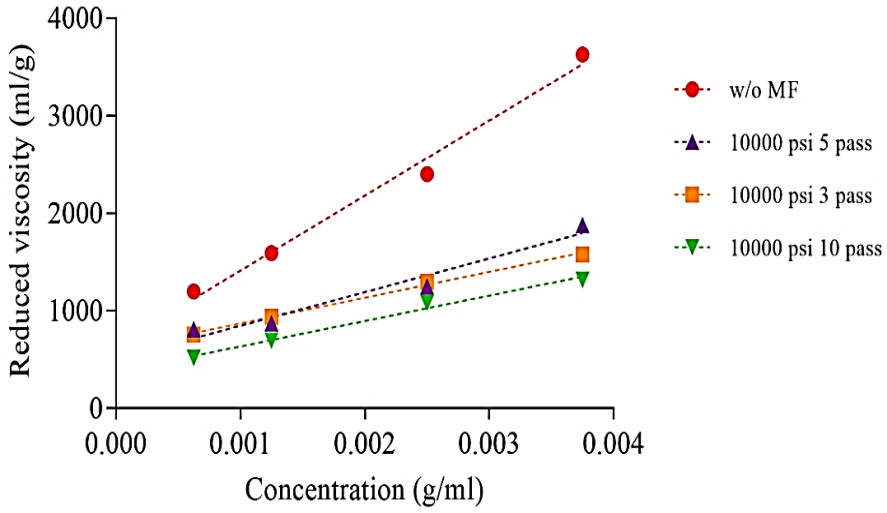

Figure 4. 3. Reduced viscosity versus concentration graph of chitosan solution

Table 4. 2. Linear regression equations defining the reduced viscosity

Groups	**Regression Equation**	**R^2**
w/o MF	$y = 769489X + 641.8$	0.99
10,000 psi 3 pass	$y = 264653X + 605.4$	0.99
10,000 psi 5 pass	$y = 345158X + 501.1$	0.95
10,000 psi 10 pass	$y = 260444X + 374.4$	0.99

The molecular weight values were calculated with the Mark-Houwink-Sakurada empirical correlation by using the intrinsic viscosity values (Eq. 3.4). A reduction of intrinsic viscosity of chitosan resulted with a decrease in viscosity average molecular weight. Intrinsic viscosity and the molecular weight of non-treated and microfluidizer treated chitosan were given in Table 4.3. The decrease in molecular weight can be linked

with the increase in the energy flow in microfluidizer that leads increase in degradation efficiency. Microfluidizer treatment caused a very slight change in molecular weight at 10,000 psi with 3 passes. However, it was observed that molecular weight decrease is more after 5 pass number. As seen in Table 4.3, the molecular weight of the non-treated chitosan was found as 141.75 kDa. The molecular weight of chitosan solution was decreased from 131 to 101.43 kDa while pass number increases 3 to 5. The molecular weight of chitosan homogenized with conditions of 10,000 psi 10 pass was further decreased to 68.55 kDa, which can be attributed to reduction due to chain scission of chitosan backbone. Therefore, it was found that pass numbers of 3 and 5 at 10,000 psi could be convenient for the electrospray application. In a study, it was indicated that the molecular weight of the chitosan solution significantly decreases with the microfluidizer pass number at a constant pressure of 117.2 MPa (17,000 Psi) (Tsai et al., 2009). Therefore, our findings are in good agreement with the literature and 10,000 psi pressure with 3 and 5 pass numbers are selected as the optimum homogenization conditions for chitosan solution.

Table 4. 3. Intrinsic viscosity and viscosity average molecular weight of chitosan

	w/o MF	**10,000 psi 3 pass**	**10,000 psi 5 pass**	**10,000 psi 10 pass**
Intrinsic viscosity	641.8±12.0	605.4±9.2	501.1±31.7	374.4±7.3
Molecular weight (kDa)	141.8±8.8	131.0±5.5	101.5±20.0	68.6±3.5

4.1.3. Deacetylation Degree

Deacetylation degree (DD) can be simply defined as the molar percentage of monomeric units carrying amino groups. The degree of deacetylation is the ratio of a number of moles of β-(1→4)-2-amino-2-deoxy-D-glucopyranose units over the summation of the β-(1→4)-2-amino-2-deoxy-D-glucopyranose units and β-(1→4)-2-acetamido-2-deoxy-D-glucopyranose units (dos Santos et al., 2009). The deacetylation of chitin results with the formation of free amine groups that gives the solubility property to chitosan, so it is one of the most structural parameters that affect the physical, chemical and biological properties of the chitosan solution and chitosan based materials. It was

proven that DD effects the water uptake capacity, contact angle and crystallinity of chitosan films (Baskar and Kumar, 2009).

In a study, the effect of DD of chitosan films on physicochemical properties was investigated and it was found that higher DD causes improvement in mechanical properties, higher crystallinity index and lower water uptake capacity when compared to those with lower DD (Yuan et al., 2011).

DD also ensures increased biological properties in perspective of biomaterial studies. In literature, the effect of DD on wound healing properties was investigated and it was found that activated fibroblasts were highly seen in the more deacetylated group. Besides, it was observed that the wound break strength is stronger in highly deacetylated groups (Minagawa et al., 2007). In addition, due to amino residue increase, collagenase activity and wound healing process were accelerated in highly deacetylated groups. Stronger antimicrobial activity was observed with highly deacetylated chitosan samples since the active amino groups on backbone were increased (Pakravan et al., 2011).

In this study, the effect of MF homogenization conditions on the deacetylation degree of chitosan was investigated. The degree of deacetylation of chitosan solutions treated with different parameters of microfluidizer was evaluated based on FT-IR analysis (Figure 4.4). The amide I band at 1655 cm^{-1} is used for residual -CO-NH- group determination. The OH band at 3455 cm^{-1} is used as reference band and the deacetylation degree (%) was calculated from the ratio of the absorbances.

The baselines were attentively described according to the reference and illustrated in Figure 4.5 (Miya et al., 1980). The height of the peaks of amide I and -OH groups were adjusted as a baseline with the IR Solution (Shimadzu) software.

All groups showed similar spectra at different treatment conditions. However, the amide I band at 1655 cm^{-1} started to decay with the transformation of acetamide groups into primary amine groups by increasing the DD. In literature, it was also proven that significant deacetylation degree increase causes amide I band disappearance (Ko et al., 1997).

The DD was calculated by the absorbance ratios of the amide-I band and OH^{-1} band at 1655 cm^{-1} and 3450 cm^{-1} , respectively using the equation derived by Domszya and Roberts (1985). The deacetylation degrees of the chitosan solutions at different MF conditions were given in Table 4.4.

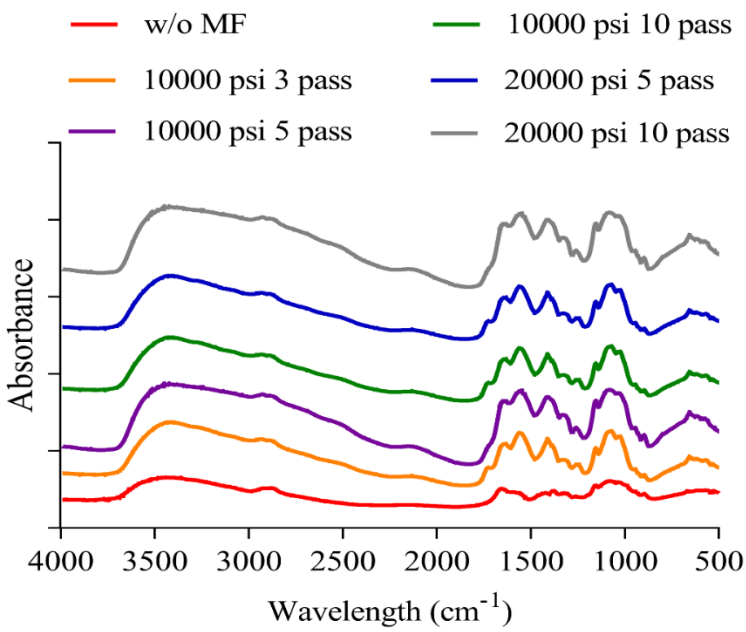

Figure 4. 4. FT-IR Spectra of chitosan exposed to MF treatment

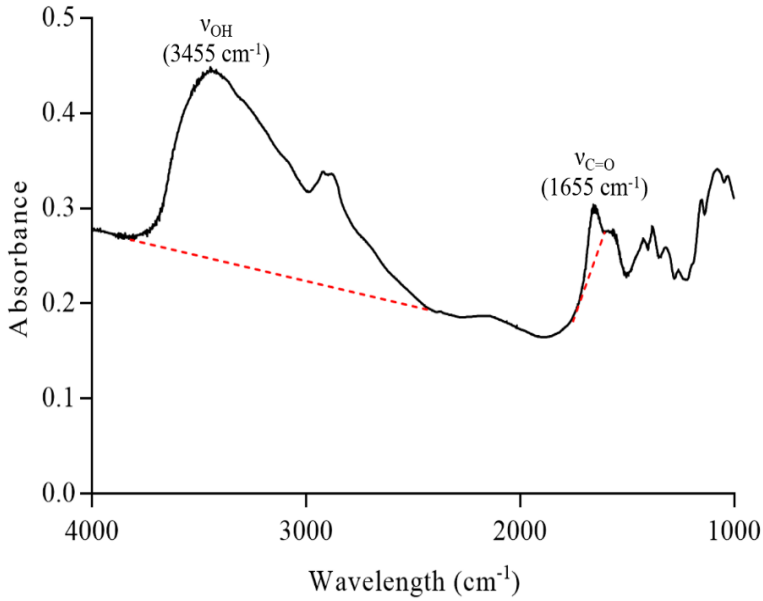

Figure 4. 5. Reference bands and corresponding baselines regarding the deacetylation degree of chitosan

It was observed that deacetylation degree of lyophilized chitosan without microfluidizer treatment had a deacetylation degree of 77.58%. The results seem reasonable since the original product was described as >75% deacetylated. The microfluidized samples showed higher deacetylation degree (80-85%) when compared to non-treated sample. The DD of samples treated with 3 and 5 passes were close to each

other. Results indicated that pass number affects the deacetylation degree more when compared to pressure term. In a study, the degree of deacetylation of chitosan was increased from 74 to 78% with a microfluidizer treatment of around 103 MPa (15000 psi) and 5 passes at 25°C (Kasaai et al., 2003).

Table 4. 4. Deacetylation degree of MF treated chitosan

Groups	Deacetylation Degree (%)
w/o MF	77.5±2.2
10,000 psi 3 pass	80.9±2.3
10,000 psi 5 pass	80.9±2.2
10,000 psi 10 pass	84.3±0.5
20,000 psi 5 pass	80.3±0.9
20,000 psi 10 pass	84.9±3.1

The deacetylation degree also plays an important role in crosslinking and stability of chitosan-based systems, which are essential factors for drug delivery systems. Gupta and Jabrail (2006) indicated that increase in DD causes higher encapsulation efficiency and more controllable release rate in chitosan microspheres. However, DD itself does not enough to draw a conclusion for characterization of chitosan that will use as drug delivery system. In the study, the effect of microfluidizer was well defined with rheology, viscosity, molecular weight and deacetylation degree results. Hence, it was found that microfluidizer parameters of 10,000 psi pressure, 3 and 5 passes were convenient for nanosphere production according to the microfluidization optimization studies.

4.1.4. X-Ray Diffraction (XRD) Analysis

XRD study was performed to display the clay distribution and structure in the polymer matrix. Figure 4.6 depicts the XRD pattern of the chitosan, montmorillonite and CS/MMT composites homogenized with 10,000 psi, 3 and 5 passes.

The characteristic peak was depicted in 2θ=20.7° due to diffraction of chitosan powder. In literature, the characteristic peak of chitosan powder was reported at 25° according to its high crystallinity (Hosseini et al., 2013). Two hydroxyl and one amino functional group of chitosan can provide an interaction between hydroxyl edges of MMT

layers by hydrogen bonding to ensure the penetration into MMT nanosheets (Thakur, Singh, and Singh, 2016). The characteristic diffraction peak of the MMT (Cloisite 10A) was observed approximately in 2θ=7.23°.

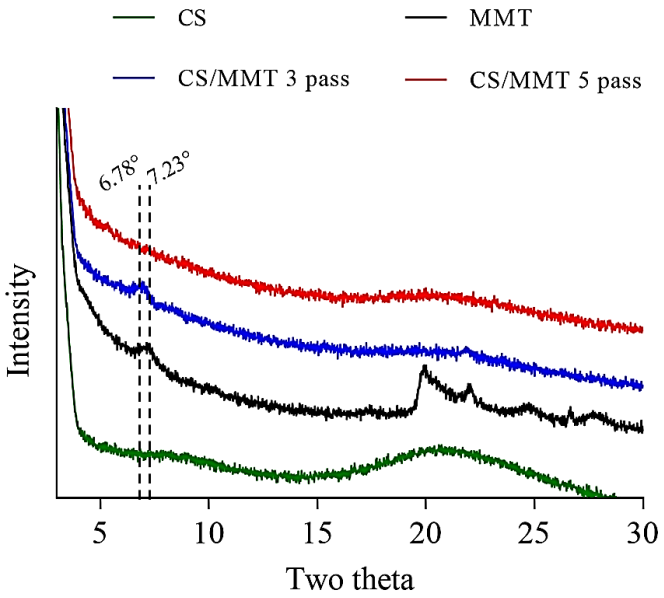

Figure 4. 6. XRD spectra of chitosan (CS), montmorillonite (MMT) and microfluidized CS/MMT nanocomposites

According to the Bragg's law (Equation 3.8), the peak at 7.23° indicates a basal d-spacing of 12.22Å. This peak has shifted left to 6.78° with microfluidizer application of 10,000 psi and 3 passes due to the intercalation of MMT layers. It was calculated that the d-spacing value increased to 13.03Å, which was significantly a sign of the intercalated structure (Wang et al., 2005). The permeation of chitosan into MMT galleries broadened the layer spacing. Furthermore, the characteristic peak was disappeared in the CS/MMT group microfluidized with 10,000 psi 5 passes that indicate the exfoliated structure. The cyclic application of a microfluidizer homogenization caused exfoliation of the single clay layers in the polymer matrix. In a study of Albalawi et al. (2016), it was observed that the characteristic peak for pristine nanoclay at 2θ=7° shifted to small angles with increasing the chitosan content due to the intercalation.

The exfoliated structure in nanocomposite system is preferable in drug delivery since it serves a tortuous pathway to drug for diffusion. Therefore, the exfoliated structure of MMT nanosheets can act as a cross-linker to ensure stability and slower release rate of hydrophilic drugs.

4.2. The Optimization of Electrospray Process Parameters

Electrospraying is a one-step technique that serves the advantage of production of micro-nanoscaled spheres with high yield. Fiber or sphere morphology can be achieved by tailoring the working parameters. Since chitosan has a polycationic nature, the strong electric field causes stretching during the whipping and bending motion of the solution. These charges cause a repulsive interaction, resulting with the liquid explosion forming spherical droplets in the electrical field. The sprayability of the chitosan solution is limited with electrospray method; since there are many inhibitor factors such as rigid chemical structure, polycationic nature and specific molecular interactions (Pakravan et al., 2011). In addition, hydrogen bonds in the solution increase the chain entanglements that supports fiber formation.

Needle gauge, applied voltage, the distance between needle and collector and the flowrate are the main parameters that affect the sprayability and the size of the spheres. Solution concentration, solvent type and the viscosity are the solution parameters that influence the morphology of the product. In this study, 2% (w/v) HMW chitosan solution was prepared in 90% (v/v) acetic acid solution to obtain nanospheres with electrospraying method. The acetic acid concentration of the solution was kept constant at 90% (v/v) since this concentration was found as optimal to decrease the surface tension of the chitosan solution and increases the charge density of jet (Geng et al., 2005).

In order to obtain uniformly sized perfectly spherical particles, the voltage, distance and the flow rate were optimized in terms of the nanospheres morphology and sizes. Firstly, the effect of needle gauge on the morphology was investigated as a preliminary study. Figure 4.7 shows the SEM images showed that decreasing the needle size causes fiber and irregularly shaped particle formation (Figure 4.7). In contrary, the solution flowed freely in larger sized needle gauge caused spherically shaped nanospheres with a size of 86.67±3.51 nm. Hence, the needle inner diameter was selected as 1.27 mm for spherical nanoparticle production.

The best voltage range for the electrospray (10-20 kV) was determined by observation of stable and continuous spray at the tip of the needle. Groups of electrospray parameters were depicted in Table 4.5. Experiments were carried out in triplicates and performed randomly. Furthermore, the effects of voltage, distance and the flowrate on

nanospheres morphology were investigated according to the SEM images of nanospheres (Figure 7).

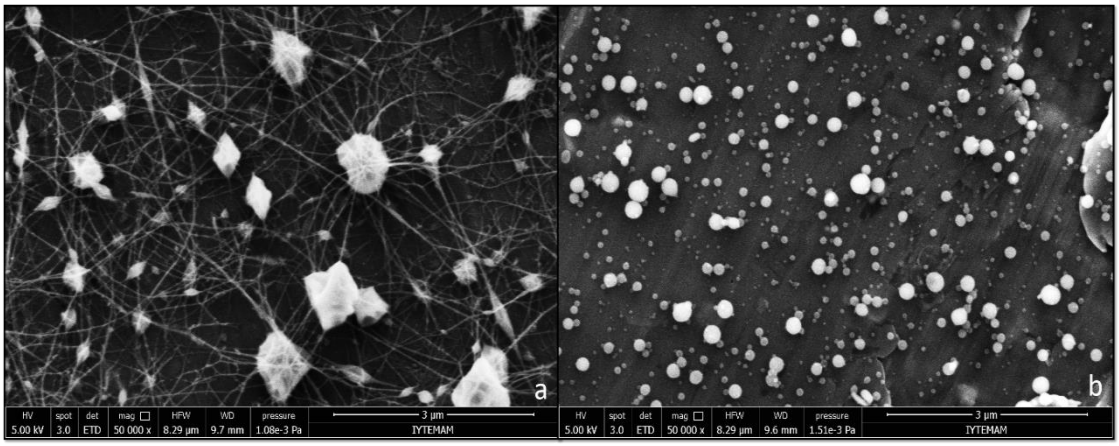

Figure 4. 7. The effect of needle size on particle morphology; needle inner diameters of 0.51mm (a) and 1.27 mm (b)

Table 4. 5. Electrospray group codes

Group	Voltage (kV)	Distance (cm)	Flowrate (ml/h)
A	10	5	5
B	20	5	5
C	10	10	5
D	20	10	5
E	10	5	10
F	20	5	10
G	10	10	10
H	20	10	10

The diameters of nanospheres were measured with ImageJ software and tabulated in Table 4.6. The histogram of size distribution was illustrated in Figure 4.9. According to the SEM images, fabricated nanospheres were found in an average size range of 87-141 nm. In literature, it was indicated that the increase in voltage causes narrow particle size distribution as well as size decrease (Hayati et al., 1987b). The same effect was observed in the groups by increasing the voltage from 10 to 20 kV while keeping flowrate and distance constant at 5 cm and 10 ml/h, respectively. In contrary, minimum flowrate (5ml/h) with minimum distance (5 cm) caused a wider distribution and formation of sticky spheres due to poor solvent evaporation (Figure 4.9).

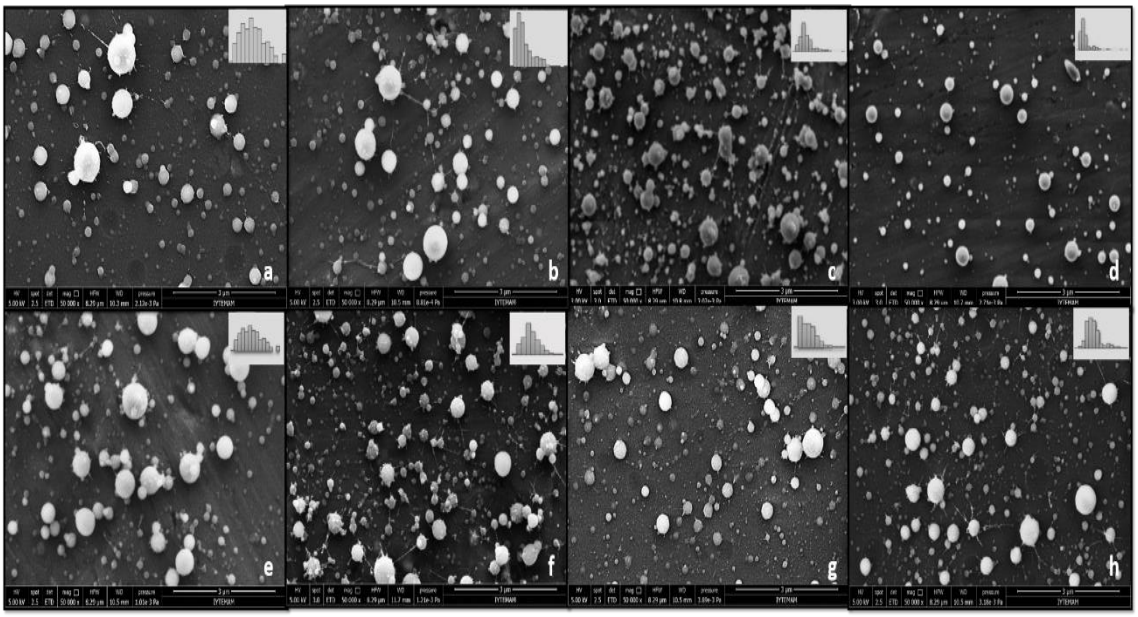

Figure 4. 8. Electrosprayed chitosan nanospheres (Groups were depicted in Table 5)

Table 4. 6. Mean sizes of nanospheres fabricated in various electrospray parameters

Voltage (kV)	**Distance (cm)**	**Flowrate (ml/h)**	**Diameter (nm)**
10	5	5	127.04±7.7
10	5	10	141.75±4.0
10	10	5	87.67±2.1
10	10	10	104.73±5.1
20	5	5	111.75±4.7
20	5	10	116.91±2.0
20	10	5	86.67±3.5
20	10	10	96.45±4.0

According to the observations, smaller nanospheres can be obtained by increasing the distance. SEM images show that decrease in distance significantly affects the nanosphere yield and morphology (Figure 4.10). When the voltage and flowrate were kept constant at 20 kV and 5 ml/h, average sizes were reduced from 111.7 to 86.67 nm by increasing the distance from 5 cm to 10 cm. The same reduction was observed with different voltage and flowrate values. The distance lets polymeric droplets to scatter and form smaller sized particles. In addition, the decrease in the voltage prohibits the fiber formation between spheres. However, lower voltage causes more solvent accumulation on the surface, which may degrade spheres.

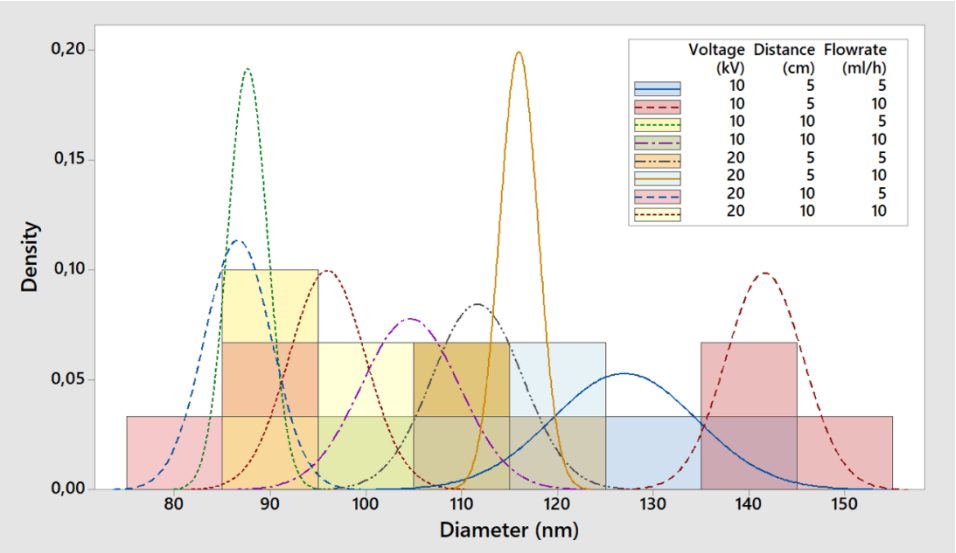

Figure 4. 9. Size distribution of nanospheres in various electrospray parameters

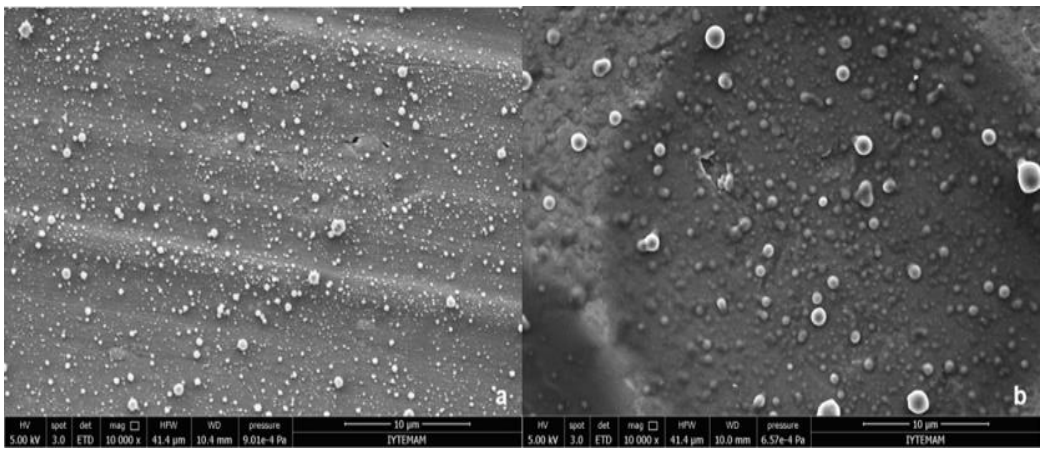

Figure 4. 10. The effect of distance on nanosphere morphology: 10 cm (a); 5 cm (b) (Voltage and flowrate were kept constant at 20 kV and 5 ml/h, respectively)

2 level full factorial design was performed to optimize the electrospray parameters with 95% two-sided confidence interval. The main effects of each parameter on average nanosphere diameter were shown in Figure 4.11.

Results implied that smaller nanosphere size could be achieved with higher voltage, higher distance and lower flowrate. It was inferred that each main effect significantly affects the response (Figure 4.12.b). In addition, two-way interactions of voltage-distance and voltage-flowrate also affect the size. However, two-way interactions of distance and flowrate, and the three-way interaction were not statistically significant in determining the nanosphere size. Therefore, these terms were canceled while performing the regression analysis.

- **Effect of voltage (A)**

In the study, a stable cone-jet was observed continuously in the applied voltage range of 10-20 kV. This fact can be attributed to the Rayleigh limit, the minimum magnitude of charge per solution drop that overcomes the surface tension that is the basis of sprayability of a solution. According to Pareto chart (Figure 4.12.b), the voltage (A) was found as a significant factor ($P<0.05$). In addition, the voltage interactions between distance and flowrate also affect the nanosphere diameter.

In each parametric case, the nanosphere diameters were reduced with increasing voltage which was supported with the literature (Zhang and Kawakami, 2010). The increase in voltage affects the jet current positively by increasing the number of charge carriers, and so leads to the formation of smaller sized nanospheres. Increased Coulombic forces at the tip of the needle cause more repulsion between the solution droplets, which induces the solution droplets to split up followed by size reduction. According to the observations, the voltage was set at 20 kV.

- **Effect of distance (B)**

It was found that distance is the main factor that affects the nanosphere diameter ($P<0.05$). The polymer solution is exposed to electrical charge more as the distance increases. Thus, droplets split up more and become smaller. The size reduction of particles by increasing the distance between needle and collector was illustrated in Figure 4.11. Therefore, a distance of 10 cm was found convenient for further studies.

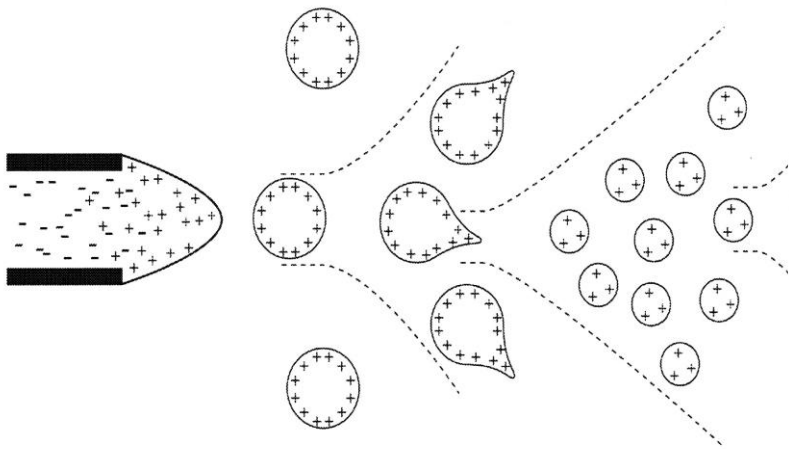

Figure 4. 11. Size reduction of particles due to increase in distance (Source: Ho et al., 2003)

➢ **Effect of flow rate (C)**

A significant increase in particle size was observed by increasing the flowrate. It could be explained by required electrical force to overcome hydrodynamic forces were lowered with the decreasing flow rate. A solution flowing out of the needle causes an elongation of the meniscus to form a jet. Therefore, the optimum flow rate occurs when spraying of the polymer solution leads to the formation of a stable jet, and forms smaller sized particles. At a higher flow rate, the effective flow rate of the polymer solution increases and the drops are formed very quickly, leading to the formation of larger sized particles. Songsurang et al. explained that solution drops are formed very quickly with an increased flowrate, leading to large particle formation (Songsurang et al., 2011). In a study, it was found that increasing the flowrate from 4 to 8 ml/h significantly increases the size of chitosan microcapsules (Xu and Hanna, 2007).A flowrate of 5 ml/h was selected for further studies. The response surface methodology (RSM) was applied to understand the main and interaction effects of the factors (Figure 4.13).

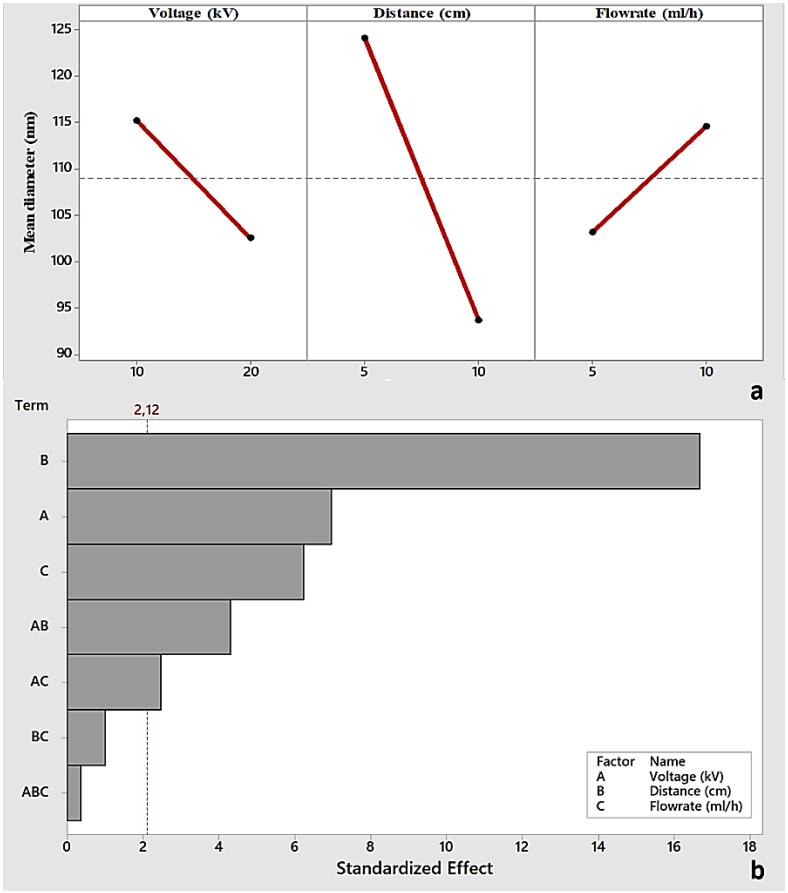

Figure 4. 12. Main effects for nanospheres diameter (a); Pareto chart for standardized effects (α=0.05) (b)

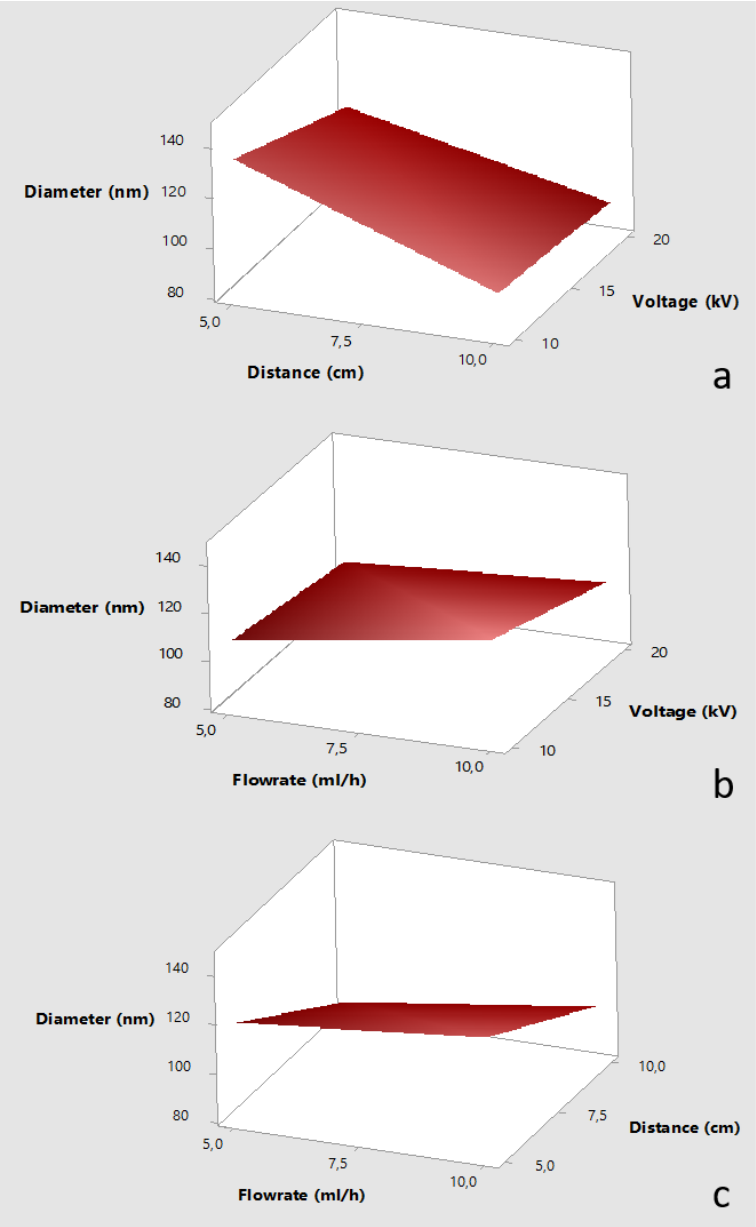

Figure 4. 13. Surface plots of nanosphere diameter, constant values: 5ml/h flowrate (a); 10 cm distance (b); 20 kV voltage (c)

In the latter case, insignificant terms were discarded from the ANOVA table and the nanosphere diameter was fit into an empirical equation by using a regression analysis tool of Minitab. The regression equation with uncoded terms was given in Equation 4.1.

$$D\ (nm) = 171.4 - 2.267A - 10.77B + 4.97C + 0.3133AB - 0.18AC \qquad (4.1)$$

where D is diameter, A is the voltage (kV), B is the distance (cm) and C is the flowrate (ml/h).

In the determined range, fabricated nanosphere sizes could be achieved with a good precision (R^2=0.9579, P<0.05). Normal probability plot of residuals for average nanosphere diameters (Figure 4.14) represents the precision of the observed results to the theoretical model. It could be observed that the experimental points are closely aligned.

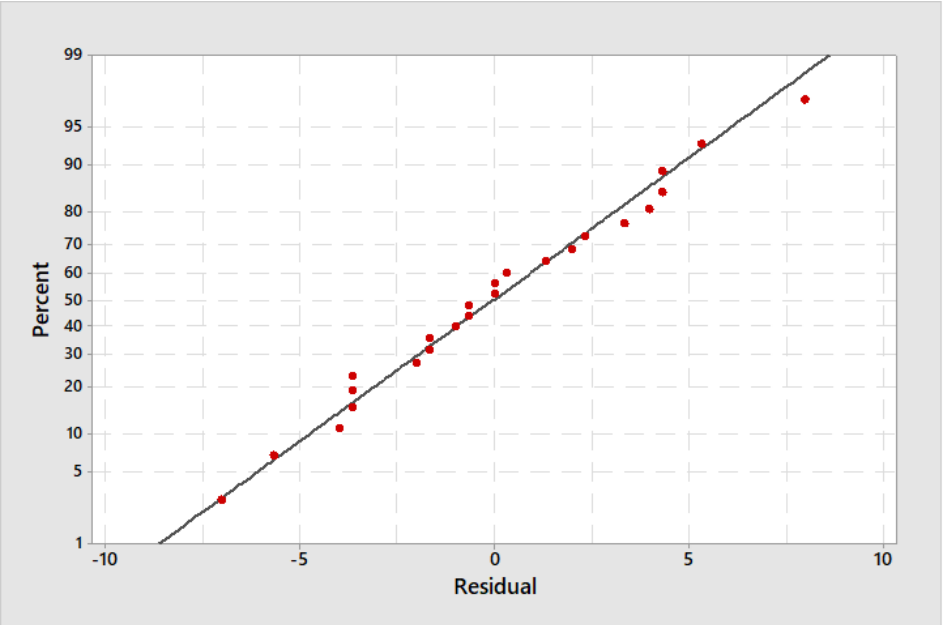

Figure 4. 14. Normal probability plot

As a result of the statistical design of the electrospray parametric optimization experiments followed by regression, electrospray parameters were set as a voltage of 20 kV, a distance of 10 cm and a flowrate of 5 ml/h that results with uniformly distributed nanospheres with the perfectly spherical shape.

Finally, MF treated CS/MMT nanocomposites were electrosprayed with parameters of 20 kV, 10 cm and 5 ml/h to observe the effect of homogenization parameters on sprayability of the solution. Figure 4.15 illustrates the SEM images of electrosprayed CS and CS/MMT nanocomposites. CS/MMT nanospheres treated with 10,000 psi were found smaller when compared with pure CS nanospheres. It was observed that solutions homogenized with a pressure of 20,000 psi are not suitable for electrospraying process, which was previously explained in microfluidizer parametric studies.

It was observed that all groups homogenized with 10,000 psi pressure results with nanosphere formation. The average size of the nanospheres homogenized with a pressure of 10,000 psi was given in Figure 4.16. It was observed that the average nanoparticle size

was reduced with the cyclic application of microfluidizer homogenization. The group treated with 10,000 psi 5 passes gave the most uniform size distribution.

By combining the knowledge of microfluidizer optimization results and SEM images of final products, it was decided to produce drug loaded nanospheres with MF conditions of 10,000 psi pressure with 5 passes.

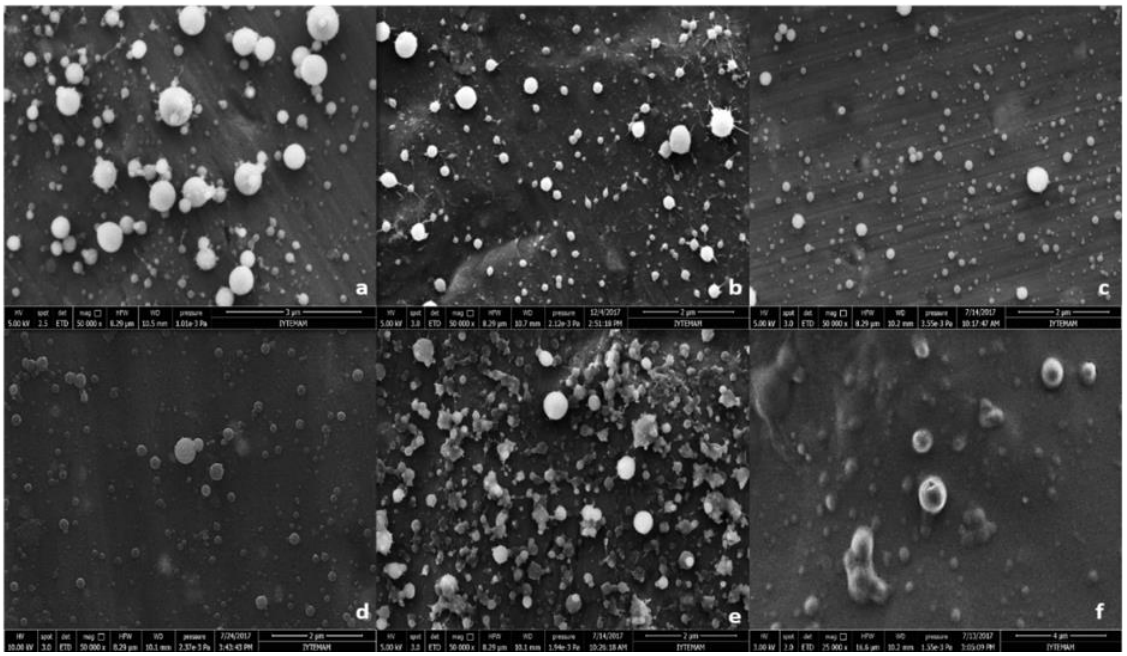

Figure 4. 15. SEM images of microfluidized CS and CS/MMT nanospheres: pure CS (a); 10,000 psi 3 pass (b); 10,000 psi 5 pass (c); 10,000 psi 10 pass (d); 20,000 psi 5 pass (e); 20,000 psi 10 pass (f)

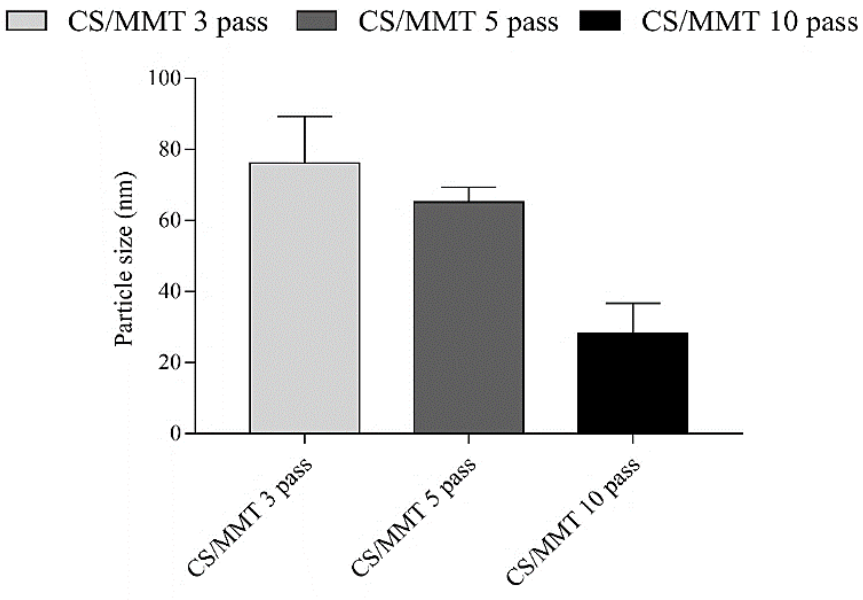

Figure 4. 16. Average diameters of nanospheres microfluidized with 10,000 psi pressure; 3, 5 and 10 passes

4.3. Characterization of Chitosan Nanoclay Composite Nanospheres

4.3.1. Morphology of the Nanospheres

In this study, prepared nanospheres were characterized in terms of their morphology, hydrodynamic sizes and surface charges. The size and the surface charge of the carriers has a major influence on release profile and circulation in body fluid in nanoparticulate drug delivery systems. Hence, these terms should be well-characterized to enlighten the major factors affecting the release mechanism.

Chitosan micro or nanospheres cannot be used for long-term drug release systems without the presence of crosslinker or nanofiller since they degrade in aqueous media in a short time. Therefore, low stability of chitosan-based drug carriers should be compensated with using crosslinkers or nanofillers. In literature, several studies have attempted to form polyelectrolyte complexes with chitosan to overcome the low-stability of the chitosan (Hamman, 2010). However, crosslinkers or composite formation is better to ensure the stability of long-term drug release systems. In this study, stability improvement was achieved by the addition of MMT clay into chitosan. Similarly, MMT nanoclay provided an improved stability in cinnamon oil capsulated chitosan microspheres (Güneş, 2016). This fact was proven with the DLS analysis. According to the SEM images of chitosan nanospheres, the average size was found as 86.67±3.512 nm for the optimum electrospraying conditions (Table 4.6). Figure 4.17 shows hydrodynamic sizes the pure chitosan nanospheres at the two different measurement times (t=0 and t=60 min) As seen in Figure 4.17.a, the average hydrodynamic size of chitosan nanospheres at the first scan of DLS analysis is 78±3 nm, however, it could be seen that chitosan nanospheres were disintegrated as 2 and 25-30 nm in sizes and some part of particles formed aggregates after 60 min measurement time (Figure 4.17.b).

The MMT nanofiller ensures the stability in particulate systems by acting as a physical cross-linker (Zheng et al., 2011; Ennajih et al., 2012). Therefore, MMT nanoclay was used to ensure stability and create a tortuous pathway for sustained drug release in this study.

In Figures 4.18 and 4.19, the morphology CS/MMT nanospheres were illustrated with SEM and AFM analysis, respectively. It can be observed that nanospheres have a

smooth surface and perfectly spherical shape (Figure 4.18). In AFM analysis, the electrosprayed particles were dispersed in deionized water, diluted 10000-fold and dried under ambient conditions. Hence, size reduction of nanospheres was easily observed with AFM images. Particle Analysis tool of Nanoscope Analysis software (Bruker) was used to determine the average diameter of nanospheres in the AFM image. The average diameter of nanospheres was found as 61.04±7 nm (Figure 4.19).

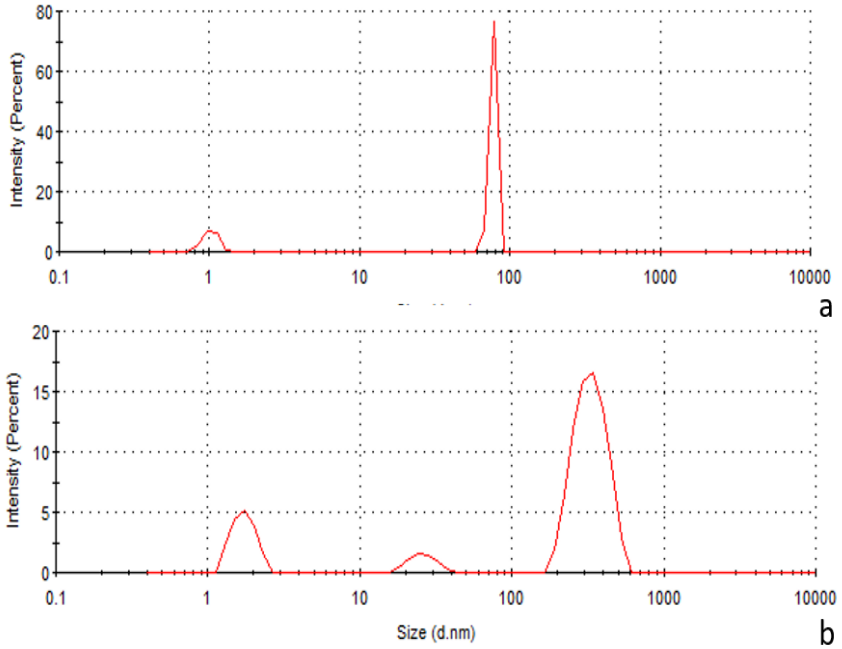

Figure 4.17. Hydrodynamic sizes of non-stable chitosan nanospheres; measurements taken at the initial time (t_0) (a) and 60 minutes (b)

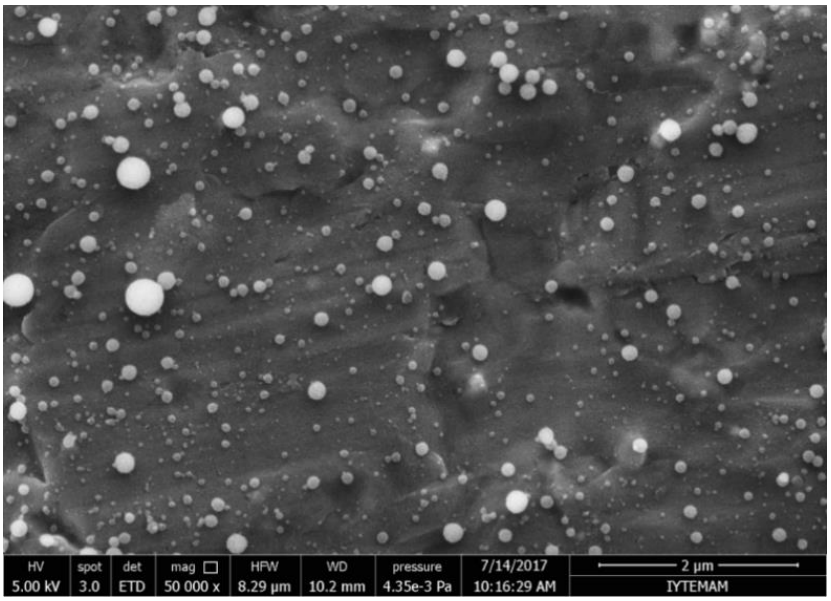

Figure 4. 18. SEM image of electrosprayed CS/MMT nanospheres

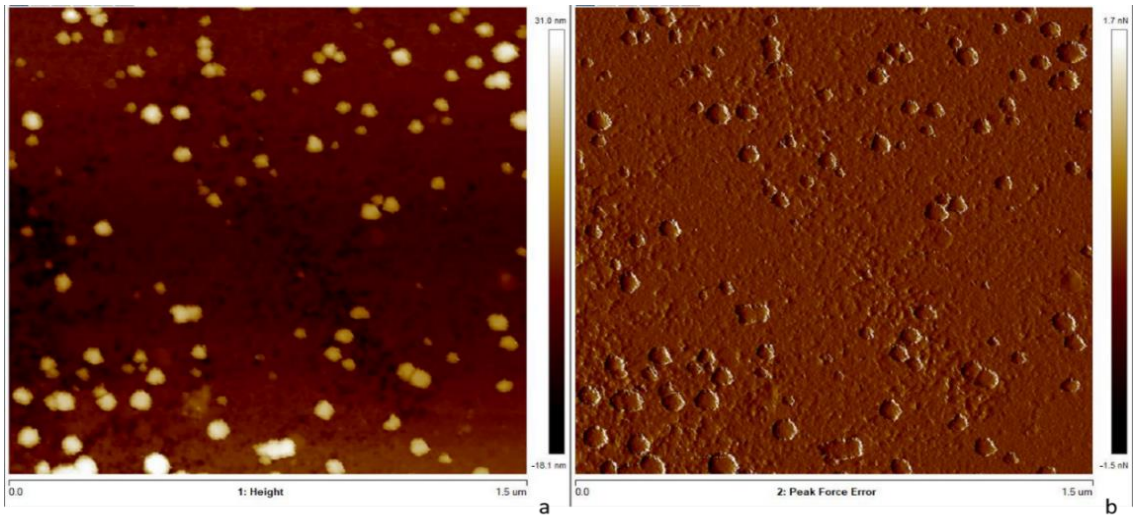

Figure 4. 19. AFM image of electrosprayed CS/MMT nanospheres (1.5µm x 1.5µm)

Furthermore, DLS analysis was performed to obtain the hydrodynamic sizes of the nanospheres. The size distribution of CS/MMT nanospheres dispersed in 1x PBS (pH=7.4) was given by intensity % (Figure 4.20). According to the results, narrow size distribution was obtained. The average hydrodynamic size of CS/MMT nanospheres homogenized with microfluidizer conditions of 10,000 psi 5 passes were found as 65.17±4.3 nm, which is in very good agreement with the AFM results (69.17±7 nm).

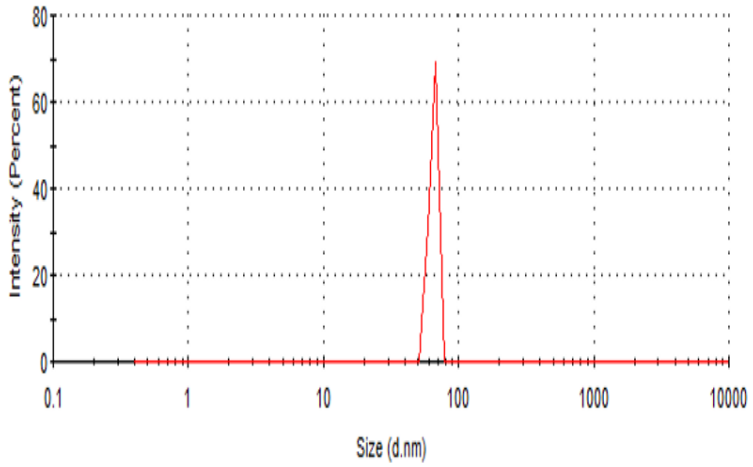

Figure 4. 20. Intensity size distribution of CS/MMT nanospheres

Antibiotic (Vancomycin and Gentamicin sulfate) loaded nanospheres were also observed with SEM and AFM analysis with two different magnitudes. According to the SEM results, vancomycin loaded nanospheres with a polymer:drug ratio of 4:1 and 8:1 has an average diameter of 224±5.13 and 168.93±4.96 nm, respectively (Figure 4.21).

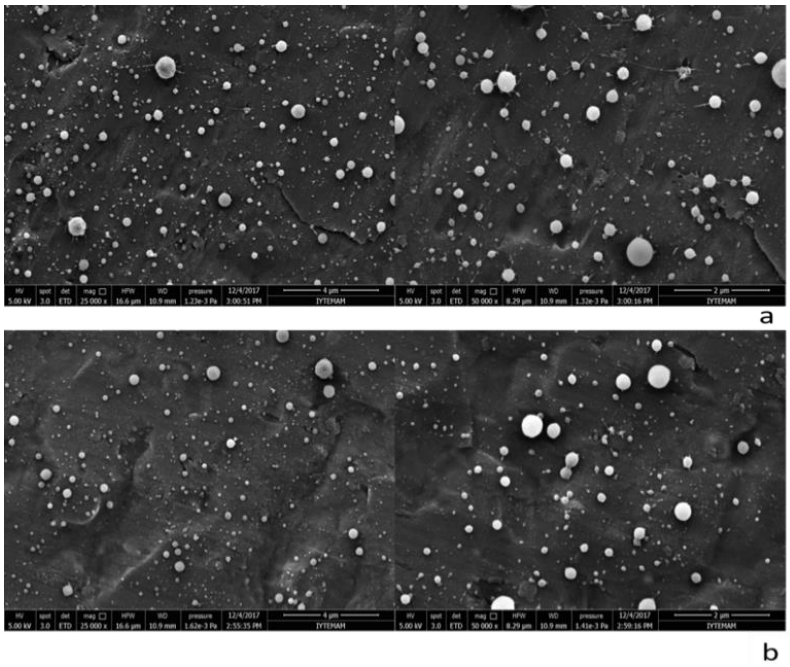

Figure 4. 21. SEM images of Vancomycin loaded nanospheres with a polymer:drug ratio of 4:1 (a) and 8:1 (b).

The AFM images of the Vancomycin loaded nanospheres with a P:D of 4:1 and 8:1 were given in Figures 4.22 and 4.23. AFM images showed that Vancomycin loaded groups carried their spherical shape after immersion in PBS and drying with a vacuum oven. According to the SEM and AFM imaging, sizes of fabricated nanospheres were in nanometer scale range. However, the most accurate sizes of the particles in the liquid media were determined with DLS analysis.

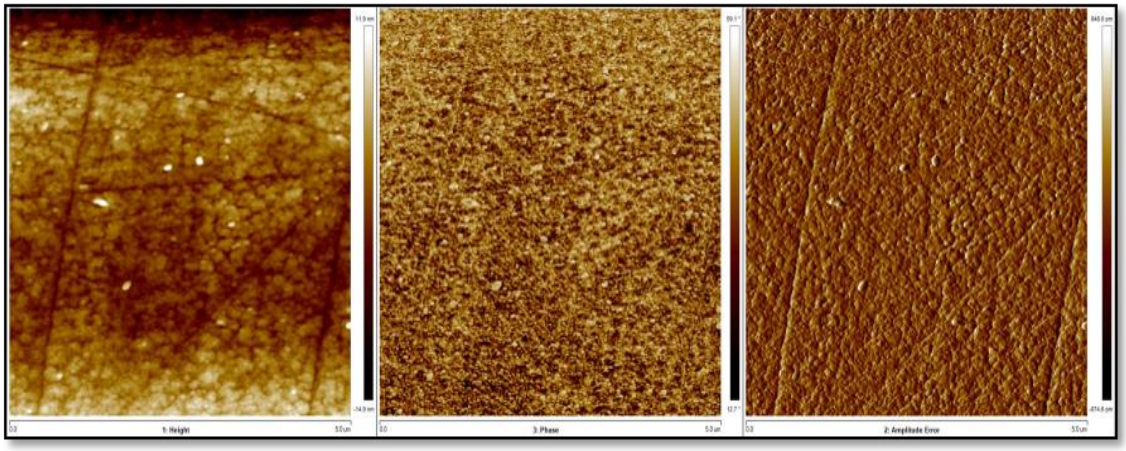

Figure 4. 22. AFM images of Vancomycin loaded nanospheres with a polymer:drug ratio of 4:1.

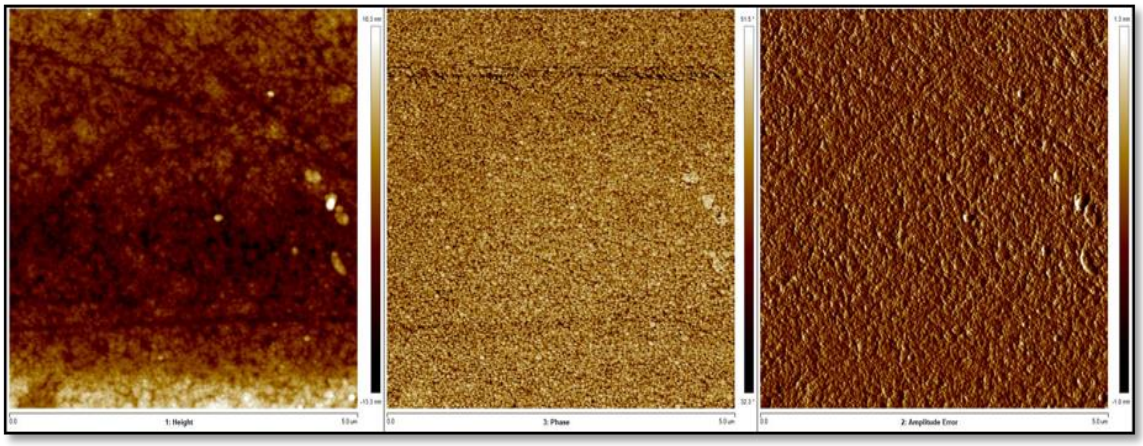

Figure 4. 23. AFM images of Vancomycin loaded nanospheres with a polymer:drug ratio of 8:1.

The AFM results were compared with the hydrodynamic sizes measured by DLS analysis (Figure 4.24). The mean hydrodynamic size was found as 351±20.18 nm and 210±19.25 nm for the groups having chitosan to Vancomycin ratio of 4:1 and 8:1, respectively. As it is known, DLS analysis gives the hydrodynamic size distributions of particles swollen in solution, while the nanospheres were dry and non-treated in SEM analysis. Therefore, higher mean size values were achieved by DLS analysis compared to SEM, which was also proven in the literature findings (Songsurang et al., 2011; Bai and Hu, 2014).

It was observed that particle sizes were reduced with the increase in polymer:drug ratio (P:D) as it was expected. In this thesis study, the polymer concentration was kept constant while drug concentration was altered. The increase in nanosphere size can be attributed to drug integration on the polymer matrix. Our results were found in good agreement with VC loaded CS microspheres (3-5 μm range sizes) prepared by spray drying (Cevher et al., 2006) and salicylic acid and gentamicin loaded CS nanoparticles prepared by ionic crosslinking method (Ji et al., 2011). Particle size decreased with an increase in P:D ratio. However, ciprofloxacin loaded chitosan nanoparticles prepared by ionic gelation showed that particle sizes increased with an increase in P:D ratio.

Furthermore, same analyses were performed on Gentamicin releasing nanospheres. Figure 4.25 represents the SEM images of gentamicin loaded nanospheres having a P:D ratio of 10:1 and 20:1, respectively. According to the SEM images, produced gentamicin loaded nanospheres have perfectly spherical shapes.

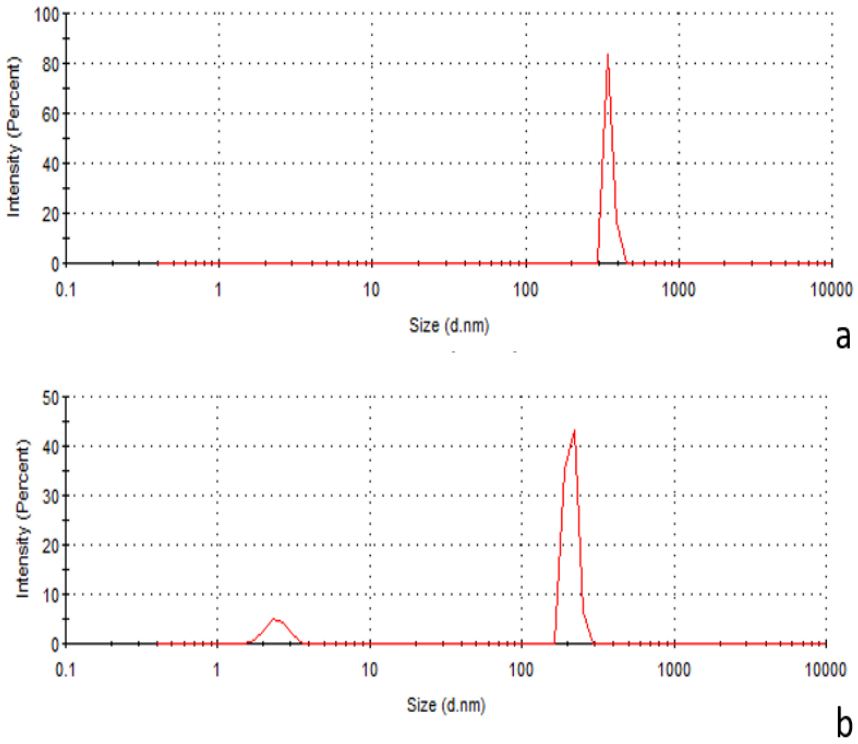

Figure 4. 24. Intensity size distributions of Vancomycin loaded nanospheres with polymer:drug ratio of 4:1 (a) and 8:1 (b) respectively

The AFM images of the Gentamycin loaded nanospheres with a P:D of 10:1 and 20:1 were given in Figures 4.26 and 4.27, respectively.

The nanospheres attached on aluminum foil was collected by washing the collector surface and making serial dilutions to observe nanosphere morphology with the AFM analysis. The AFM images of the nanospheres indicated that the spherical shape was preserved even they were hydrated and air-dried. They did not show any aggregate formation and they observed as individual particles.

DLS results indicated that hydrodynamic sizes were increased with drug incorporation when compared to the control (unloaded) CS/MMT nanospheres (65.17±4.3 nm). Additionally, it can be concluded that nanosphere sizes were increased by increasing the drug concentration.

The mean hydrodynamic size was found as 246.4nm and 181.6nm for the groups having P:D of 10:1 and 20:1, respectively (Figure 4.28). Literature findings also support that drugs adsorbing on the particle surface and incorporating in polymer matrix increase the particle sizes compared to unloaded drug sphere (Esmaeili et al., 2007).

The particle size of the carrier material is a critical parameter in drug release systems. In general, the release rate is fastened as particle size decreases. In literature, it

was found that smaller polystyrene particles lead to faster coumarin-6 release because of their larger surface area per unit volume (Yin Win and Feng, 2005).

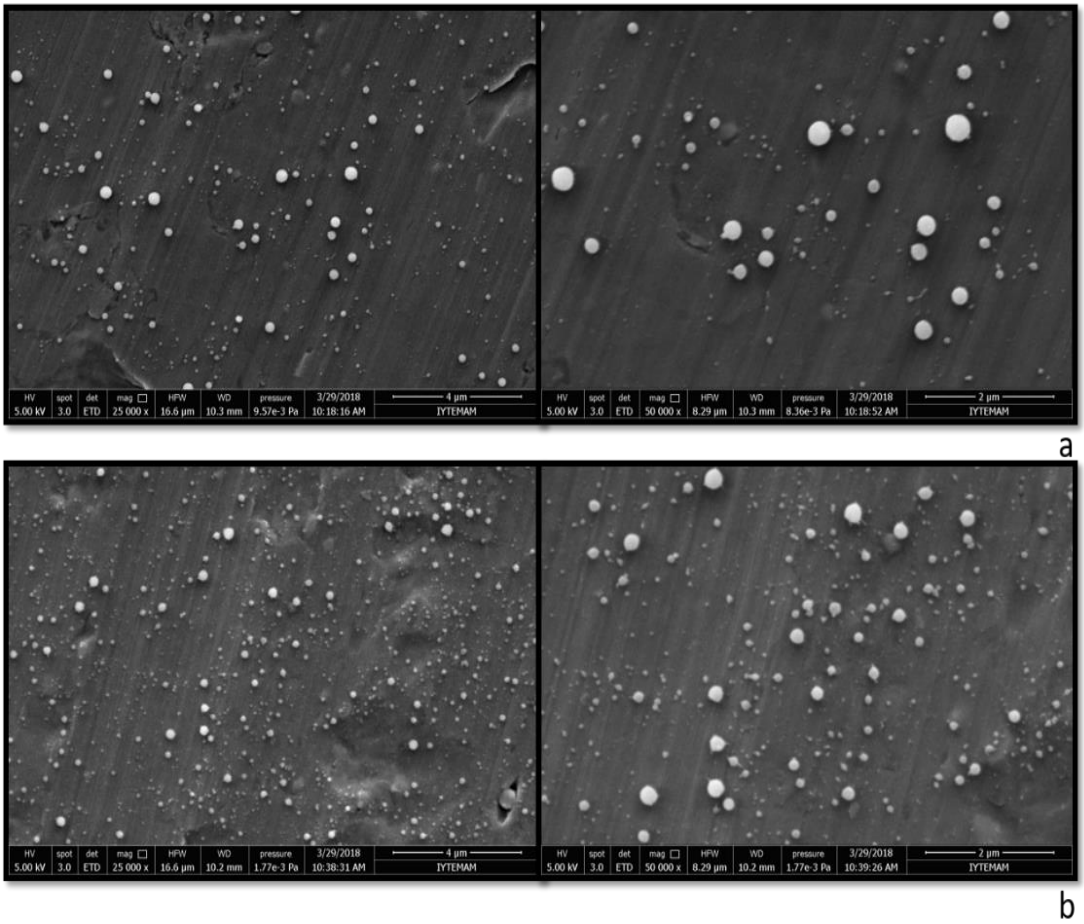

Figure 4. 25. SEM images of Gentamicin loaded nanospheres with a polymer:drug ratio of 10:1 (a) and 20:1 (b)

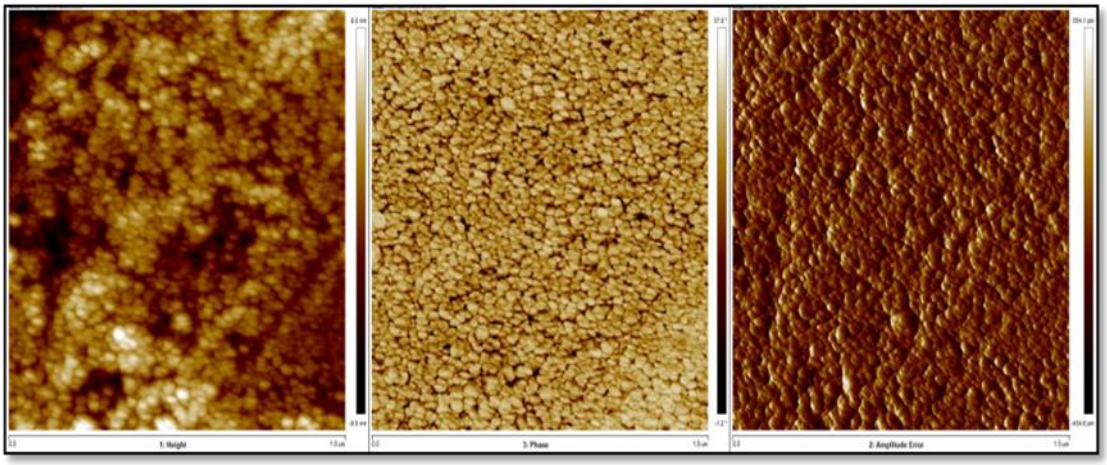

Figure 4. 26. AFM images of Gentamicin loaded nanospheres with a polymer:drug ratio of 10:1

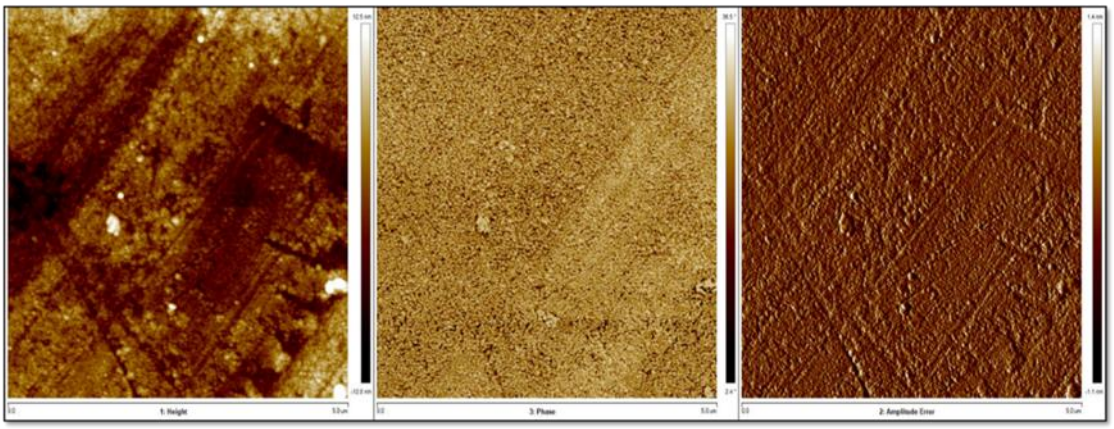

Figure 4. 27. AFM images of Gentamicin loaded nanospheres with a polymer:drug ratio of 20:1

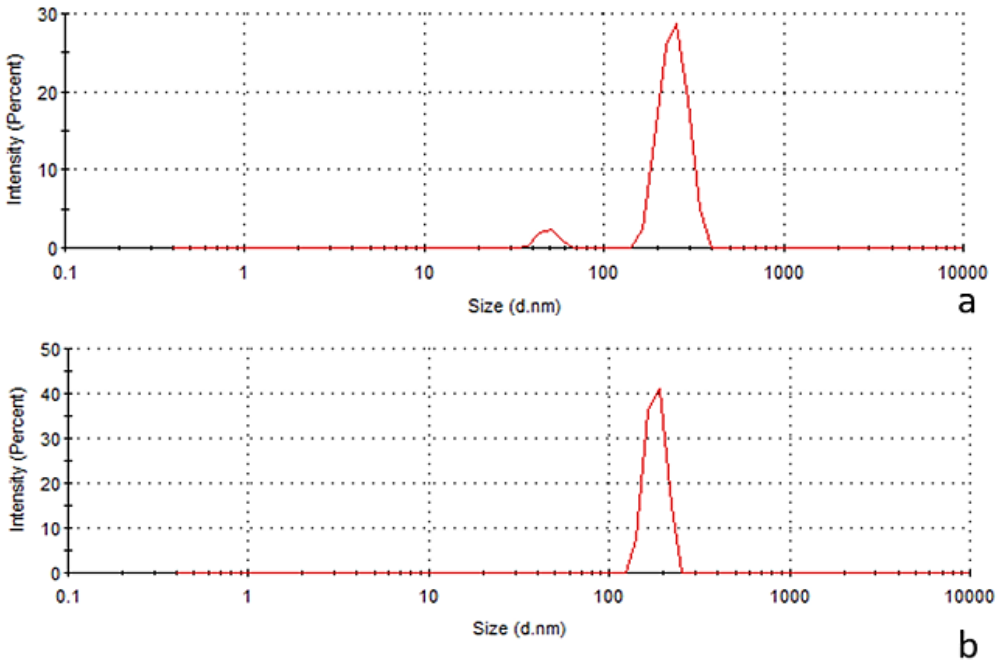

Figure 4. 28. Intensity size distributions of Gentamicin loaded nanospheres with polymer:drug ratio of 10:1 (a) and 20:1 (b) respectively

4.3.2. Zeta potential

The stability of the particles in a surrounding fluid is important criteria to overcome the aggregate formation of nanosized drug delivery systems. According to DLVO electrostatic theory, the stability of a system can be expounded as a balance between the electrical repulsion and attractive van der Waals' forces (Honary and Zahir, 2013). The surface charge of the drug carrier nanoparticle should be characterized since

it affects the interaction with surfaces and drug release profile in a different type of media. Thus, the zeta potential of the drug carrier composite nanospheres was determined to investigate the electrostatic interactions.

Therefore, the point of zero charges (PZC) of MMT was determined by measuring its zeta potential by increasing pH (Figure 4.29). According to the findings, the PZC of MMT is 6.2. In literature, it was indicated that the PZC of MMT varies between 6.4 – 7.2 (Kosmulski, 2011). The zeta potential of MMT varied at different pH values due to proton adsorption or desorption on edge -OH- groups and isomorphous substitutions at the faces of platelets (Forano, 2004). The amphoteric parts were positively or negatively charged due to the pH of the media. Some parts of cations do not strongly hold to the structure hence readily exchanged by other ions.

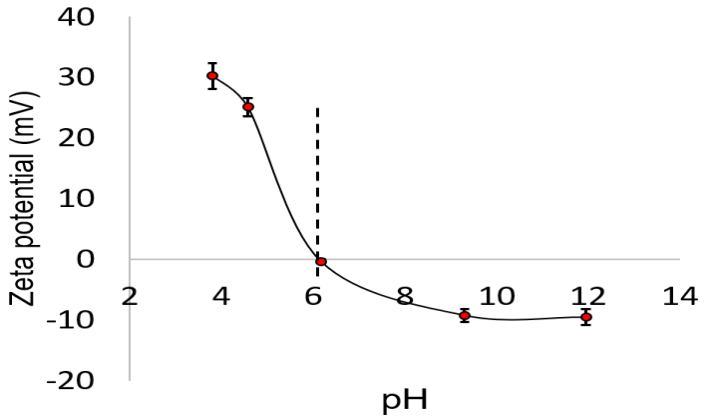

Figure 4. 29. The zeta potential of MMT in various pH

Moreover, surface charges of nanospheres were measured immediately after suspension in deionized water and PBS with sonication. Table 4.7 indicates the zeta potential of nanospheres in ultrapure water and PBS. The surface charges of CS/MMT nanospheres were found higher in ddH2O when compared to PBS. This fact was well explained in the study of Huang et al. (2016). The continuous dissolution of atmospheric CO_2 lead to pH reduction in water that paves the way for protonation of amine groups of chitosan. Therefore, relatively positive zeta potential values were observed. It was found that prepared CS/MMT nanospheres are positively charged due to polycationic nature of chitosan. The surface charge of neat CS nanospheres was found in a range of 24-29 mV. However, the zeta potential of neat CS/MMT nanospheres were measured as 13.3-18.7 mV due to the negative charge of MMT nanoclay in the working pH. Hence, prepared drug loaded nanospheres carried their stability in aqueous media according to their

repulsive forces. In literature, it was indicated that Vancomycin and Gentamicin are positively charged drug molecules (Williams and Domen, 1990; Huang et al., 2016). However, the zeta potentials of drug-loaded nanospheres were decreased when compared to neat CS/MMT. The decreased zeta potential of drug loaded nanospheres may be attributed to stability decrease due to initial diffusion of drugs attached to nanosphere surface to the medium. All antibiotic loaded nanospheres have a positive zeta potential showing good physical stability of the dispersions. In addition, the positive zeta potential is advantageous in antibiotic delivery systems since most of the cellular membrane surfaces are negatively charged (Honary and Zahir, 2013).

When the results were evaluated together with the DLS study, it was observed that particles having smaller zeta potential values have larger sizes. The fact can be attributed to relatively higher zeta potential prevents particles to form aggregates. The same effect was also observed for insulin-releasing chitosan nanoparticles prepared by Avadi et al. (2010) and gentamicin/salicylic acid releasing nanoparticles by Ji et al. (2006). It can be concluded that fabricated nanospheres will ensure the good stability in the bloodstream at incubation time to demonstrate the therapeutic drug release.

Table 4. 7. Surface charges of CS/MMT nanospheres

Groups	**Zeta Potential (mV)**	
	in PBS	**in ddH_2O**
CS	24.0±3.6	29.0±2.1
CS/MMT	13.3±1.3	18.7±0.1
CS/MMT-VC (4-1)	5.7±0.2	8.2±1.1
CS/MMT-VC (8-1)	12.3±1.7	17.4±2.3
CS/MMT-GC (10-1)	4.3±0.1	7.8±1.5
CS/MMT-GC (20-1)	6.9±0.6	9.9±0.8

4.3.3. Fourier Transform Infrared (FT-IR) Analysis

Functional groups of chitosan, MMT nanoclay and drugs were investigated with FT-IR analysis. Firstly, chitosan and MMT nanoclay interactions were studied (Figure 4.30). Main characteristic bands and their presence in groups were depicted in Table 4.8.

The FT-IR spectrum of chitosan consists of characteristic bands appeared at 1655 cm^{-1} (C=O stretching of amide I), 1560 cm^{-1} (N-H bending of amine) and 1380 cm^{-1} (C-N stretching and N-H bending of amide linkages). The main characteristic peaks of MMT are at 3667 cm^{-1} (Al-OH stretching), 1020 cm^{-1} (Si-O stretching), 913 cm^{-1} (Al-Al-OH). The peaks of number 5 (-CH- stretching) and 6 ($-CH_2$ vibration) were located on MMT spectra due to the organic modification (Cervantes-Uc et al., 2007). In the case of CS/MMT composite groups, the IR spectra showed that the characteristic bands of both CS and MMT that appeared in the CS/MMT composite.

The characteristic amide I (1655 cm^{-1}), amine (1560 cm^{-1}) and amide III (1380 cm^{-1}) peaks of chitosan slightly shifted to left in CS/MMT composite. The characteristic band of MMT due to $-CH_2$ vibration (2916 cm^{-1}) was seen in the CS/MMT composite. The interaction of CS and MMT was ensured by the hydrogen bonding due to hydroxylated silicates of MMT and, amino and hydroxyl groups of CS (Wang et al., 2005). The MMT Si-O stretching (1020 cm^{-1}) was overlapped with CS peaks in the IR spectra of CS/MMT group.

The peak at 2990 cm^{-1} due to OH stretching was shifted to 2934 cm^{-1} and overlapped with the characteristic peak of MMT due to $-CH_2-$ vibration at 2916 cm^{-1}. The intensities of the characteristic peak of MMT due to Al-OH-Al stretching (913 cm^{-1}) and -CH- bending (2852 cm^{-1}) were decreased in composite groups when compared to pure MMT. This fact also confirms the interaction between chitosan and MMT (Abdollahi et al., 2012).

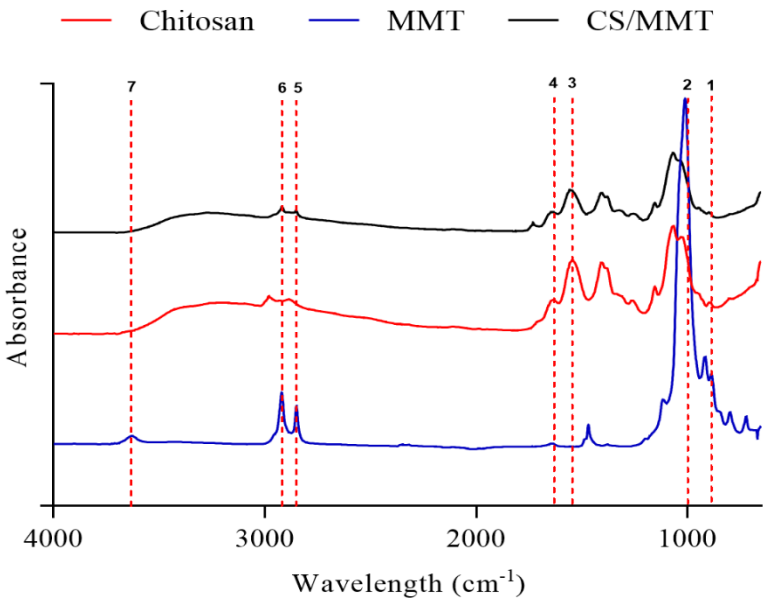

Figure 4. 30. IR spectrum of chitosan, MMT and CS/MMT composite groups.

Table 4. 8. Characteristic bands of CS and MMT

No	Wavenumber (cm^{-1})	Band	Formulation	Reference
1	913	Al-Al-OH stretching	MMT CS/MMT	Long et al., 2007
2	1020	Si-O stretching	MMT	Koosha et al., 2015
3	1560	N-H bending	Chitosan (amine)	Baxter et al., 1992
4	1655	C=O stretching	Chitosan (amide I)	
5	2852	-CH- stretching	MMT CS/MMT	Huang et al., 2015
6	2916	$-CH_2$ vibration	MMT CS/MMT	
7	3667	AlOH and SiOH stretching	MMT	Long et al., 2007

Additionally, chemical interactions between the drug (Vancomycin and Gentamicin) with CS/MMT nanocomposite was analyzed with FT-IR analysis. Figure 4.31 shows the IR spectra of the CS/MMT, Vancomycin and the vancomycin loaded CS/MMT groups with a polymer to drug ratio of 4:1 and 8:1. Vancomycin has a characteristic absorption band of -OH- stretching (3450 cm^{-1}), C=O stretching (1652 cm^{-1}), aromatic C=C stretching (1502 cm^{-1}) and phenolic groups (1232cm^{-1}) (Yang et al., 2013; Yao et al., 2013). The existence of most of these bands confirmed the presence of Vancomycin in the prepared nanospheres and moreover, the interaction between the polymer matrix and vancomycin was supported with hydrogen bonds (3750-2250 cm^{-1}) and observed as a shifted and broadened band.

The FT-IR spectra of CS/MMT, Gentamicin and Gentamicin loaded CS/MMT groups with a polymer to drug ratio of 10:1 and 20:1 were depicted in Figure 4.32. In literature, it was indicated that the Gentamicin spectra includes a strong absorption band due to stretching vibrations of C-N and C-O between 1300-900 cm^{-1}; N-H vibration at 1650-1400 cm^{-1} (Rapacz-Kmita et al., 2015). Most of the characteristic peaks of

Gentamicin were depicted in the IR spectra of Gentamicin incorporated groups. The Gentamicin incorporation in the chitosan-MMT matrix can be explained by hydrogen bonding due to shifts of amide I and II groups of the CS.

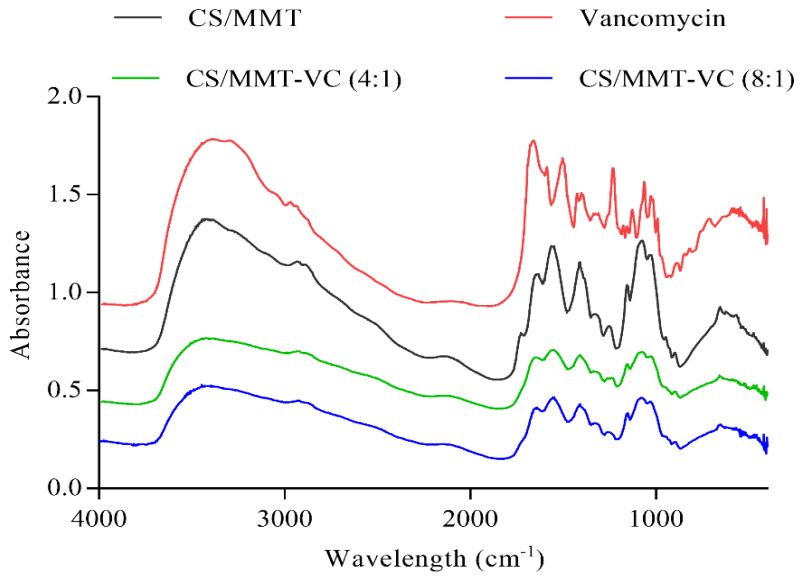

Figure 4. 31. The IR Spectra of CS/MMT, Vancomycin (VC) and VC loaded CS/MMT groups with a polymer: drug ratio of 4:1 and 8:1

The intensity of hydroxyl peak (3420 cm^{-1}) was weakened and broadened in Gentamicin loaded matrix. This change was linked with the merge of chitosan and gentamicin -OH- bending at 3415 cm^{-1} (Ji et al., 2011; Huang et al., 2016).

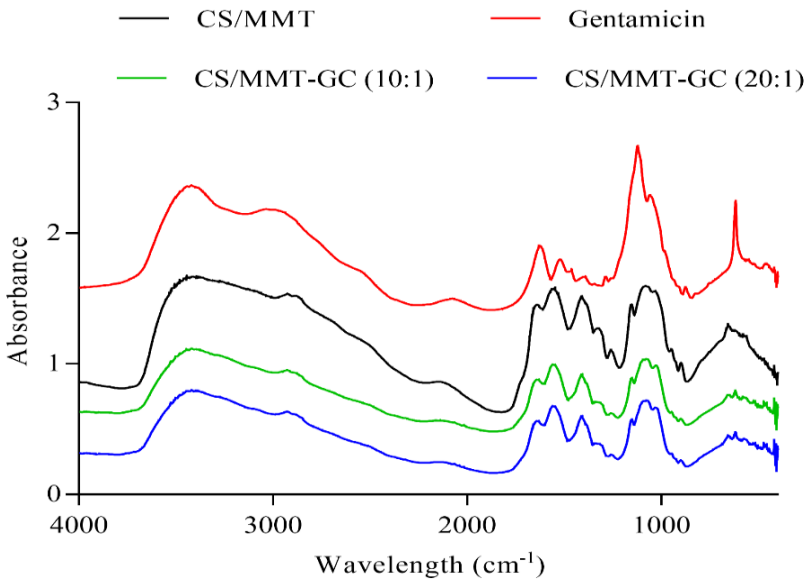

Figure 4. 32. The IR Spectra of CS/MMT, Gentamicin (GC) and GC loaded CS/MMT groups with a polymer: drug ratio of 10:1 and 20:1

4.4. *In vitro* Drug Release Profile and Kinetics

The drug loaded chitosan nanospheres were aimed to be sustained drug releasing materials to prevent the inflammations in bone tissue. Therefore, encapsulation efficiency and the drug release profiles were determined.

4.4.1. Encapsulation Efficiency

The drug encapsulation efficiency (EE) is the ratio of drug entrapped in polymer matrix over the amount of drug that was given in system. Therefore, entrapment efficiencies of the nanospheres were determined according to the standard calibration curves and depicted in Table 4.9. The calibration curves were given in Appendix B. It was observed that the nanocomposite formation significantly increased the encapsulation efficiency. The nanocomposite structure improved the Vancomycin entrapment of the matrix from 80 to 86% with a same P:D ratio. Similarly, gentamicin incorporation was significantly increased from 76 to 94% with nanofiller dispersion in the chitosan matrix. According to the results, it could be concluded that the entrapment efficiency of the CS/MMT matrix increases as a polymer to drug ratio (P:D) increases. The entrapment efficiencies of Vancomycin loaded groups were found as 79.04 and 86.56 for the P:D of 4:1 and 8:1, respectively. The incorporation of drug into polymer matrix becomes easier with the increase in the ratio of polymer to drug, which results in increasing entrapment efficiency. Similarly, the entrapment efficiencies of gentamicin loaded groups were found as 90.59 and 94.73 for the P:D of 10:1 and 20:1, respectively. The polymer to drug ratio is known as a significant factor that affects the drug release. It was found that encapsulation efficiency of the nanospheres increased with the increase in the polymer to drug ratio (Desai and Park 2005; Ji et al., 2011).

Studies revealed that the drug encapsulation efficiency strongly depends on particle size and processing method. In a study, spray-dried chitosan nanoparticles showed higher Vancomycin encapsulation efficiencies (72-76.2%) compared to that of freeze-dried nanoparticles (32.3-38.4%). On the other hand, spray dried microparticles with the same formulation showed an encapsulation efficiency ranging between 7.2-12.6% (Cerchiara et al., 2015). In another study, it was found that spray-dried

Vancomycin releasing chitosan microparticles prepared different polymer to drug ratio of 1:1 to 4:1 have encapsulation efficiency over 98% (Cevher et al., 2006).

The Gentamicin encapsulation efficiency of TPP crosslinked chitosan nanoparticles prepared by Ji et al. (2011) showed an EE in a range of 63.3-79.8%. Similarly, they observed an enhanced EE due to increase in the polymer to drug ratio. In a study by Huang et al. (2016), it was reported that prepared Gentamicin releasing chitosan/fucoidan nanoparticles have an encapsulation efficiency over 90% that is higher than previous studies.

Table 4. 9. Encapsulation efficiencies of drug loaded nanospheres

Material	**Drug**	**Polymer:Drug**	**Encapsulation efficiency (%)**
CS	Vancomycin	8:1	80±3
CS/MMT		4:1	79±1
CS/MMT		8:1	87±3
CS	Gentamicin	20:1	76±2
CS/MMT		10:1	91±5
CS/MMT		20:1	95±4

4.4.2. Drug Release Profile and Kinetics

Controlled release up to 10 days is appropriate for acute osteomyelitis treatment. In the sub-acute infections, the controlled release profile in a period of 2-4 weeks is required. However, chronic osteomyelitis requires several months of therapy due to incorrect treatment of acute phase (Dorati et al., 2017). Therefore, antibiotic treatment of 2 weeks is required to overcome possible chronic osteomyelitis.

In this thesis study, the *in vitro* release behavior of gentamicin and vancomycin loaded nanospheres were identified to evaluate the feasibility of CS/MMT nanocomposites as drug carrier systems. *İn vitro* release was carried out in pH=7.4 at 37 °C. Cumulative percentage of released drug was calculated as the ratio of the amount of drug released from nanosphere at a certain time (t=t) the initial amount (t:0) of the drug in the nanosphere using calibration curve. The cumulative drug release profiles of both drug with two different P:D ratio were given in Figures 4.33 and 4.34. As seen in the

figures, two-step release was observed as initial burst release and sustained release in nanocomposite groups. According to the cumulative release plot of Gentamicin loaded nanospheres, neat CS released the entrapped drug in 4 hours. However, the release was sustained up to 30 days with the composite structure. 84 and 88% of the drug in PBS released from CS/MMT-GS (20:1) and CS/MMT-GS (10:1) in 30 days, respectively. 87 and 94% of entrapped vancomycin in CS/MMT matrix were released in groups with a P:D ratio of 4 and 8, respectively. The release rate decreased when P:D ratio increases as expected and found in the literature (Ji et al. 2011).

Burst release occurred from the nanospheres is generally due to the hydrophilic antibiotic drug molecules adsorbed on CS/MMT nanosphere surface that released to incubation media rapidly and therefore caused burst effect. A burst release in 6 hours was desired since most of the local infections after surgery occurs at this post-implantation period (Rumian et al., 2016). However, it is not enough to protect the defect region against bacterial inflammation. Studies indicated that biofilm formation can be seen at the tissue-material interface if long-term drug release cannot be achieved (Ordikhani et al., 2014). In this study, initial burst release was followed by 30 days of sustained release period which was desired in the post-implantation period (Rao and Lipsky, 2007)

CS/MMT nanospheres that contain less amount of drug decelerated the burst release effect by entrapping the drug stronger inside the polymer matrix. In CS/MMT-GC 10:1 group, the relatively linear trend was observed after the burst release until it reaches the plateau on the 20^{th} day. CS/MMT-GC (20:1) group showed biphasic trend due to possible degradation of nanospheres at day 14. In literature, Wers et al. (2015) hypothesized that Gentamicin release from chitosan matrix occurs with the breaking of hydrogen bonds between each other. The gentamicin release from various type of biomaterials has been monitored during incubation times ranging from minutes to weeks. Zhang and Zhang (2002) reinforced the chitosan scaffolds with beta-tricalcium phosphate to prolong the Gentamicin release rate for more than 3 weeks. Composite structure reduced the initial burst effect. In a study of Wu et al. (2013), beta-tricalcium phosphate composite scaffolds were doped with gentamicin and the drug was completely released in 10 hours. Furthermore, the scaffold was coated with gelatin/genipin layer and the sustained release was achieved for 28 days.

Rumian and co-workers fabricated poly(lactide-co-glycolide) microparticles were loaded with gentamicin and immobilized on the surface of the ceramic scaffolds. The

initial burst release for 8 hours was followed by a sustained release profile up to day 50. 90% of doped gentamicin was diffused into solution media (Rumian et al., 2016).

In a study, the Gentamicin release rate was monitored by adjusting the component ratio of Chitosan/Gelatin blend films. The increase in gelatin content reduced the release rate due to electrostatic interactions between positively charged drug and negatively charged gelatin. However, the release profile was obtained only for 48 hours of incubation (Sionkowska et al., 2016).

It was reported that gentamicin concentration should be in therapeutic level (1-10 ng/mL) at the defect site to promote bone healing (Selvig et al., 1994). In order to verify whether the released drug amount is sufficient to kill bacteria or not, minimum inhibitory concentrations (MIC) of the Gentamicin and Vancomycin were determined.

The results showed that released drug concentrations in all time intervals were higher than MIC values ensuring the antimicrobial activity (Appendix C). In this study, the therapeutic drug level was achieved without exceeding the toxic concentration.

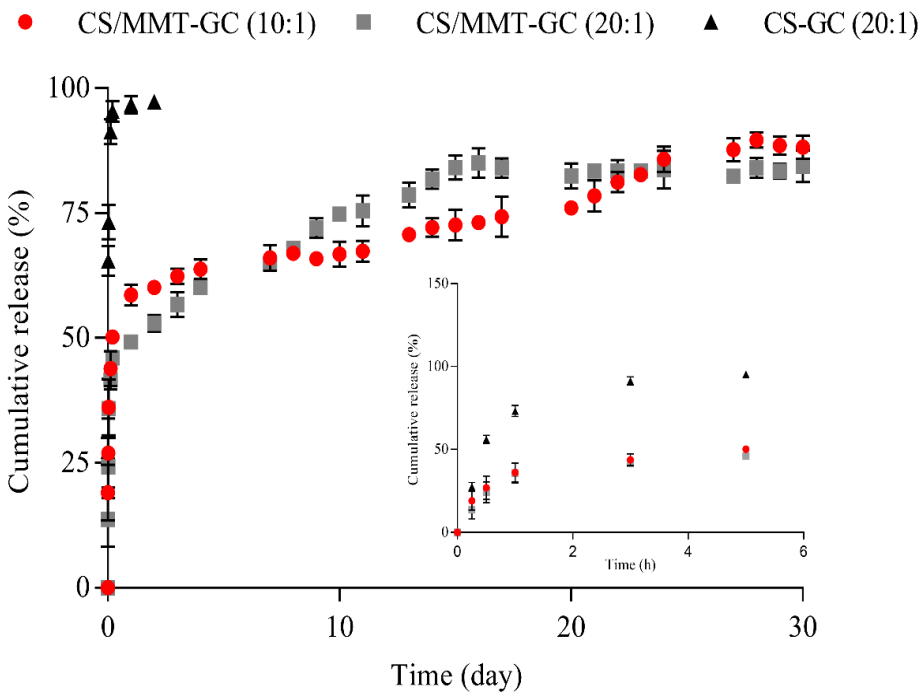

Figure 4. 33. The cumulative release of Gentamicin from CS and CS/MMT nanospheres

The Vancomycin release in neat CS nanospheres could be monitored up to 4 hours of incubation with a burst release profile. However, the drug release was monitored up to 30 days in a sustained manner with a nanocomposite structure.

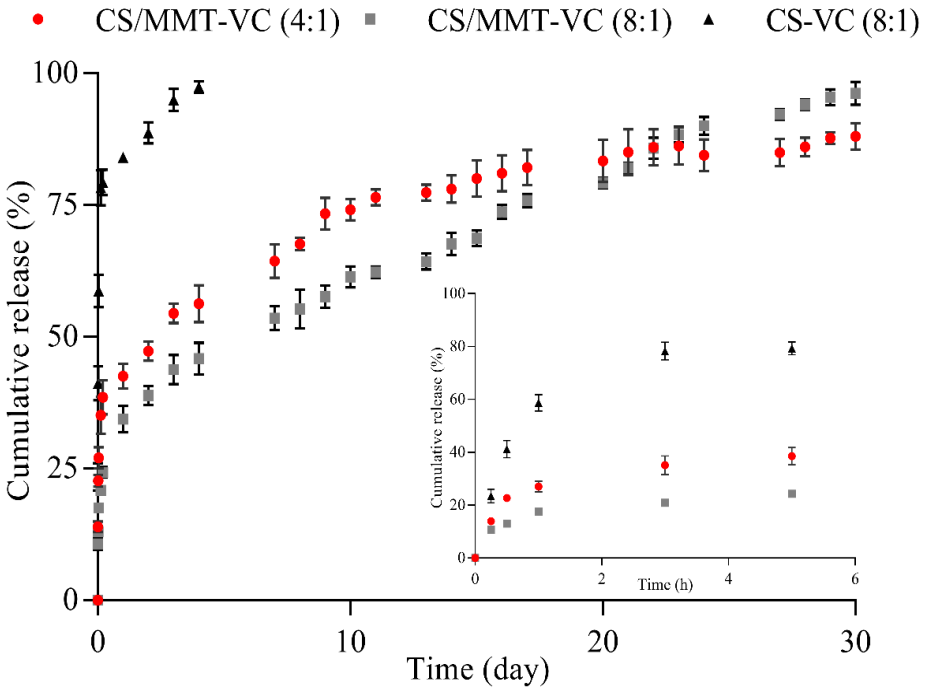

Figure 4. 34. The cumulative release of Vancomycin from CS and CS/MMT nanospheres

In composite groups, the burst release in 6 hours was followed by a controlled release profile. 38±1.86% of Vancomycin has released from CS/MMT-VC (4:1) nanospheres in 6 hours of incubation, followed by a controlled release of 88±1.53% of the total amount of drug. For the CS/MMT-VC (8:1) groups, the 24±0.58 % of the entrapped drug was released in 6 hours. Finally, 96±1.15% of the Vancomycin released to the incubation media. Similarly, it was observed that nanospheres containing less amount of Vancomycin (CS/MMT-VC (8:1)) showed a slower release rate when compared to CS/MMT-VC (4:1) group.

In recent studies, Vancomycin delivery from implant coatings, scaffolds and particulate systems have been investigated against bone infections. In a study, Yang et al. (2013) evaluated a hydroxyapatite/Ti-6Al-4V alloy bar coated with vancomycin loaded chitosan solution by electrodeposition method. The 55% of the drug was released at the initial burst period in several hours and the release was controlled by hydration and degradation of the polymer. Ordikhani et al. (2015) prepared Vancomycin-loaded chitosan-Laponite composite films with a similar approach to coat titanium implants. The initial burst effect at pure chitosan films was more apparent and the release was completed on 12th day of incubation. In contrary, Chitosan-Laponite composites showed controlled and slower release rate up to 28 days.

In literature, faster release profiles are observed with immersion and direct mixing of the vancomycin to the scaffolds. In a study of Ezazi et al. (2018), polypyrrole-based composite scaffolds were loaded with vancomycin. However, most of the loaded vancomycin have eluted at the crosslinking and washing due to the porous structure of the material. The increasing trend of cumulative release was continued up to day 20 with an 80% of cumulative release.

The sustained vancomycin release rate for sub-acute osteomyelitis treatment can be achieved with the particulate carriers. Zhou et al. (2011) coated vancomycin loaded-PCL microspheres with silk and extended the complete release from 8 to 33 days. In a study, vancomycin loaded poly(trimethylene carbonate) nanoparticles were fabricated with lyophilization technique to overcome osteomyelitis and increase the sustained effectiveness. *İn vitro* drug release studies indicated that the cumulative release in PBS (pH=7.4) was reached a plateau at approximately 17 days (18-24%) whereas drug release in lipase medium continued up to day 36 (83-90%). However, complete drug diffusion could not be achieved. Then, the *in vivo* study has been performed with an *S.aureus*-induced rabbit model and observed that produced nanoparticles inhibited bacteria colonization and promoted the bone healing (Zhang et al., 2017).

Mathematical relations corresponding drug release at incubation period were evaluated to predict the release rate at the specified time. Therefore, First-order, Higuchi, Korsmeyer-Peppas, Hixson-Crowell, Weibull and Baker-Lonsdale empirical models were applied to determine the release kinetics and the dominant mechanism of Vancomycin and Gentamicin release from CS/MMT nanospheres (Eqns. 2.9-2.14). Mathematical models were applied to experimental data and illustrated in Figures 35-40. The release coefficients(k), Korsmeyer-Peppas release exponent (n) and the correlation coefficients (R^2) were depicted in Table 4.10.

Results showed that Korsmeyer-Peppas model fits CS/MMT-VC (8-1) and CS/MMT-GC (10:1) group well whereas Weibull model was more matched with CS/MMT-VC (4:1) and CS/MMT-GC (20:1) groups. Weibull model is generally applicable for erodible matrix formulations, which verifies the biphasic release due to particle erosion at day 14. Korsmeyer-Peppas exponent “n” gives an insight into dominating mechanism in a release from CS/MMT nanospheres. According to the results, it was found that each system has a “n” value below 0.45 indicating that Fickian diffusion is the main mechanism in drug delivery from spherical CS/MMT nanocomposites.

Therefore, it can be inferred that the release rate is not dependent on the drug concentration in the matrix.

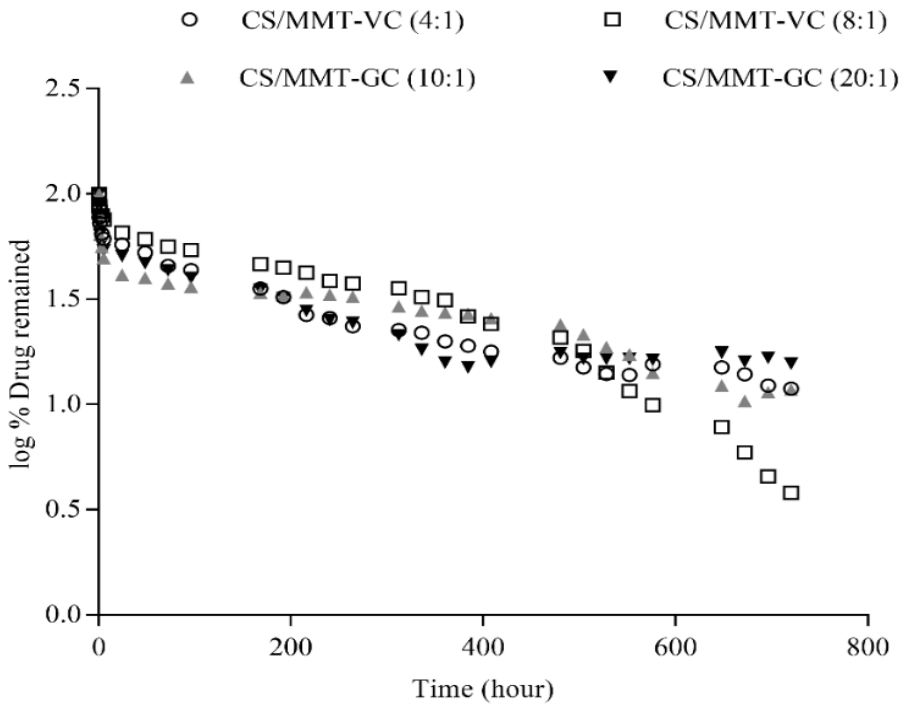

Figure 4. 35. First-order release model for CS/MMT nanospheres

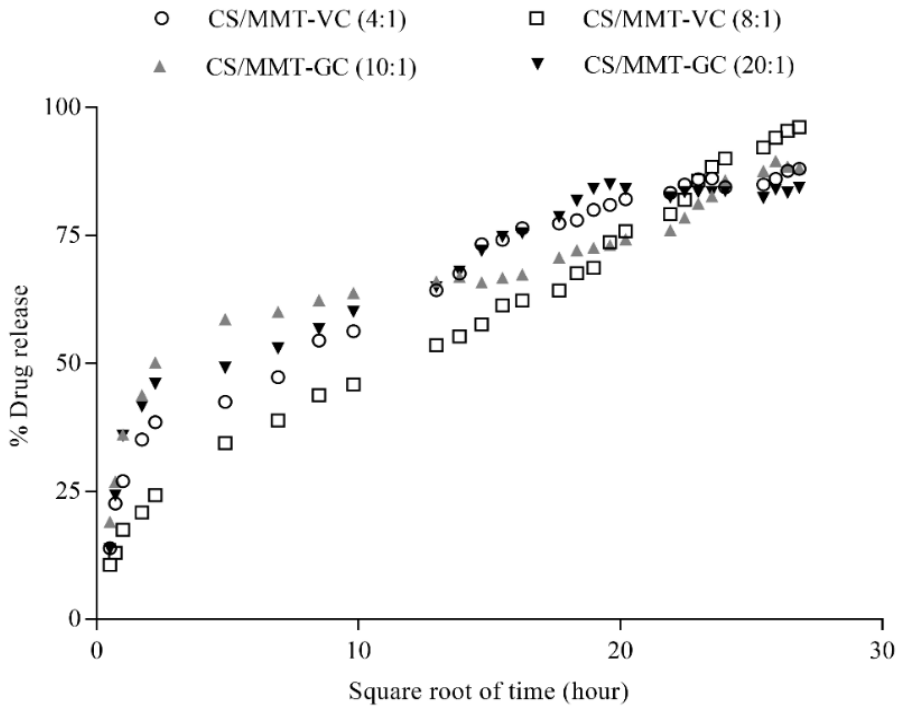

Figure 4. 36. Higuchi release model for CS/MMT nanospheres

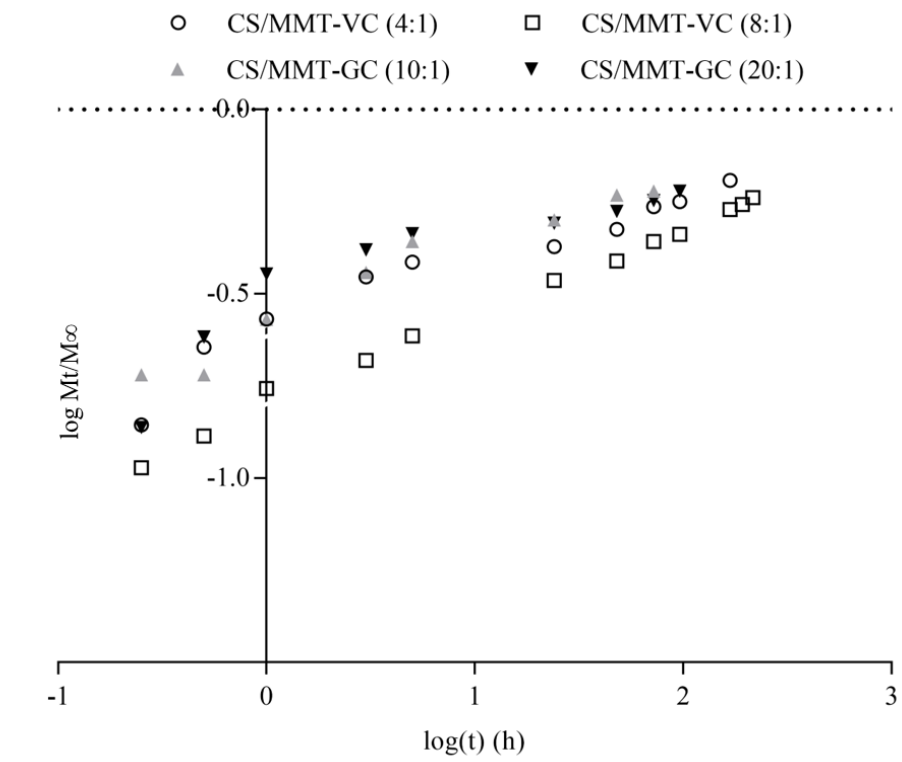

Figure 4. 37. Korsmeyer-Peppas release model for CS/MMT nanospheres

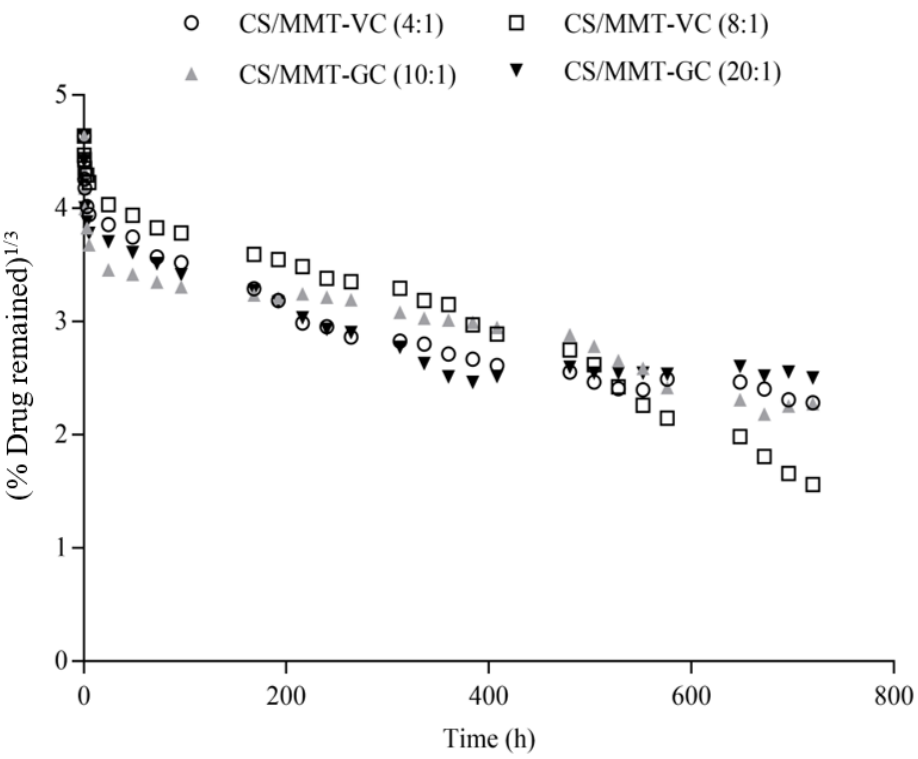

Figure 4. 38. Hixson Crowell release model for CS/MMT nanospheres

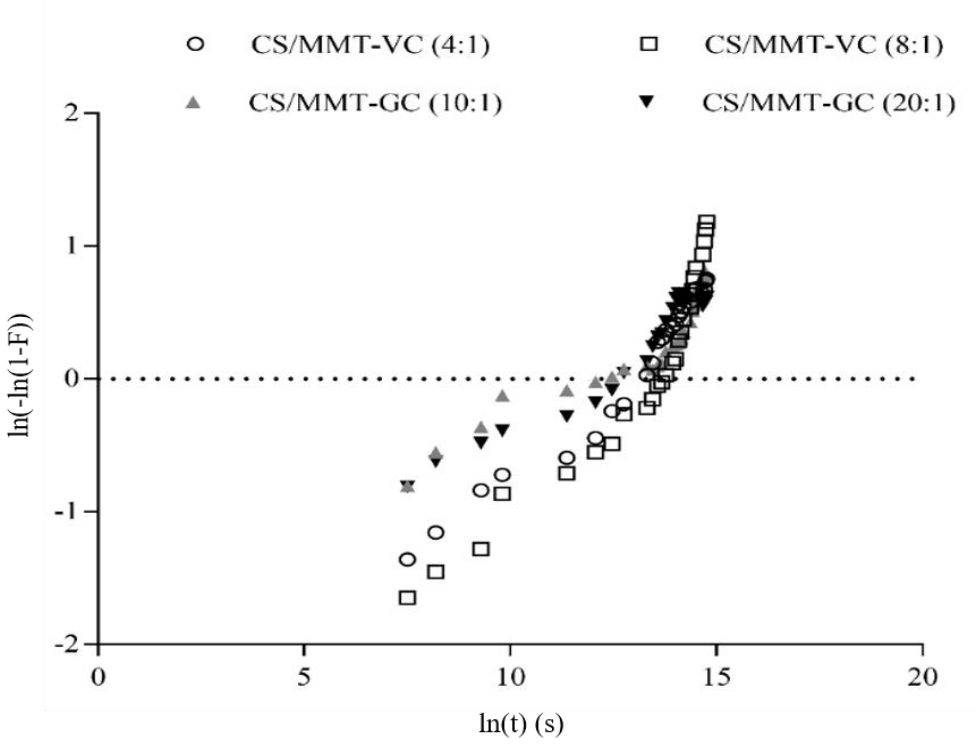

Figure 4. 39. Weibull release model for CS/MMT nanospheres

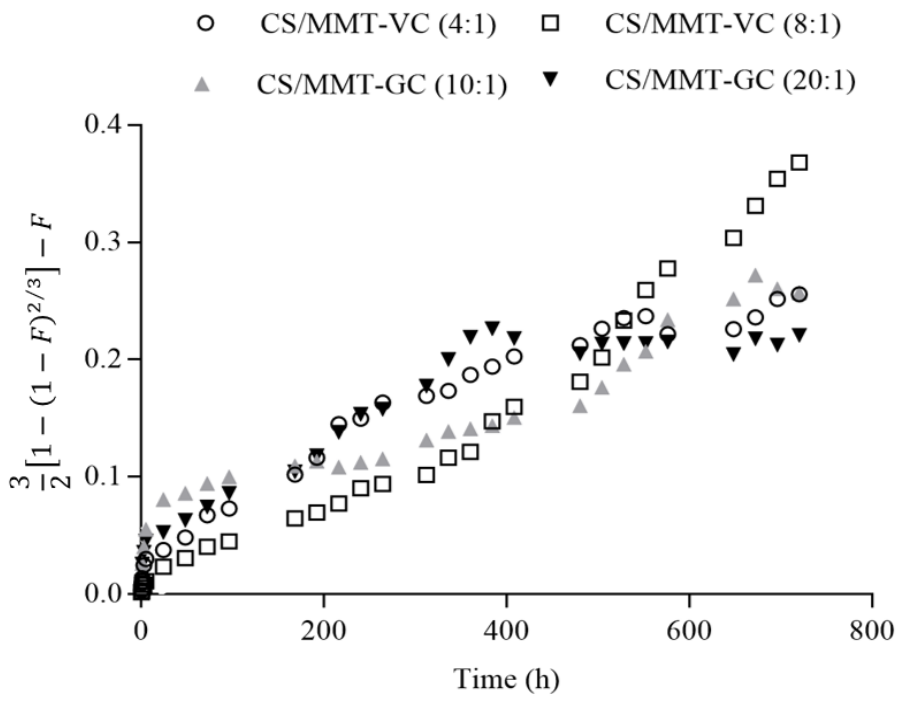

Figure 4. 40. Baker-Lonsdale model for CS/MMT nanospheres

Ji et al. (2011) fabricated GC and salicylic acid loaded chitosan nanoparticles and the release kinetics were mostly fit to Weibull model. In addition, the Korsmeyer-Peppas

exponent proved that the release was controlled by Fickian diffusion at the initial portion. The release kinetics could be monitored up to 70 hours. The cumulative release of gentamicin was found as 92% at the end of the incubation period.

Huang et al. (2016) investigated the GC release kinetics of CS/fucoidan nanoparticles for pulmonary drug delivery and they obtained a biphasic profile. In first 10 hours, the release was controlled by diffusion and swelling whereas Fickian diffusion dominates the 10-72 h period.

In literature, there are several studies related to Vancomycin release kinetics in bone implantations to prevent bone infections. Pon-On et al. (2013) fabricated Vancomycin releasing calcium phosphate/collagen scaffolds for bone implantations. They observed that the kinetic model was fit to Korsmeyer-Peppas non-Fickian (anomalous transport) in 14 days. In the study of Sezer et al. (2017), Vancomycin release from levan microparticles was mostly fit to Higuchi model with an R^2 of 0.98-0.99.

In addition, Kopcha's empirical equation (Eq. 2.16) was applied to the systems in order to verify the dominant mechanism for CS/MMT nanospheres. Since A/B value was higher than 1 in each group, it was suggested that diffusion was the main mechanism for Vancomycin and Gentamicin release from CS/MMT nanospheres (Table 4.11).

Furthermore, the Crank equation for long-term release (Eq. 2.6) was found as applicable to the release profile of the Vancomycin and Gentamicin loaded CS/MMT composite nanospheres since the dominating mechanism in 30 days of incubation was found to be diffusion. In the latter case, diffusion coefficients of drugs from the CS/MMT matrix were calculated by analyzing the final portions of the release profiles ($M_t/M_0>0.7$) with the Fickian theory. The Table 4.12. represents the Vancomycin and Gentamicin effective diffusion coefficients in CS/MMT nanosphere matrix with two different P:D ratio.

It was seen that diffusion coefficient of groups with higher P:D is prone to decrease. This fact was also proving the release profiles of the CS/MMT nanospheres. Groups having higher D showed faster drug release.

In a study of Kumbar et al. (2003), it was also observed that groups showing faster drug release have higher diffusion coefficients. The similar effect was observed in both Vancomycin and Gentamicin loaded CS/MMT nanocomposite spheres.

Table 4. 10. Release kinetic coefficients for CS/MMT nanospheres

Drug	P:D	First-order Release		Higuchi		Korsmeyer-Peppas		Hixson-Crowell		Weibull	Baker-Lonsdale
		K	R^2	k	R^2	N	R^2	k	R^2	R^2	R^2
Vancomycin	4:1	0.0026	0.9085	2.47	0.9354	0.1928	0.9216	-0.0073	0.8593	0.9552	0.9308
	8:1	0.0037	0.9537	3.037	0.9915	0.238	0.995	-0.0036	0.9789	0.8734	0.9622
Gentamicin	10:1	0.0023	0.8998	1.935	0.8847	0.2152	0.9515	-0.0023	0.8531	0.8369	0.9383
	20:1	0.0022	0.8064	2.17	0.8781	0.1913	0.8015	-0.0023	0.7667	0.9354	0.8330

Table 4. 11. Kopcha diffusion and erosion coefficients of CS/MMT nanospheres

Groups	A	B	R^2
CS/MMT-VC (4-1)	101.7	6.192	0.99
CS/MMT-VC (8-1)	43.91	2.839	0.98
CS/MMT-GC (10-1)	17.48	1.126	0.99
CS/MMT-GC (20-1)	7.365	0.393	0.98

Table 4. 12. Diffusion coefficients of CS/MMT nanospheres according to Crank long term release equation

Samples	D $x10^{-15}$ (m^2/s)
CS/MMT-VC (4-1)	5.13
CS/MMT-VC (8-1)	1.84
CS/MMT-GC (10-1)	2.52
CS/MMT-GC (20-1)	1.37

4.5. Antimicrobial Activity

In chronic osteomyelitis, mostly described bacterial isolates are staphylococci and Gram-negative bacteria. *S. aureus* is known as an important bone pathogen that causes bone destruction and failure in orthopedic implants (Kanellakopoulou and Giamarellos-Bourboulis, 2000). In addition, it was reported that total knee replacement operations can result in a bacterial infection caused by *E. coli* (Dixon et al., 2004). Therefore, local Vancomycin and Gentamicin release is selectively used in bone infection cases since they are both broad-spectrum antibiotics. To confirm the relevance of the *in vitro* release study, the antimicrobial activity of the release media was investigated for gram-negative *E. coli* and Gram-positive *Staphylococcus aureus*.

Inhibition zones were clearly observed on discs diffusing the release media of nanospheres taken at specific time intervals (6 hours, 24 hours and 25 days). In negative control (blank disc), no inhibition zone was observed. Inhibition zones to the release media diffused from discs to the culture environment were observed after 24 hours of incubation. Effect of released drugs against *E. coli* and *S. aureus* were depicted in Figures

4.41 and 4.42, respectively. Results indicated that Gentamicin and Vancomycin were locally released at given intervals and affected by both pathogens.

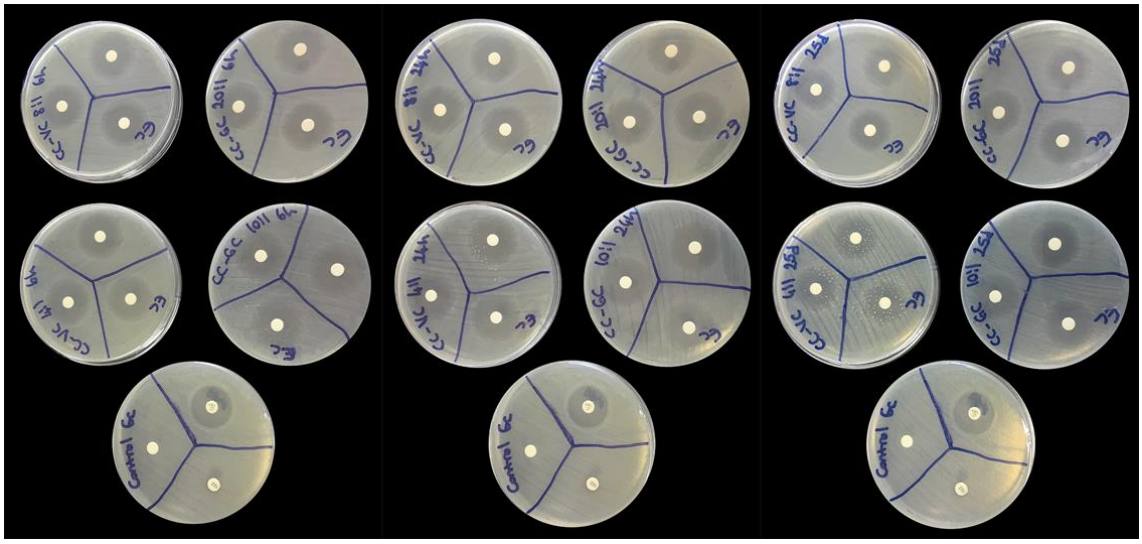

Figure 4. 41. Effect of release media against *E. coli* at incubation times of 6h, 24h and 25 days.

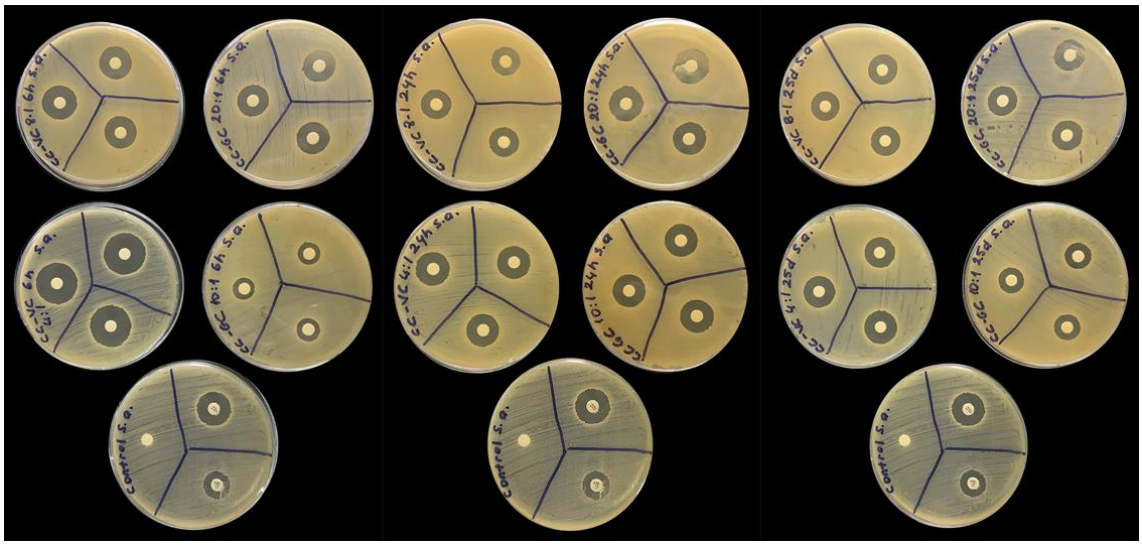

Figure 4. 42. Effect of release media against *S. aureus* at incubation times of 6h, 24h at 25 days.

The inhibition zones were given in Tables 4.13 and 4.14. It can be observed that antimicrobial activity against *S. aureus* was increased with the antibiotic concentration. It may be due to increased penetration of Vancomycin to bacterial cell wall and inhibition of the growth. In addition, the inhibition zone at the 6 h period was larger, which was attributed to burst release at the short-time period. Similarly, Ryu et al. (2014) studied the effect of release kinetics on antimicrobial activity of Gentamicin releasing PCL

microspheres against *S. aureus* and *E. coli*. It was indicated that larger inhibition zone was achieved in the group which has a greater release at the initial period. In literature, it was indicated that Vancomycin loaded polymeric microparticles have antimicrobial activity against gram-positive *S. aureus*, gram-negative *S. epidermidis* and *P. Aeruginosa* (Noel et al., 2010; Rumian et al., 2017). In addition, Lertsutthiwong et al. (2012) have proved the antimicrobial activity of CS/MMT composites against *E. coli* bacteria.

Table 4. 13. Effect of *in vitro* release media (6h, 24h, 25 days) against *E. coli*

	Inhibition zone (mm)		
Groups	**6 hours**	**24 hours**	**25 days**
Positive control 1 (Amoxycylin)	10		
Positive control 2 (Vancomycin)	5		
Negative control (Blank disc)	-		
CS/MMT-VC (4:1)	14±0.00	11.3±0.01	10.0±0.01
CS/MMT-VC (8:1)	14.7±0.01	10.7±0.01	9±0.00
CS/MMT-GC (10:1)	14.7±0.02	10.0±0.01	10.3±0.01
CS/MMT-GC (20:1)	11.7±0.02	9.7±0.01	8.8±0.00

Table 4. 14. Effect of *in vitro* release media (6h, 24h, 25 days) against *S. aureus*

	Inhibition zone (mm)		
Groups	**6 hours**	**24 hours**	**25 days**
Positive control 1 (Amoxycylin)	6		
Positive control 2 (Vancomycin)	11.3±0.01		
Negative control (Blank disc)	-		
CS/MMT-VC (4:1)	07.9±0.01	5.3±0.03	5.3±0.03
CS/MMT-VC (8:1)	05.5±0.01	4.8±0.02	4.4±0.02
CS/MMT-GC (10:1)	2.8±0.01	4±0.00	3.1±0.01
CS/MMT-GC (20:1)	3.8±0.01	4.1±0.01	3.8±0.01

The maximum pathogen activity was obtained with the antimicrobial tests since the culture environment supply optimum conditions for test microorganisms in terms of medium composition, pH and temperature (Altiok et al., 2010). Consequently, higher antimicrobial activity is expected in the real case since pure strains cultured in laboratory conditions show maximum growth.

4.6. *In vitro* Cytotoxicity

Cytotoxicity of the nanospheres on NIH/3T3 and SaOS-2 cell lines was evaluated by 24 h extraction of nanospheres in 24, 48 and 72 hours of incubation and depicted in Figure 4.43 and 4.44, respectively. It was observed that nanospheres did not cause any cytotoxic effect on cells. Indeed, all groups showed good viability (>95%). According to the ANOVA results, drug loaded nanospheres showed the significant viability on both cell line ($P<0.05$). In some groups, non-significant viability decrease at 72 hours of incubation was observed according to the possible contact inhibition of cells. In literature, *in vitro* cytotoxicity of CS/MMT based materials were evaluated and it was found that nanocomposites also do not show any cytotoxic behavior to Caco-2 cells and rat stem cells (Wang et al., 2008; Zhuang et al., 2007). The results suggested that neat CS/MMT and drug loaded nanospheres were found to be cytocompatible with fibroblast and human osteoblast-like cell lines.

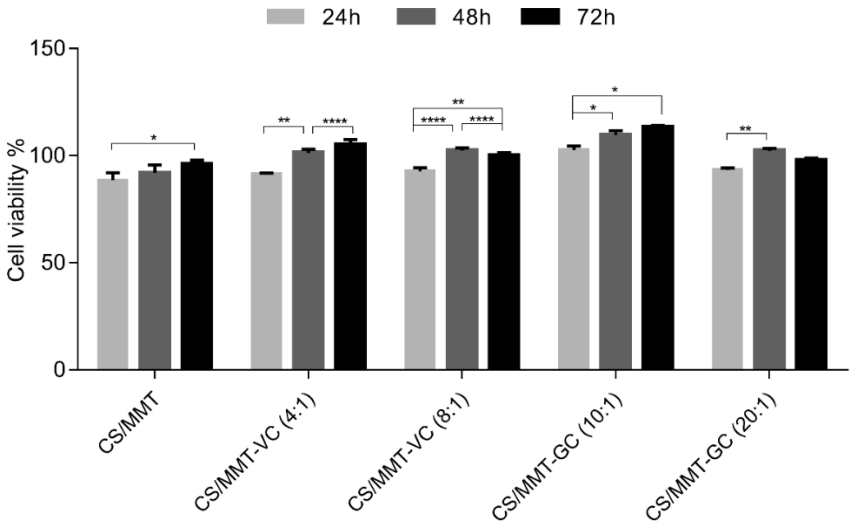

Figure 4. 43. *In vitro* cytotoxicity of nanospheres against NIH/3T3 cell line

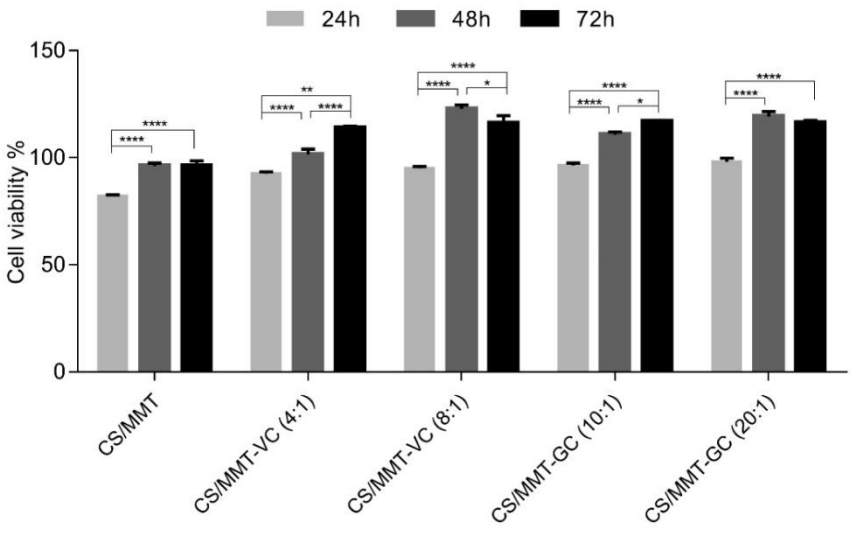

Figure 4. 44. *In vitro* cytotoxicity of nanospheres against SaOS-2 cell line

CHAPTER 5

CONCLUSIONS

Infection is one of the most serious drawbacks of bone implantation operations which can cause necrosis of the tissue. Therefore, antibiotic treatment should be applied to the defect region in order to eliminate possible infections. Prolonged antibiotic delivery is needed at the implant site to guarantee the prevention from microbial contamination of the implant.

The main objective of this dissertation was to fabricate controlled antibiotic releasing chitosan/montmorillonite (CS/MMT) nanocomposite spheres to improve antimicrobial efficacy while reducing the systemic toxicity of the antibiotics. MMT nanoclay was implicated in chitosan matrix with microfluidizer homogenization to prolong the drug diffusion pathway and ensure the stability of the system. Electrospray method was selected for nanosphere fabrication. The study comprises the effect of microfluidizer treatment on chitosan characteristics, electrospray parametric optimization, characterization of CS/MMT nanospheres, drug release profile and kinetics, antimicrobial activity and *in vitro* cytotoxicity of the nanospheres.

As a first step, microfluidizer working parameters were optimized by evaluating the effects on chitosan characteristics such as viscosity, molecular weight, deacetylation degree and solution rheology. Operation conditions of 10,000 psi and 5 passes were selected to prepare chitosan nanospheres. Then, the electrospray process parameters on nanosphere morphology and size were evaluated statistically. Response surface methodology (RSM) was applied to determine the effects of working parameters. A voltage of 20 kV, a distance of 10 cm and 5 ml/h flowrate were chosen as optimal electrospray conditions for fabrication of CS/MMT nanospheres. Drug loaded CS/MMT nanospheres were physically characterized by their morphology, size distribution, surface charge and encapsulation efficiencies. The hydrodynamic sizes of the CS/MMT nanospheres were found in a range of 65-250 nm. All groups obtain positive surface charge due to the polycationic nature of chitosan. The drug encapsulation efficiency of nanospheres was found as 79-86% for Vancomycin and 90-94% for Gentamicin loading,

respectively. It was observed that drug entrapment was increased with decreasing the loading amount. The chemical interactions between drug, clay and polymer were determined with the FT-IR studies.

The drug release profiles of nanospheres were investigated for 30 days. The slower release rate was achieved with nanospheres containing less amount of drug. Initial burst release for 5 hours was achieved which is a critical period for bone infections. The drug release was proceeded in a controlled manner up to 30 days. First order, Higuchi, Korsmeyer-Peppas, Hixson-Crowell and Weibull models were applied in order to predict the release kinetics and determine the dominating mechanism. It was found that Korsmeyer-Peppas and Weibull models fit the drug release rate according to their R^2 values. According to the Korsmeyer-Peppas empirical equation, Gentamicin and Vancomycin release from CS/MMT matrix were dominated with diffusion mechanism. The Kopcha equation parameters also verified the results by indicating diffusion was more efficient than erosion for CS/MMT nanospheres.

In vitro release media of CS/MMT nanospheres showed strong antimicrobial activity against *E. coli* and *S. aureus* bacteria demonstrating that both antibiotics can be used against bone infections. In addition, these CS/MMT nanocomposites did not show any cytotoxic activity against fibroblast and human osteoblast-like cells.

The overall evaluations suggested that these antibiotic loaded CS/MMT nanospheres have a promising potential effect on bacterial infections at the post-implantation period. The efficacy of antibiotic therapy was increased when compared to conventional methods. The antibiotic release from CS/MMT matrix can be controlled by the alteration of polymer:drug ratio. Nanocomposites made of biopolymers and natural inorganic fillers can be a new notion in controlled drug delivery systems.

Further studies could comprise spraying drug loaded CS/MMT nanospheres on scaffolds to be implanted to bone defects. *In vivo* studies are recommended as a further step to determine the efficacy of these composite drug delivery systems.

REFERENCES

Abarrategi, A., A. Civantos, V. Ramos, J. V. Sanz Casado, and J. L. López-Lacomba (2008). Chitosan Film as RhBMP2 Carrier: Delivery Properties for Bone Tissue Application. *Biomacromolecules 9*(2), 711–718.

Abdollahi, M., M. Rezaei, and G. Farzi (2012). A Novel Active Bionanocomposite Film Incorporating Rosemary Essential Oil and Nanoclay into Chitosan. *Journal of Food Engineering 111*(2), 343–350.

Agnihotri, S. A, N. N. Mallikarjuna, and T. M. Aminabhavi (2004). Recent Advances on Chitosan-Based Micro-and Nanoparticles in Drug Delivery. *Journal of Controlled Release 100*(1), 5–28.

Aimin, C., H. Chunlin, B. Juliang, Z. Tinyin, and D. Zhichao (1999). Antibiotic Loaded Chitosan Bar. An in vitro, in Vivo Study of a Possible Treatment for Osteomyelitis. *Clinical Orthopaedics and Related Research, 366*, 239–247.

Albalawi, M.A., W.S. Mohamed, and N.H. Elsayed (2016). Utilization of MMT Clay and MMT-Chitosan for Platinol Drug Delivery. *Der Pharma Chemica 8*(23), 27-34.

Albuhairan, B., D. Hind, and A. Hutchinson (2008). Antibiotic prophylaxis for wound infections in total joint arthroplasty: a systematic review. *Bone & Joint Journal* 90(7), 915-919.

Altiok, D., E. Altiok, and F. Tihminlioglu (2010). Physical, Antibacterial and Antioxidant Properties of Chitosan Films Incorporated with Thyme Oil for Potential Wound Healing Applications. *Journal of Materials Science: Materials in Medicine 21*(7), 2227–2236.

Anal, A. K., and W. F. Stevens (2005). Chitosan-Alginate Multilayer Beads for Controlled Release of Ampicillin. *International Journal of Pharmaceutics 290*(1–2), 45–54.

Arca, H.Ç., and S. Şenel (2008). Chitosan Based Systems for Tissue Engineering Part 1: Hard Tissues. *Fabad Journal of Pharmaceutical Sciences 33*(1), 35–49.

Arya, N., S. Chakraborty, N. Dube, and D. S. Katti (2009). Electrospraying: A Facile Technique for Synthesis of Chitosan-Based Micro/Nanospheres for Drug Delivery Applications. *Journal of Biomedical Materials Research - Part B Applied Biomaterials 88*(1), 17–31.

Avadi, M. R., A. M. M. Sadeghi, N. Mohammadpour, S. Abedin, F. Atyabi, R. Dinarvand, and M. Rafiee-Tehrani (2010). Preparation and Characterization of Insulin Nanoparticles Using Chitosan and Arabic Gum with Ionic Gelation Method. *Nanomedicine: Nanotechnology, Biology, and Medicine 6*(1), 58-63.

Bai, M. Y., and Y. M. Hu (2014). Development of Alpha-Lipoic Acid Encapsulated Chitosan Monodispersed Particles Using an Electrospray System: Synthesis, Characterisations and Anti-Inflammatory Evaluations. *Journal of Microencapsulation 31*(4), 373–381.

Balakumar, P., A. Rohilla, and A. Thangathirupathi (2010). Gentamicin-Induced Nephrotoxicity: Do We Have a Promising Therapeutic Approach to Blunt It? *Pharmacological Research 62*(3), 179–186.

Bao, H., Y. Pan, Y. Ping, N. G. Sahoo, T. Wu, L. Li, J. Li, and L. H. Gan (2011). Chitosan-Functionalized Graphene Oxide as a Nanocarrier for Drug and Gene Delivery. *Small 7*(11), 1569–1578.

Barna, J. C. J., and D. H. Williams (1984). The Structure and Mode of Action of Glycopeptide Antibiotics of the Vancomycin Group. *Annual Review of Microbiology 38*, 339–357.

Baskar, D., and T. S. Sampath Kumar (2009). Effect of Deacetylation Time on the Preparation, Properties and Swelling Behavior of Chitosan Films. *Carbohydrate Polymers 78*(4), 767–772.

Bastami, F., Z. Paknejad, M. Jafari, M. Salehi, M. R. Rad, and A. Khojasteh (2017). Fabrication of a Three-Dimensional β-Tricalcium-Phosphate/Gelatin Containing Chitosan-Based Nanoparticles for Sustained Release of Bone Morphogenetic Protein-2: Implication for Bone Tissue Engineering. *Materials Science and Engineering C 72*, 481–491.

Baxter, A., M. Dillon, K. A. Taylor, and G. A. Roberts (1992) Improved method for ir determination of the degree of N-acetylation of chitosan. *International Journal of Biological Macromolecules* 14(3), 166-169.

Berridge, M. V., P. M. Herst, and A. S. Tan (2005). Tetrazolium Dyes as Tools in Cell Biology: New Insights into Their Cellular Reduction. *Biotechnology Annual Review 11*, 127-152.

Blanco-Príeto, M. J., C. Lecaroz, M. J. Renedo, J. Kunkova, and C. Gamazo (2002). *İn vitro* Evaluation of Gentamicin Released from Microparticles. *International Journal of Pharmaceutics 242*(1–2), 203–206.

Bonilla, J., L. Atarés, M. Vargas, and A. Chiralt (2012). Effect of Essential Oils and Homogenization Conditions on Properties of Chitosan-Based Films. *Food Hydrocolloids 26*(1), 9–16.

Burg, K. J. L., S. Porter, and J. F. Kellam (2000). Biomaterial Developments for Bone Tissue Engineering. *Biomaterials 21*(23), 2347–2359.

Calabrese, I., G. Cavallaro, C. S., M. Licciardi, M. Merli, L. Sciascia, and M. L. Turco Liveri (2013). Montmorillonite Nanodevices for the Colon Metronidazole Delivery. *International Journal of Pharmaceutics 457*(1), 224–236.

Caramella, C., B. Conti, T. Modena, F. Ferrari, M. C. Bonferoni, I. Genta, S. Rossi, M.R. Torre, G. Sandri, M. Sorrenti, L. Catenacci, R. Dorati and G. Tripodo (2016). Controlled Delivery Systems for Tissue Repair and Regeneration. *Journal of Drug Delivery Science and Technology 32*, 206-228.

Casariego, A., B.W.S. Souza, M. A. Cerqueira, J. A. Teixeira, L. Cruz, R. Díaz, and A. A. Vicente (2009). Chitosan/Clay Films' Properties as Affected by Biopolymer and Clay Micro/Nanoparticles' Concentrations. *Food Hydrocolloids 23*(7), 1895–1902.

Cerchiara, T., A. Abruzzo, M. Di Cagno, F. Bigucci, A. Bauer-Brandl, C. Parolin, B. Vitali, M. C. Gallucci, and B. Luppi (2015). Chitosan Based Micro- and Nanoparticles for Colon-Targeted Delivery of Vancomycin Prepared by Alternative Processing Methods. *European Journal of Pharmaceutics and Biopharmaceutics 92*, 112–119.

Cervantes-Uc, J. M., J. V. Cauich-Rodríguez, H. Vázquez-Torres, L. F. Garfias-Mesías, and D. R. Paul (2007). Thermal Degradation of Commercially Available Organoclays Studied by TGA-FTIR. *Thermochimica Acta 457*(1–2), 92–102.

Cevher, E., Z. Orhan, L. Mülazimoğlu, D. Şensoy, M. Alper, A. Yildiz, and Y. Özsoy (2006). Characterization of Biodegradable Chitosan Microspheres Containing Vancomycin and Treatment of Experimental Osteomyelitis Caused by Methicillin-Resistant Staphylococcus Aureus with Prepared Microspheres. *International Journal of Pharmaceutics 317*(2), 127–135.

Cha, Y., and C. G. Pitt (1988). A One-Week Subdermal Delivery System for l-Methadone Based on Biodegradable Microcapsules. *Journal of Controlled Release 7*(1), 69–78.

Chen, J., R. H. Liang, W. L., C. M. L., T. Li, Z. C. Tu, and J. Wan (2012). Degradation of High-Methoxyl Pectin by Dynamic High Pressure Microfluidization and Its Mechanism. *Food Hydrocolloids 28*(1), 121–129.

Chen, R. H., J. R. Huang, M. L. Tsai, L. Z. Tseng, and C. H. Hsu (2011). Differences in Degradation Kinetics for Sonolysis, Microfluidization and Shearing Treatments of Chitosan. *Polymer International 60*(6), 897–902.

Chen, Y., A. Zhou, B. Liu, and J. Liang (2010). Tramadol Hydrochloride/Montmorillonite Composite: Preparation and Controlled Drug Release. *Applied Clay Science 49*(3), 108–112.

Chevalier, E., M. Viana, A. Artaud, S. Haddouchi, and D. Chulia (2009). A Novel Application of the T-Cell for Flow-through Dissolution: The Case of Bioceramics Used as Ibuprofen Carrier. *Talanta 77*(4), 1545–1548.

Cho, B. C., J. Y. Kim, J. H. Lee, H. Y. Chung, J. W. Park, K. H. Roh, G. U. Kim, I. C. Kwon, K. H. Jang, D. Lee, N. W. Park and I. S. Kim (2004). The Bone Regenerative Effect of Chitosan Microsphere-Encapsulated Growth Hormone on Bony Consolidation in Mandibular Distraction Osteogenesis in a Dog Model. *Journal of Craniofacial Surgery 15*(2), 299-311.

Cojocariu, A., L. Profire, M. Aflori, and C. Vasile. (2012). *İn vitro* Drug Release from Chitosan/Cloisite 15A Hydrogels. *Applied Clay Science 57*, 1–9.

Costa-Pinto, A. R., R. L. Reis, and N. M. Neves (2011). Scaffolds Based Bone Tissue Engineering: The Role of Chitosan. *Tissue Engineering Part B: Reviews 17*(5), 331–347.

Croisier, F., and C. Jérôme (2013). Chitosan-Based Biomaterials for Tissue Engineering. *European Polymer Journal 49*(4), 780–792.

Darder, M., M. Colilla, and E. Ruiz-Hitzky (2005). Chitosan-Clay Nanocomposites: Application as Electrochemical Sensors. *Applied Clay Science 28*(1–4), 199–208.

Darley, E. S. R., and A. P. MacGowan (2004). Antibiotic Treatment of Gram-Positive Bone and Joint Infections. *Journal of Antimicrobial Chemotherapy 53*(6), 928-935.

Dash, M., F. Chiellini, R. M. Ottenbrite, and E. Chiellini (2011). Chitosan - A Versatile Semi-Synthetic Polymer in Biomedical Applications. *Progress in Polymer Science 36*(8), 981–1014.

Depan, D., A. P. Kumar, and R. P. Singh (2009). Cell Proliferation and Controlled Drug Release Studies of Nanohybrids Based on Chitosan-g-Lactic Acid and Montmorillonite. *Acta Biomaterialia 5*(1), 93–100.

Desai, K. G H, and H. J. Park (2005). Encapsulation of Vitamin C in Tripolyphosphate Cross-Linked Chitosan Microspheres by Spray Drying. *Journal of Microencapsulation 22*(2), 179–192.

Dinçer, A., S. Becerik, and T. Aydemir (2012). Immobilization of Tyrosinase on Chitosan-Clay Composite Beads. *International Journal of Biological Macromolecules 50*(3), 815–820.

Dixon, P., E. N. Parish, and M. J. Cross (2004). Arthroscopic Debridement in the Treatment of the Infected Total Knee Replacement. *The Journal of Bone and Joint Surgery. British Volume 86*(1), 39–42.

Domszya, J. G., and G. A. F. Roberts (1985). Evaluation of Infrared Spectroscopic Techniques for Analysing Chitosan. *Makromolekulare Chemie: Macromolecular Chemistry and Physics 186*(8), 1671–1677.

Dorati, R., A. DeTrizio, T. Modena, B. Conti, F. Benazzo, G. Gastaldi, and I. Genta

(2017). Biodegradable Scaffolds for Bone Regeneration Combined with Drug-Delivery Systems in Osteomyelitis Therapy. *Pharmaceuticals 10*(4), 96.

Doshi, J., and D.H. Reneker (1993). Electrospinning Process and Applications of Electrospun Fibers. *Conference Record of the 1993 IEEE Industry Applications Conference Twenty-Eighth IAS Annual Meeting 35*, 151–160.

Ehrlich, H., B. Krajewska, T. Hanke, R. Born, S. Heinemann, C. Knieb, and H. Worch (2006). Chitosan Membrane as a Template for Hydroxyapatite Crystal Growth in a Model Dual Membrane Diffusion System. *Journal of Membrane Science 273*, 124–128.

Ennajih, H., R. Bouhfid, E. M. Essassi, M. Bousmina, and A. E. Kadib (2012). Chitosan-Montmorillonite Bio-Based Aerogel Hybrid Microspheres. *Microporous and Mesoporous Materials 152*, 208–213.

Esmaeili, F., M. Hosseini-Nasr, M. Rad-Malekshahi, N. Samadi, F. Atyabi, and R. Dinarvand (2007). Preparation and Antibacterial Activity Evaluation of Rifampicin-Loaded Poly Lactide-Co-Glycolide Nanoparticles. *Nanomedicine: Nanotechnology, Biology, and Medicine 3*(2), 161–167.

Ezazi, N. Z., M. A. Shahbazi, Y. V. Shatalin, E. Nadal, E. Mäkilä, J. Salonen, M. Kemell, A. Correia, J. Hirvonen, and H. A. Santos (2018). Conductive Vancomycin-Loaded Mesoporous Silica Polypyrrole-Based Scaffolds for Bone Regeneration. *International Journal of Pharmaceutics 536*(1), 241–250.

Forano, C. (2004). Clay Surfaces - Fundamentals and Applications. *Interface Science and Technology 1*, 425-458.

Fu, X., and S. Qutubuddin (2001). Polymer – Clay Nanocomposites : Exfoliation of Organophilic Montmorillonite Nanolayers in Polystyrene. *Polymer 42*, 807–813.

Gao, F. (2004). Clay/Polymer Composites: The Story. *Materials Today 7*(11), 50-55.

Gao, P., X. Nie, M. Zou, Y. Shi, and G. Cheng (2011). Recent Advances in Materials for Extended-Release Antibiotic Delivery System. *Journal of Antibiotics 64*(9), 625-634.

Geankoplis, C. J. (2003). *Transport Processes and Unit Operations*. Prentice Hall Professional Technical Reference.

Geng, X., O. H. Kwon, and J. Jang (2005). Electrospinning of Chitosan Dissolved in Concentrated Acetic Acid Solution. *Biomaterials 26*(27), 5427–5432.

Gierszewska, M., and J. Ostrowska-Czubenko (2016). Chitosan-Based Membranes with Different Ionic Crosslinking Density for Pharmaceutical and Industrial Applications. *Carbohydrate Polymers 153*, 501–511.

Gumusderelioglu, M., E. T. Tunçay, G. Kaynak, T. T. Demirtaş, S. T. Aydin, and S. S. Hakki (2015). Encapsulated Boron as an Osteoinductive Agent for Bone Scaffolds. *Journal of Trace Elements in Medicine and Biology 31*, 120–128.

Günister, E., D. Pestreli, C. H. Ünlü, O. Atici, and N. Güngör (2007). Synthesis and Characterization of Chitosan-MMT Biocomposite Systems. *Carbohydrate Polymers 67*(3), 358–365.

Gupta, K. C., and F. H. Jabrail (2006). Glutaraldehyde and Glyoxal Cross-Linked Chitosan Microspheres for Controlled Delivery of Centchroman. *Carbohydrate Research 341*(6), 744–756.

Hadjitheodorou, A., and G. Kalosakas (2014). Analytical and Numerical Study of Diffusion-Controlled Drug Release from Composite Spherical Matrices. *Materials Science and Engineering C 42*, 681–690.

Hamman, J. H. (2010). Chitosan Based Polyelectrolyte Complexes as Potential Carrier Materials in Drug Delivery Systems. *Marine Drugs 8*(4), 1305-1322.

Hammett-Stabler, C. A., and T. Johns (1998). Laboratory Guidelines for Monitoring of Antimicrobial Drugs. *Clinical Chemistry 44*, 1129–1240.

Hao, S., Y. Wang, B. Wang, J. Deng, X. Liu, and J. Liu (2013). Rapid Preparation of PH-Sensitive Polymeric Nanoparticle with High Loading Capacity Using Electrospray for Oral Drug Delivery. *Materials Science and Engineering C 33*(8), 4562–4567.

Hayati, I., A. I. Bailey, and T. F. Tadros (1987). Investigations into the Mechanisms of Electrohydrodynamic Spraying of Liquids. I. Effect of Electric Field and the

Environment on Pendant Drops and Factors Affecting the Formation of Stable Jets and Atomization. *Journal of Colloid And Interface Science 117*(1), 205–221.

Hayati, I., A. Bailey, and T. F. Tadros (1987). Investigations into the Mechanism of Electrohydrodynamic Spraying of Liquids. II. Mechanism of Stable Jet Formation and Electrical Forces Acting on a Liquid Cone. *Journal of Colloid And Interface Science 117*(1), 222–223.

Hidayat, L. K., D. I. Hsu, R. Quist, K. A. Shriner, and A. Wong-Beringer (2006). High-Dose Vancomycin Therapy for Methicillin-Resistant Staphylococcus Aureus Infections. *Archives of Internal Medicine 166*(19), 2138.

Hirota, K., A. C. Doty, R. Ackermann, J. Zhou, K. F. Olsen, M. R. Feng, Y. Wang, S. Choi, W. Qu, A. S. Schwendemann and S. P. Schwendemann (2016). Characterizing Release Mechanisms of Leuprolide Acetate-Loaded PLGA Microspheres for IVIVC Development I: *İn vitro* Evaluation. *Journal of Controlled Release 244*, 302–313.

Hixson, A. W., and J. H. Crowell (1931). Dependence of Reaction Velocity upon Surface and Agitation: III—Experimental Procedure in Study of Agitation. *Industrial and Engineering Chemistry 23*(10), 1160–1168.

Hogan, A., V. G. Heppert, and A. J. Suda (2013). Osteomyelitis. *Archives of Orthopaedic and Trauma Surgery 133*(9), 1183–1196.

Honary, S., and F. Zahir (2013). Effect of Zeta Potential on the Properties of Nano - Drug Delivery Systems - A Review (Part 2). *Tropical Journal of Pharmaceutic Al Research 12*(2), 265–273.

Hosseini, S. F., M. Zandi, M. Rezaei, and F. Farahmandghavi (2013). Two-Step Method for Encapsulation of Oregano Essential Oil in Chitosan Nanoparticles: Preparation, Characterization and in vitro Release Study. *Carbohydrate Polymers 95*(1), 50–56.

Hua, S., H. Yang, W. Wang, and A. Wang (2010). Controlled Release of Ofloxacin from Chitosan-Montmorillonite Hydrogel. *Applied Clay Science 50*(1), 112–117.

Huang, Y., J. Huang, J. Cai, W. Lin, Q. Lin, F. Wu, and J. Luo (2015). Carboxymethyl chitosan/clay nanocomposites and their copper complexes: fabrication and property.

Carbohydrate polymers 134, 390-397.

Huang, Y. C., R. Y. Li, J. Y. Chen, and J. K. Chen (2016). Biphasic Release of Gentamicin from Chitosan/Fucoidan Nanoparticles for Pulmonary Delivery. *Carbohydrate Polymers 138*, 114–122.

Hulbert, S. F., F. A. Young, R. S. Mathews, J. J. Klawitter, C. D. Talbert, and F. H. Stelling (1970). Potential of Ceramic Materials as Permanently Implantable Skeletal Prostheses. *Journal of Biomedical Materials Research 4*(3), 433–456.

Jantzen, G. M., and J. R. Robinson (2002). Sustained- and Controlled-Release Drug Delivery Systems *Drugs and the Pharmaceutical Sciences 121*, 501–528.

Jaworek, A., and A. T. Sobczyk (2008). Electrospraying Route to Nanotechnology: An Overview. *Journal of Electrostatics 66*(3–4), 197–219.

Jayaraman, P., C. Gandhimathi, J. R. Venugopal, D. L. Becker, S. Ramakrishna, and D. K. Srinivasan (2015). Controlled Release of Drugs in Electrosprayed Nanoparticles for Bone Tissue Engineering. *Advanced Drug Delivery Reviews 94*, 77–95.

Jeong Park, Y., Y. M. Lee, S. N. Park, S. Y. Sheen, C. P. Chung, and S. J. Lee (2000). Platelet Derived Growth Factor Releasing Chitosan Sponge for Periodontal Bone Regeneration. *Biomaterials 21*(2), 153–159.

Ji, J., S. Hao, D. Wu, R. Huang, and Y. Xu (2011). Preparation, Characterization and in vitro Release of Chitosan Nanoparticles Loaded with Gentamicin and Salicylic Acid. *Carbohydrate Polymers 85*(4), 803–808.

Jia, W. T., X. Zhang, S. H. Luo, X. Liu, W. H. Huang, M. N. Rahaman, D. E. Day, C. Q. Zhang, Z. P. Xie, and J. Q. Wang (2010). Novel Borate Glass/Chitosan Composite as a Delivery Vehicle for Teicoplanin in the Treatment of Chronic Osteomyelitis. *Acta Biomaterialia 6*(3), 812–819.

Jong, W. H. D., and P. J. A. Borm (2008). Drug Delivery and Nanoparticles:Applications and Hazards. *International Journal of Nanomedicine 3*(2), 133–149.

Joshi, G. V., B. D. Kevadiya, H. A. Patel, H. C. Bajaj, and R. V. Jasra (2009). Montmorillonite as a Drug Delivery System: Intercalation and in vitro Release of

Timolol Maleate. *International Journal of Pharmaceutics 374*(1–2), 53–57.

Joshi, G. V., H. A. Patel, B. D. Kevadiya, and H. C. Bajaj (2009). Montmorillonite Intercalated with Vitamin B1 as Drug Carrier. *Applied Clay Science 45*(4), 248–253.

Kanellakopoulou, K., and E. J. Giamarellos-Bourboulis (2000). Carrier Systems for the Local Delivery of Antibiotics in Bone Infections. *Drugs 59*(6), 1223-1232.

Kang, X., J. Wang, H. Wu, I. A. Aksay, J. Liu, and Y. Lin (2009). Glucose Oxidase-Graphene-Chitosan Modified Electrode for Direct Electrochemistry and Glucose Sensing. *Biosensors and Bioelectronics 25*(4), 901–905.

Kasaai, M.R., G. Charlet, P. Paquin, and J. Arul (2003). Fragmentation of Chitosan by Microfluidization Process. *Innovative Food Science and Emerging Technologies 4*, 403–413.

Kaushik, A., R. Khan, P. R. Solanki, P. Pandey, J. Alam, S. Ahmad, and B. D. Malhotra (2008). Iron Oxide Nanoparticles-Chitosan Composite Based Glucose Biosensor. *Biosensors and Bioelectronics 24*(4), 676–683.

Kevadiya, B. D., G. V. Joshi, and H. C. Bajaj (2010). Layered Bionanocomposites as Carrier for Procainamide. *International Journal of Pharmaceutics 388*(1–2), 280–286.

Khan, A., K. D. Vu, G. Chauve, J. Bouchard, B. Riedl, and M. Lacroix (2014). Optimization of Microfluidization for the Homogeneous Distribution of Cellulose Nanocrystals (CNCs) in Biopolymeric Matrix. *Cellulose 21*(5), 3457–3468.

Khlibsuwan, R., and T. Pongjanyakul (2016). Chitosan-Clay Matrix Tablets for Sustained-Release Drug Delivery: Effect of Chitosan Molecular Weight and Lubricant. *Journal of Drug Delivery Science and Technology 35*, 303–313.

Kim, I. Y., S. J. Seo, H. S. Moon, M. K. Yoo, I. Y. Park, B. C. Kim, and C. S. Cho (2008). Chitosan and Its Derivatives for Tissue Engineering Applications. *Biotechnology Advances 26*(1), 1–21.

Kim, S. B., Y. J. Kim, T. L. Yoon, S. A. Park, I. H. Cho, E. J. Kim, I. A. Kim, and J. W. Shin (2004). The Characteristics of a Hydroxyapatite-Chitosan-PMMA Bone

Cement. *Biomaterials 25*(26), 5715–5723.

Klekamp, J., J. M. Dawson, D. W. Haas, D. DeBoer, and M. Christie (1999). The Use of Vancomycin and Tobramycin in Acrylic Bone Cement: Biomechanical Effects and Elution Kinetics for Use in Joint Arthroplasty. *Journal of Arthroplasty 14*(3), 339–346.

Konermann, L. (2009). A Simple Model for the Disintegration of Highly Charged Solvent Droplets during Electrospray Ionization. *Journal of the American Society for Mass Spectrometry 20*(3), 496–506.

Kong, L., Y. Gao, W. Cao, Y. Gong, N. Zhao, and X. Zhang (2005). Preparation and Characterization of Nano-Hydroxyapatite/Chitosan Composite Scaffolds. *Journal of Biomedical Materials Research - Part A 75*(2), 275–282.

Koosha, M., H. Mirzadeh, M. A. Shokrgozar, and M. Farokhi (2015). Nanoclay-reinforced electrospun chitosan/PVA nanocomposite nanofibers for biomedical applications. *RSC Advances 5*(14), 10479-10487.

Kosmulski, M. (2011). The PH-Dependent Surface Charging and Points of Zero Charge. V. Update. *Journal of Colloid and Interface Science 353*(1), 1–15.

Kumari, A., S. K. Yadav, and S. C. Yadav (2010). Biodegradable Polymeric Nanoparticles Based Drug Delivery Systems. *Colloids and Surfaces B: Biointerfaces 75*(1), 1–18.

Kumbar, S. G., K. S. Soppimath, and T. M. Aminabhavi (2003). Synthesis and Characterization of Polyacrylamide-Grafted Chitosan Hydrogel Microspheres for the Controlled Release of Indomethacin. *Journal of Applied Polymer Science 87*(9), 1525–1536.

Lagoueyte, N., and P. Paquin (1998). Effects of Microfluidization on the Functional Properties of Xanthan Gum. *Food Hydrocolloids 12*(3), 365–371.

Lan, Y., W. Li, Y. Jiao, R. Guo, Y. Zhang, W. Xue, and Y. Zhang (2014). Therapeutic Efficacy of Antibiotic-Loaded Gelatin Microsphere/Silk Fibroin Scaffolds in Infected Full-Thickness Burns. *Acta Biomaterialia 10*(7), 3167–3176.

Lavorgna, M., F. Piscitelli, P. Mangiacapra, and G. G. Buonocore (2010). Study of the Combined Effect of Both Clay and Glycerol Plasticizer on the Properties of Chitosan Films. *Carbohydrate Polymers 82*(2), 291–298.

Lee, D. S., and C. T. Huynh (2014). Controlled Release. *Encyclopedia of Polymeric Nanomaterials*, 1-12.

Lee, Y. H., F. Mei, M. Y. Bai, S. Zhao, and D. R. Chen (2010). Release Profile Characteristics of Biodegradable-Polymer-Coated Drug Particles Fabricated by Dual-Capillary Electrospray. *Journal of Controlled Release 145*(1), 58–65.

Lertsutthiwong, P., K. Noomun, S. Khunthon, and S. Limpanart (2012). Influence of Chitosan Characteristics on the Properties of Biopolymeric Chitosan–montmorillonite. *Progress in Natural Science: Materials International 22*(5), 502–508.

Liu, K. H., T. Y. Liu, S. Y. Chen, and D. M. Liu (2008). Drug Release Behavior of Chitosan-Montmorillonite Nanocomposite Hydrogels Following Electrostimulation. *Acta Biomaterialia 4*(4), 1038–1045.

Long, B., C. A. Wang, W. Ling, Y. Huang, and J. Sun (2007) Polyacrylamide-clay nacre-like nanocomposites prepared by electrophoretic deposition. *Composites Science and Technology 67*(13), 2770-2774.

Lowenstam, H. A., and S. Weiner (1989). *On Biomineralization*. *Oxford University Press, Oxford*.

Mader, J. T., and K. Adams (1989). Comparative Evaluation of Daptomycin (LY146032) and Vancomycin in the Treatment of Experimental Methicillin-Resistant Staphylococcus Aureus Osteomyelitis in Rabbits. *Antimicrobial Agents and Chemotherapy 33*(5), 689–692.

Mahdi Jafari, S., Y. He, and B. Bhandari (2006). Nano-Emulsion Production by Sonication and Microfluidization - A Comparison. *International Journal of Food Properties 9*(3), 475–485.

Marks, S. C., and S. N. Popoff (1988). Bone Cell Biology: The Regulation of

Development, Structure, and Function in the Skeleton. *The American Journal of Anatomy 183*(1), 1–44.

Martino, A. D., M. Sittinger, and M. V. Risbud (2005). Chitosan: A Versatile Biopolymer for Orthopaedic Tissue-Engineering. *Biomaterials 26*(30), 5983–5890.

Midhun, B. T., K. T. Shalumon, K. Manzoor, R. Jayakumar, S. V. Nair, and M. Deepthy (2011). Preparation of Budesonide-Loaded Polycaprolactone Nanobeads by Electrospraying for Controlled Drug Release. *Journal of Biomaterials Science, Polymer Edition 22*(18), 2431–2444.

Miller, S. C., and W. S. S. Jee (1987). The Bone Lining Cell: A Distinct Phenotype? *Calcified Tissue International 41*(1), 1-5.

Minagawa, T., Y. Okamura, Y. Shigemasa, S. Minami, and Y. Okamoto (2007). Effects of Molecular Weight and Deacetylation Degree of Chitin/Chitosan on Wound Healing. *Carbohydrate Polymers 67*(4), 640–644.

Mitra, S., U. Gaur, P. C. Ghosh, and A. N. Maitra (2001). Tumour Targeted Delivery of Encapsulated Dextran – Doxorubicin Conjugate Using Chitosan Nanoparticles as Carrier. *Journal of Controlled Release 74*(1–3), 317–23.

Miya, M., R. Iwamoto, S. Yoshikawa, and S. Mima (1980). I.r. Spectroscopic Determination of CONH Content in Highly Deacylated Chitosan. *International Journal of Biological Macromolecules 2*(5), 323–324.

Moura, M. R. D., R. J. Avena-Bustillos, T. H. McHugh, D. F. Wood, C. G. Otoni, and L. H. C. Mattoso (2011). Miniaturization of Cellulose Fibers and Effect of Addition on the Mechanical and Barrier Properties of Hydroxypropyl Methylcellulose Films. *Journal of Food Engineering 104*(1), 154–160.

Murphy, C. M., M. G. Haugh, and F. J. O'Brien (2010). The Effect of Mean Pore Size on Cell Attachment, Proliferation and Migration in Collagen-Glycosaminoglycan Scaffolds for Bone Tissue Engineering. *Biomaterials 31*(3), 461–466.

Nath, S. D., S. Son, A. Sadiasa, Y. K. Min, and B. T. Lee (2013). Preparation and Characterization of PLGA Microspheres by the Electrospraying Method for

Delivering Simvastatin for Bone Regeneration. *International Journal of Pharmaceutics 443*(1–2), 87–94.

Nigmatullin, R., F. Gao, and V. Konovalova (2008). Polymer-Layered Silicate Nanocomposites in the Design of Antimicrobial Materials. *Journal of Materials Science 43*(17), 5728–3573.

Niranjan, R., C. Koushik, S. Saravanan, A. Moorthi, M. Vairamani, and N. Selvamurugan (2013). A Novel Injectable Temperature-Sensitive Zinc Doped Chitosan/β-Glycerophosphate Hydrogel for Bone Tissue Engineering. *International Journal of Biological Macromolecules 54*(1), 24–29.

Noel, S. P., H. Courtney, J. D. Bumgardner, and W. O. Haggard (2008). Chitosan Films: A Potential Local Drug Delivery System for Antibiotics. *Clinical Orthopaedics and Related Research 466*(6), 1377–1382.

Noel, S. P., H. S. Courtney, J. D. Bumgardner, and W. O. Haggard (2010). Chitosan Sponges to Locally Deliver Amikacin and Vancomycin: A Pilot in vitro Evaluation. *Clinical Orthopaedics and Related Research 468*(8), 2074–2080.

Oguzlu, H., and F. Tihminlioglu (2010). Preparation and Barrier Properties of Chitosan-Layered Silicate Nanocomposite Films. *Macromolecular Symposia 298*(1), 91–98.

Ohya, Y., T. Takei, H. Kobayashi, and T. Ouchi (1993). Release Behaviour of 5-Fluorouracil from Chitosan-Gel Microspheres Immobilizing 5-Fluorouracil Derivative Coated with Polysaccharides and Their Cell Specific Recognition. *Journal of Microencapsulation 10*(1), 1–9.

Ordikhani, F., E. Tamjid, and A. Simchi (2014). Characterization and Antibacterial Performance of Electrodeposited Chitosan-Vancomycin Composite Coatings for Prevention of Implant-Associated Infections. *Materials Science and Engineering C 41*, 240–248.

Ordikhani, F., M. Dehghani, and A. Simchi (2015). Antibiotic-Loaded Chitosan–Laponite Films for Local Drug Delivery by Titanium Implants: Cell Proliferation and Drug Release Studies. *Journal of Materials Science: Materials in Medicine 26*(12), 269.

Orhan, Z. (2006). The Preparation of Ciprofloxacin Hydrochloride-Loaded Chitosan and Pectin Microspheres: Their Evaluation in an Animal Osteomyelitis Model. *Journal of Bone and Joint Surgery - British Volume 88–B*(2), 270–275.

Ozcan, A. V., M. Demir, G. Onem, I. Goksin, A. Baltalarli, V. K. Topkara, and I. Kaleli (2006). Topical versus Systemic Vancomycin for Deep Sternal Wound Infection Caused by Methicillin-Resistant Staphylococcus Aureus in a Rodent Experimental Model. *Texas Heart Institute Journal 33*(2), 107–110.

Pakravan, M., M. C. Heuzey, and A. Ajji (2011). A Fundamental Study of Chitosan/PEO Electrospinning. *Polymer 52*(21), 4813–4824.

Panagiotou, T., J.M. Bernard, and S.V. Mesite (2008). Deagglomeration and Dispersion of Carbon Nanotubes Using Microfluidizer High Shear Fluid Processors. *Nano Science and Technology Institute-Nanotech 1*, 39–42.

Park, J. K., Y. B. Choy, J. M. Oh, J. Y. Kim, S. J. Hwang, and J. H. Choy (2008). Controlled Release of Donepezil Intercalated in Smectite Clays. *International Journal of Pharmaceutics 359*(1–2), 198–204.

Patel, V. R., and M. M. Amiji (1996). Preparation and Characterization of Freeze-Dried Chitosan-Poly(Ethylene Oxide) Hydrogels for Site-Specific Antibiotic Delivery in the Stomach. *Pharmaceutical Research 13*(4), 588–593.

Peppas, N. A., and B. Narasimhan (2014). Mathematical Models in Drug Delivery: How Modeling Has Shaped the Way We Design New Drug Delivery Systems. *Journal of Controlled Release 190*, 75–81.

Perdones, A., L. Sánchez-González, A. Chiralt, and M. Vargas (2012). Effect of Chitosan-Lemon Essential Oil Coatings on Storage-Keeping Quality of Strawberry. *Postharvest Biology and Technology 70*, 32–41.

Pillai, C. K. S. , W. Paul, and C. P. Sharma (2009). Chitin and Chitosan Polymers: Chemistry, Solubility and Fiber Formation. *Progress in Polymer Science 37*(4), 641-678.

Pillai, O., and R. Panchagnula (2001). Polymers in Drug Delivery. *Current Opinion in*

Chemical Biology 5(4), 447-451.

Pon-On, W., N. Charoenphandhu, J. Teerapornpuntakit, J. Thongbunchoo, N. Krishnamra, and I. M. Tang (2013). *İn vitro* Study of Vancomycin Release and Osteoblast-like Cell Growth on Structured Calcium Phosphate-Collagen. *Materials Science and Engineering C 33*(3), 1423–1431.

Porter, J. R., T. T. Ruckh, and K. C. Popat (2009). Bone Tissue Engineering: A Review in Bone Biomimetics and Drug Delivery Strategies. *Biotechnology Progress 25*(6), 1539–1560.

Prabhakaran, M. P., M. Zamani, B. Felice, and S. Ramakrishna (2015). Electrospraying Technique for the Fabrication of Metronidazole Contained PLGA Particles and Their Release Profile. *Materials Science and Engineering C 56*, 66–73.

Ranganath, S. H., I. Kee, W. B. Krantz, P. K. H. Chow, and C. H. Wang (2009). Hydrogel Matrix Entrapping PLGA-Paclitaxel Microspheres: Drug Delivery with near Zero-Order Release and Implantability Advantages for Malignant Brain Tumour Chemotherapy. *Pharmaceutical Research 26*(9), 2101–2114.

Rao, N., and B. A. Lipsky (2007). Optimising Antimicrobial Therapy in Diabetic Foot Infections. *Drugs 67*(2), 195–214.

Rapacz-Kmita, A., E. Stodolak-Zych, M. Ziabka, A. Rozycka, and M. Dudek (2015). Instrumental Characterization of the Smectite Clay-Gentamicin Hybrids. *Bulletin of Materials Science 38*(4), 1069–1078.

Rapoport, N., A. I. Smirnov, W. G. Pitt, and A. A. Timoshin (1999). Bioreduction of Tempone and Spin-Labeled Gentamicin by Gram-Negative Bacteria: Kinetics and Effect of Ultrasound. *Archives of Biochemistry and Biophysics 362*(2), 233–241.

Razak, S. I. A., N. F. A. Sharif, and W. A. A. Rahman (2012). Biodegradable Polymers and Their Bone Applications : A Review. *International Journal of Engineering & Sciences 12*(1), 31–49.

Reznikov, N., R. Shahar, and S.Weiner (2014). Bone Hierarchical Structure in Three Dimensions. *Acta Biomaterialia*, *10*(9), 3815–3826.

Roul, J., R. Mohapatra, and S. K. Sahoo (2006). Antimicrobial Activity of Novel Chitosan/Cloisite 10A Nanocomposite: Preparation, Optimization , Characterization and Drug Delivery Behavior, *Pakistan Journal of the Pharmaceutic Sciences 29*(4), 1145–1150.

Rumian, Ł., H. Tiainen, U. Cibor, M. Krok-Borkowicz, M. Brzychczy-Włoch, H. J. Haugen, and E. Pamuła (2016). Ceramic Scaffolds Enriched with Gentamicin Loaded Poly(Lactide-Co-Glycolide) Microparticles for Prevention and Treatment of Bone Tissue Infections. *Materials Science and Engineering C 69*, 856–64.

Rumian, Ł., H. Tiainen, U. Cibor, M. Krok-Borkowicz, M. Brzychczy-Włoch, H. J. Haugen, and E. Pamuła (2017). Ceramic Scaffolds with Immobilized Vancomycin-Loaded Poly(Lactide-Co-Glycolide) Microparticles for Bone Defects Treatment. *Materials Letters 190*, 67–70.

Ryu, T. K., S. E. Kim, J. H. Kim, S. K. Moon, and S. W. Choi (2014). Biodegradable Uniform Microspheres Based on Solid-in-Oil-in-Water Emulsion for Drug Delivery: A Comparison of Homogenization and Fluidic Device. *Journal of Bioactive and Compatible Polymers 29*(5), 445–57.

Salata, O. (2005). Tools of Nanotechnology: Electrospray. *Current Nanoscience 1*(1), 25–33.

Salcedo, I., C. Aguzzi, G. Sandri, M. C. Bonferoni, M. Mori, P. Cerezo, R. Sánchez, C. Viseras, and C. Caramella (2012). *İn vitro* Biocompatibility and Mucoadhesion of Montmorillonite Chitosan Nanocomposite: A New Drug Delivery. *Applied Clay Science 55*, 131–37.

Salcedo, I., G. Sandri, C. Aguzzi, C. Bonferoni, P. Cerezo, R. Sánchez-Espejo, and C. Viseras (2014). Intestinal Permeability of Oxytetracycline from Chitosan-Montmorillonite Nanocomposites. *Colloids and Surfaces B: Biointerfaces 117*, 441–48.

Salvati, E. A., A. G. D. Valle, B. A. Masri, C. P. Duncan, A. G. D. Valle, A. González, and D. Valle (2003). The Infected Total Hip Arthroplasty. *Instructional Course Lectures 52*, 223–45.

Salvia-Trujillo, L., A. Rojas-Graü, R. Soliva-Fortuny, and O. Martín-Belloso (2015). Physicochemical Characterization and Antimicrobial Activity of Food-Grade Emulsions and Nanoemulsions Incorporating Essential Oils. *Food Hydrocolloids 43*, 547–56.

Sandri, G., M. C. Bonferoni, F. Ferrari, S. Rossi, C. Aguzzi, M. Mori, P. Grisoli, P. Cerezo, M. Tenci, C. Viseras and C. Caramella (2014). Montmorillonite-Chitosan-Silver Sulfadiazine Nanocomposites for Topical Treatment of Chronic Skin Lesions: *İn vitro* Biocompatibility, Antibacterial Efficacy and Gap Closure Cell Motility Properties. *Carbohydrate Polymers 102*(1), 970–77.

Santos, Z. M., A. L. P. F. Caroni, M. R. Pereira, D. R. da Silva, and J. L.C. Fonseca (2009). Determination of Deacetylation Degree of Chitosan: A Comparison between Conductometric Titration and CHN Elemental Analysis. *Carbohydrate Research 344*(18), 2591–2595.

Schurman, D. J., and R. Wheeler (1978). Gram Negative Bone and Joint Infection: Sixty Patients Treated with Amikacin. *Clinical Orthopaedics and Related Research*, 134, 268–274.

Selvig, K. A., U. M. Wikesjo, G. C. Bogle, and R. D. Finkelman (1994). Impaired Early Bone Formation in Periodontal Fenestration Defects in Dogs Following Application of Insulin-like Growth Factor (II). Basic Fibroblast Growth Factor and Transforming Growth Factor Beta 1. *Journal of Clinical Periodontology 21*, 380–85.

Sezer, A. D., H. K. Sarılmışer, E. Rayaman, A. Çevikbaş, E. T. Öner, and J. Akbuğa (2017). Development and Characterization of Vancomycin-Loaded Levan-Based Microparticular System for Drug Delivery. *Pharmaceutical Development and Technology 22*(5), 627–634.

Shaikh, H. K., R. V. Kshirsagar, and S. G. Patil (2015). Mathematical Models for Drug Release Characterization : A Review. *World Journal of Pharmacy and Pharmaceutical Sciences 4*(4), 324–338.

Shi, P., Y. Zuo, X. Li, Q. Zou, H. Liu, L. Zhang, Y. Li, and Y. S. Morsi (2010). Gentamicin-Impregnated Chitosan/Nanohydroxyapatite/Ethyl Cellulose Microspheres Granules for Chronic Osteomyelitis Therapy. *Journal of Biomedical*

Materials Research - Part A 93(3), 1020–1031.

Sibanda, W., V. Pillay, M. P. Danckwerts, A. M. Viljoen, S. van Vuuren, and R. A. Khan (2004). Experimental Design for the Formulation and Optimization of Novel Cross-Linked Oilispheres Developed for in vitro Site-Specific Release of Mentha Piperita Oil. *AAPS PharmSciTech 5*(1), 128-141.

Singhvi, G., and M. Singh (2011). Review : In-Vitro Drug Release Characterization Models. *International Journal of Pharmaceutical Studies and Research 2*, 77–84.

Sionkowska, A., B. Kaczmarek, and R. Gadzala-Kopciuch (2016). Gentamicin Release from Chitosan and Collagen Composites. *Journal of Drug Delivery Science and Technology 35*, 353–359.

Song, B. B., S. H. Sha, and J. Schacht (1998). Iron Chelators Protect from Aminoglycoside-Induced Cochleo- and Vestibulo-Toxicity. *Free Radical Biology and Medicine 25*(2), 189–195.

Songsurang, K., N. Praphairaksit, K. Siraleartmukul, and N. Muangsin (2011). Electrospray Fabrication of Doxorubicin-Chitosan-Tripolyphosphate Nanoparticles for Delivery of Doxorubicin. *Archives of Pharmacal Research 34*(4), 583–592.

Stevens, M. M. (2008). Biomaterials for Bone Tissue Engineering. *Materials Today 11*(5), 18–25.

Sunny, M. C., P. Ramesh, and H. K. Varma (2002). Microstructured Microspheres of Hydroxyapatite Bioceramic. *Journal of Materials Science: Materials in Medicine 13*(7), 623–632.

Sussman, Carrie, and Barbara Bates-Jensen (2012). *Wound Care - A Collaborative Practice Manual for Health Professionals*. *Journal of Chemical Information and Modeling 53*(9), 1-836.

Thakor, R. S., F. D. Majmudar, J. K. Patel, and G. C. Rajaput (2010). Review : Osmotic Drug Delivery Systems Current Scenario. *Journal of Pharmaceutical Research 3*(4), 771-775.

Thakur, G., A. Singh, and I. Singh (2016). Chitosan-Montmorillonite Polymer

Composites: Formulation and Evaluation of Sustained Release Tablets of Aceclofenac. *Scientia Pharmaceutica 84*(4), 603–617.

Thomas, F., L. J. Michot, D. Vantelon, E. Montargès, B. Prélot, M. Cruchaudet, and J. F. Delon (1999). Layer Charge and Electrophoretic Mobility of Smectites. In *Colloids and Surfaces A: Physicochemical and Engineering Aspects 159*, 351–358.

Tomic, I., A. Vidis-Millward, M. Mueller-Zsigmondy, and J-M M. Cardot (2016). Setting Accelerated Dissolution Test for PLGA Microspheres Containing Peptide, Investigation of Critical Parameters Affecting Drug Release Rate and Mechanism. *International Journal of Pharmaceutics 505*(1–2), 42–51.

Tsai, M. L., L. Z. Tseng, and R. H. Chen (2009). Two-Stage Microfluidization Combined with Ultrafiltration Treatment for Chitosan Mass Production and Molecular Weight Manipulation. *Carbohydrate Polymers 77*(4), 767–772.

Uskoković, V., and T. A. Desai (2014). *İn vitro* Analysis of Nanoparticulate Hydroxyapatite/Chitosan Composites as Potential Drug Delivery Platforms for the Sustained Release of Antibiotics in the Treatment of Osteomyelitis. *Journal of Pharmaceutical Sciences 103*(2), 567–579.

Vargas, M., Á. Perdones, A. Chiralt, M. Cháfer, and C. González-Martínez (2011). Effect of Homogenization Conditions on Physicochemical Properties of Chitosan-Based Film-Forming Dispersions and Films. *Food Hydrocolloids 25*(5), 1158–1164.

Villay, A., F. Lakkis de Filippis, L. Picton, D. Le Cerf, C. Vial, and P. Michaud (2012). Comparison of Polysaccharide Degradations by Dynamic High-Pressure Homogenization. *Food Hydrocolloids 27*(2), 278–86.

Vrabec, G., W. Stevenson, S. Elguizaoui, M. Kirsch, and J. Pinkowski (2016). What Is the Intraarticular Concentration of Tobramycin Using Low-Dose Tobramycin Bone Cement in TKA: An In Vivo Analysis? *Clinical Orthopaedics and Related Research 474*(11), 2441–2447.

Wagh, A. S. (2004). *Chemically Bonded Phosphate Ceramics.* (2nd Edition) Elsevier.

Wang, J., J. De Boer, and K. De Groot (2004). Preparation and Characterization of

Electrodeposited Calcium Phosphate/Chitosan Coating on Ti6Al4V Plates. *Journal of Dental Research 83*(4), 296–301.

Wang, S. F., L. Shen, Y. J. Tong, L. Chen, I. Y. Phang, P. Q. Lim, and T. X. Liu (2005). Biopolymer Chitosan/Montmorillonite Nanocomposites: Preparation and Characterization. *Polymer Degradation and Stability 90*(1), 123–31.

Wang, X., Y. Du, and J. Luo (2008). Biopolymer/Montmorillonite Nanocomposite: Preparation, Drug-Controlled Release Property and Cytotoxicity. *Nanotechnology 19*(6).

Wedmore, I., J. G. McManus, A. E. Pusateri, and J. B. Holcomb (2006). A Special Report on the Chitosan-Based Hemostatic Dressing: Experience in Current Combat Operations. *Journal of Trauma - Injury, Infection and Critical Care 60*(3), 655–58.

Wers, E., H. Oudadesse, B. Lefeuvre, O. Merdrignac-Conanec, and A. Barroug (2015). Evaluation of the Kinetic and Relaxation Time of Gentamicin Sulfate Released from Hybrid Biomaterial Bioglass-Chitosan Scaffolds. *Applied Surface Science 353*, 200–208.

Williams, L., and R. E. Domen (1990). Zeta Potential and Vancomycin-Red Blood Cell Interactions. *Archives of Pathology & Laboratory Medicine 114*(12), 1262–1263.

Wu, T., Q. Zhang, W. Ren, X. Yi, Z. Zhou, X. Peng, X. Yu, and M. Lang (2013). Controlled Release of Gentamicin from Gelatin/Genipin Reinforced Beta-Tricalcium Phosphate Scaffold for the Treatment of Osteomyelitis. *Journal of Materials Chemistry B 1*(26), 3304-3313.

Xu, Y., and M. A. Hanna (2007). Electrosprayed Bovine Serum Albumin-Loaded Tripolyphosphate Cross-Linked Chitosan Capsules: Synthesis and Characterization. *Journal of Microencapsulation 24*(2), 143–51.

Yacob, N, N. Talip, M. Mahmud, N. A. I. Sani, N.A. Samsuddin, N. A. Fabillah (2013). Determination of Viscosity - Average Molecular Weight of Chitosan Using Intrinsic Viscosity Measurement. *Journal of Nuclear and Related Technologies 10*(1), 39–44.

Yang, C. C., C. C. Lin, J. W. Liao, and S. K. Yen (2013). Vancomycin-Chitosan Composite Deposited on Post Porous Hydroxyapatite Coated Ti6Al4V Implant for Drug Controlled Release. *Materials Science and Engineering C 33*(4), 2203–2212.

Yang, J. H., J. H. Lee, H. J. Ryu, A. A. Elzatahry, Z. A. Alothman, and J. H. Choy (2016). Drug–clay Nanohybrids as Sustained Delivery Systems. *Applied Clay Science 130*, 20–32.

Yao, Q., P. Nooeaid, J. A. Roether, Y. Dong, Q. Zhang, and A. R. Boccaccini (2013). Bioglass®-Based Scaffolds Incorporating Polycaprolactone and Chitosan Coatings for Controlled Vancomycin Delivery. *Ceramics International 39*(7), 7517–7522.

Yin Win, K., and S. Feng (2005). Effects of Particle Size and Surface Coating on Cellular Uptake of Polymeric Nanoparticles for Oral Delivery of Anticancer Drugs. *Biomaterials 26*(15), 2713–2722.

Yuan, Q., J. Shah, S. Hein, and R. D.K. Misra (2010). Controlled and Extended Drug Release Behavior of Chitosan-Based Nanoparticle Carrier. *Acta Biomaterialia 6*(3), 1140–1148.

Yuan, Y., B. M. Chesnutt, W. O. Haggard, and J. D. Bumgardner (2011). Deacetylation of Chitosan: Material Characterization and in vitro Evaluation via Albumin Adsorption and Pre-Osteoblastic Cell Cultures. *Materials 4*(8), 1399–1416.

Zambaux, M. F., F. Bonneaux, R. Gref, E. Dellacherie, and C. Vigneron (1999). Preparation and Characterization of Protein C-Loaded PLA Nanoparticles. *Journal of Controlled Release 60*(2–3), 179–188.

Zhang, S., and K. Kawakami (2010). One-Step Preparation of Chitosan Solid Nanoparticles by Electrospray Deposition. *International Journal of Pharmaceutics 397*(1–2), 211–217.

Zhang, Y., R. J. Liang, J. J. Xu, L. F. Shen, J. Q. Gao, X. P. Wang, N. N. Wang, D. Shou, and Y. Hu (2017). Efficient Induction of Antimicrobial Activity with Vancomycin Nanoparticle-Loaded Poly(Trimethylene Carbonate) Localized Drug Delivery System. *International Journal of Nanomedicine 12*, 1201–1214.

Zhang, Y., J. R. Venugopal, A. El-Turki, S. Ramakrishna, B. Su, and C. T. Lim (2008). Electrospun Biomimetic Nanocomposite Nanofibers of Hydroxyapatite/Chitosan for Bone Tissue Engineering. *Biomaterials 29*(32), 4314–4322.

Zhang, Y., and M. Zhang (2002). Calcium Phosphate/Chitosan Composite Scaffolds for Controlled in vitro Antibiotic Drug Release. *Journal of Biomedical Materials Research 62*(3), 378–386.

Zhang, Y., C. Xue, Y. Xue, R. Gao, and X. Zhang (2005). Determination of the Degree of Deacetylation of Chitin and Chitosan by X-Ray Powder Diffraction. *Carbohydrate Research 340*(11), 1914–1917.

Zhao, D., J. S. Li, W. Suen, M. W. Chang, and J. Huang (2016). Preparation and Characterization of Ganoderma Lucidum Spores-Loaded Alginate Microspheres by Electrospraying. *Materials Science and Engineering C 62*, 835–842.

Zheng, J., Q. Su, C. Wang, G. Cheng, R. Zhu, J. Shi, and K. Yao (2011). Synthesis and Biological Evaluation of PMMA/MMT Nanocomposite as Denture Base Material. *Journal of Materials Science: Materials in Medicine 22*(4), 1063–1071.

Zhou, G., J. Zhang, J. Tai, Q. Han, L. Wang, K. Wang, S. Wang, and Y. Fan (2017). Comparison of Chitosan Microsphere versus O-Carboxymethyl Chitosan Microsphere for Drug Delivery Systems. *Journal of Bioactive and Compatible Polymers 32*(5), 469–486.

Zhou, J., T. L. Fang, J. Wen, Z. Shao, and J. Dong (2011). Silk Coating on Poly(ε-Caprolactone) Microspheres for the Delayed Release of Vancomycin. *Journal of Microencapsulation 28*(2), 99–107.

Zhuang, H., J. P. Zheng, H. Gao, and K. D. Yao (2007). *İn vitro* Biodegradation and Biocompatibility of Gelatin/Montmorillonite- Chitosan Intercalated Nanocomposite. *Journal of Materials Science: Materials in Medicine 18*(5), 951–57.

APPENDIX A

VISCOSITY MEASUREMENT OF MICROFLUIDIZED CHITOSAN SOLUTION

Table A. 1. Viscosity measurements of chitosan solution without microfluidizer treatment

Concentration (g/ml)	Time (s)	Relative viscosity, μ_{rel}	Specific viscosity, μ_{sp}	Reduced viscosity μ_{red} (ml/g)
0.000625	120.67±0.33	1.75	0.75	1198.07
0.00125	206.55±2.03	2.99	1.99	1592.27
0.0025	483±2.31	7	6	2400
0.00375	1008±4.16	14.61	13.61	3628.99

Table A. 2. Viscosity measurements of microfluidized chitosan solution (10,000 psi 3 pass)

Concentration (g/ml)	Time (s)	Relative viscosity, μ_{rel}	Specific viscosity, μ_{sp}	Reduced viscosity, μ_{red} (ml/g)
0.000625	91.33±0.33	1.47	0.47	756.99
0.00125	134.67±0.33	2.17	1.17	937.63
0.0025	263.33±0.33	4.25	3.25	1298.92
0.00375	429±4.73	6.92	5.92	1578.49

Table A. 3. Viscosity measurements of microfluidized chitosan solution (10,000 psi 5 pass)

Concentration (g/ml)	Time (s)	Relative viscosity, μ_{rel}	Specific viscosity, μ_{sp}	Reduced viscosity μ_{red} (ml/g)
0.000625	101±0.58	1.51	0.51	811.94
0.00125	140±1.53	2.09	1.09	871.64
0.0025	276±0.58	4.12	3.12	1247.76
0.00375	538.7±2.85	8.04	7.04	1877.28

Table A. 4. Viscosity measurements of microfluidized chitosan solution (10,000 psi 10 pass)

Concentration (g/ml)	Time (s)	Relative viscosity, μ_{rel}	Specific viscosity, μ_{sp}	Reduced viscosity μ_{red} (ml/g)
0.000625	91.33±0.33	1.32	0.32	517.87
0.00125	129±0.58	1.87	0.87	695.65
0.0025	255.67±6.74	3.71	2.71	1082.13
0.00375	410±3.21	5.94	4.94	1317.87

APPENDIX B

CALIBRATION CURVES OF MODEL DRUGS

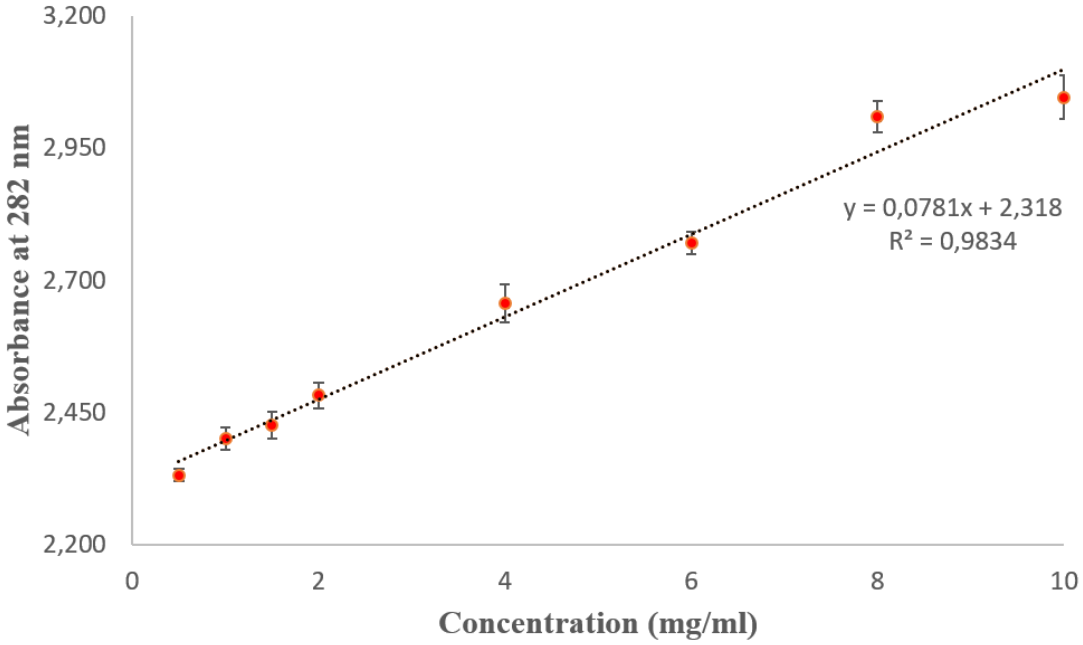

Figure B. 1. Calibration curve of Vancomycin Hydrochloride

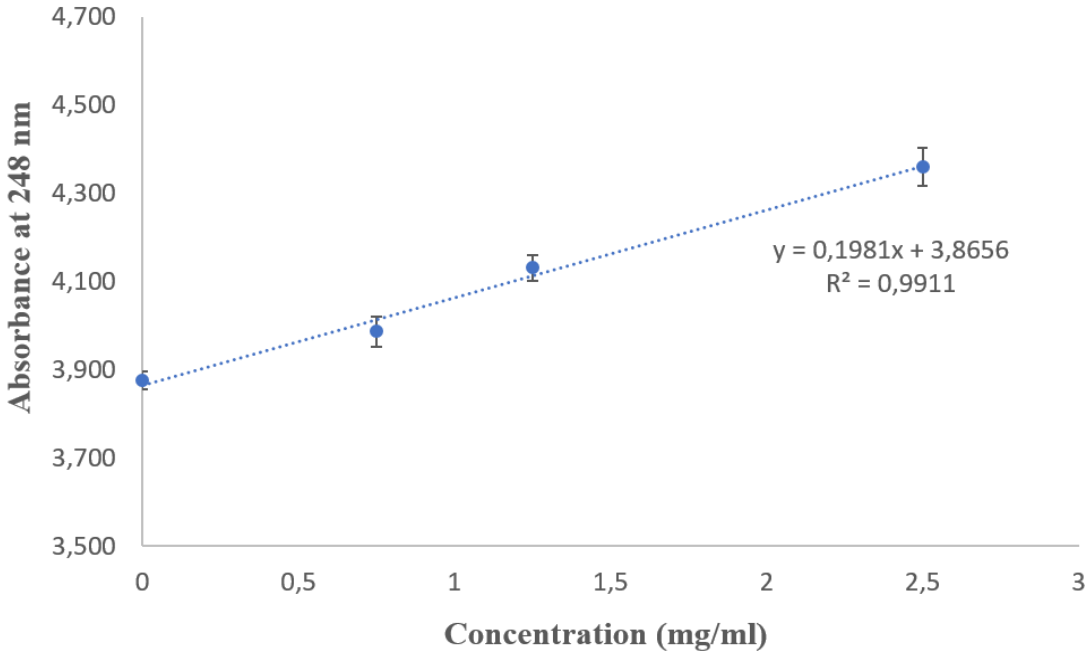

Figure B. 2. Calibration curve of Gentamicin Sulphate

APPENDIX C

MINIMUM INHIBITORY CONCENTRATION VALUES OF MODEL DRUGS

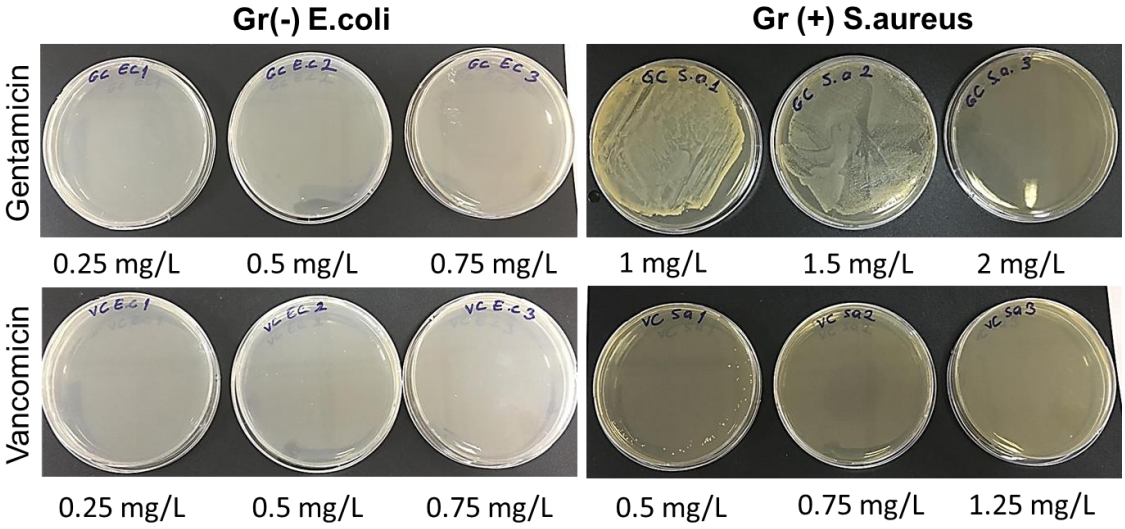

Figure C. 1. Minimum Inhibitory Concentration (MIC) determination of Vancomycin Hydrochloride and Gentamicin Sulphate